AD-A120 702 STRESS CONCENTRATIONS(U) MARYLAND UNIV COLLEGE PARK 1/2
SCHOOL OF ENGINEERING A J DURELLI SEP 82 60
N00014-81-K-0186

UNCLASSIFIED F/G 12/1 NL

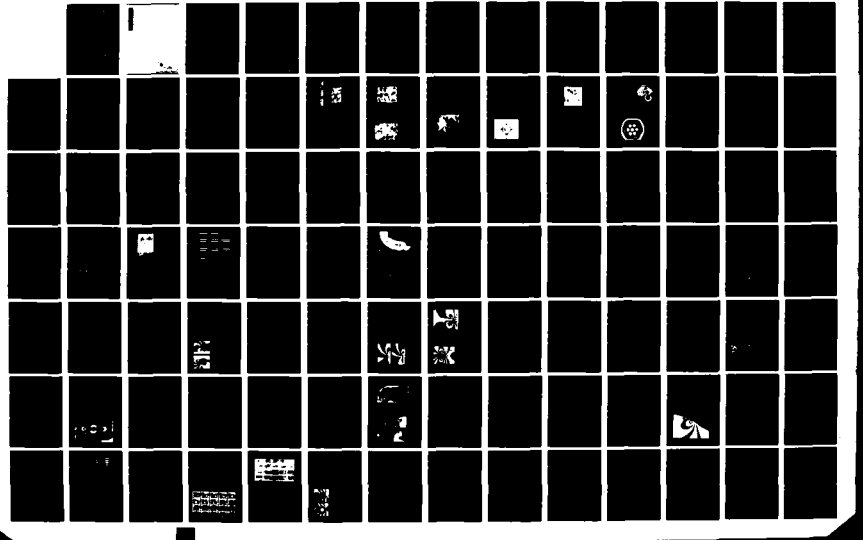

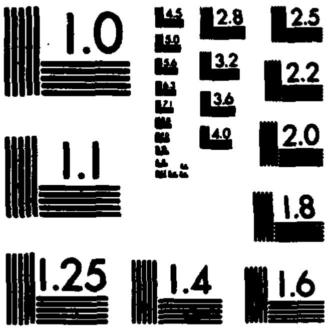

MICROCOPY RESOLUTION TEST CHART
NATIONAL BUREAU OF STANDARDS-1963-A

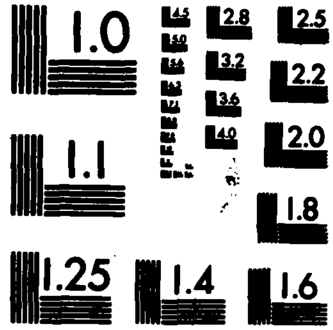

MICROCOPY RESOLUTION TEST CHART
NATIONAL BUREAU OF STANDARDS-1963-A

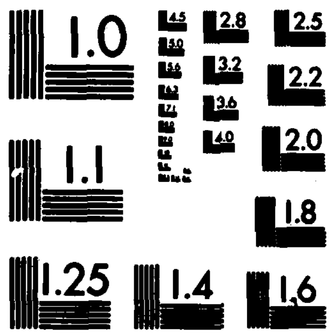

MICROCOPY RESOLUTION TEST CHART
NATIONAL BUREAU OF STANDARDS-1963-A

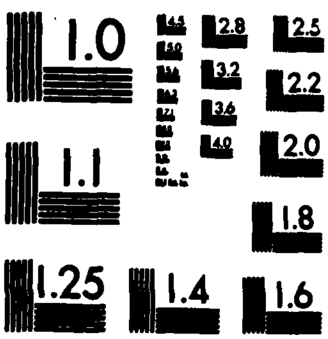

MICROCOPY RESOLUTION TEST CHART
NATIONAL BUREAU OF STANDARDS-1963-A

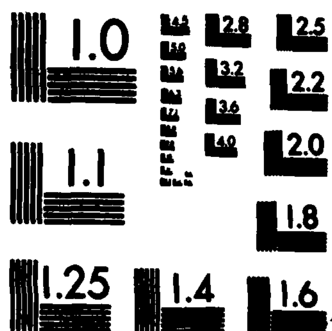

MICROCOPY RESOLUTION TEST CHART
NATIONAL BUREAU OF STANDARDS-1963-A

STRESS CONCENTRATIONS

by

A. J. Durelli

Sponsored by

Office of Naval Research
Department of the Navy
Washington, D.C. 20025

on

Contract No. N00014-81-K-0186
U.M. Project No. SF-CARS

Report No. 60

School of Engineering
University of Maryland
College Park, MD. 20742

Previous Technical Reports to the Office of Naval Research

1. A. J. Durelli, "Development of Experimental Stress Analysis Methods to Determine Stresses and Strains in Solid Propellant Grains"--June 1962.
Developments in the manufacturing of grain-propellant models are reported. Two methods are given: a) cementing routed layers and b) casting.

2. A. J. Durelli and V. J. Parks, "New Method to Determine Restrained Shrinkage Stresses in Propellant Grain Models"--October 1962.
The birefringence exhibited in the curing process of a partially restrained polyurethane rubber is used to determine the stress associated with restrained shrinkage in models of solid propellant grains partially bonded to the case.

3. A. J. Durelli, "Recent Advances in the Application of Photoelasticity in the Missile Industry"--October 1962.
Two- and three-dimensional photoelastic analysis of grains loaded by pressure and by temperature are presented. Some applications to the optimization of fillet contours and to the redesign of case joints are also included.

4. A. J. Durelli and V. J. Parks, "Experimental Solution of Some Mixed Boundary Value Problems"--April 1964.
Means of applying known displacements and known stresses to the boundaries of models used in experimental stress analysis are given. The application of some of these methods to the analysis of stresses in the field of solid propellant grains is illustrated. The presence of the "pinching effect" is discussed.

5. A. J. Durelli, "Brief Review of the State of the Art and Expected Advance in Experimental Stress and Strain Analysis of Solid Propellant Grains"--April 1964.
A brief review is made of the state of the experimental stress and strain analysis of solid propellant grains. A discussion of the aspects for the next fifteen years is added.

6. A. J. Durelli, "Experimental Strain and Stress Analysis of Solid Propellant Rocket Motors"--March 1965.
A review is made of the experimental methods used to strain-analyze solid propellant rocket motor shells and grains when subjected to different loading conditions. Methods directed at the determination of strains in actual rockets are included.

7. L. Ferrer, V. J. Parks and A. J. Durelli, "An Experimental Method to Analyze Gravitational Stresses in Two-Dimensional Problems"--October 1965.
Photoelasticity and moiré methods are used to solve two-dimensional problems in which gravity-stresses are present.

8. A. J. Durelli, V. J. Parks and C. J. del Rio, "Stresses in a Square Slab Bonded on One Face to a Rigid Plate and Shrunk"--November 1965.
A square epoxy slab was bonded to a rigid plate on one of its faces in the process of curing. In the same process the photoelastic effects associated with a state of restrained shrinkage were "frozen-in." Three-dimensional photoelasticity was used in the analysis.

9. A. J. Durelli, V. J. Parks and C. J. del Rio, "Experimental Determination of Stresses and Displacements in Thick-Wall Cylinders of Complicated Shape"--April 1966.
Photoelasticity and moiré are used to analyze a three-dimensional rocket shape with a star shaped core subjected to internal pressure.

10. V. J. Parks, A. J. Durelli and L. Ferrer, "Gravitational Stresses Determined Using Immersion Techniques"--July 1966.
The methods presented in Technical Report No. 7 above are extended to three-dimensions. Immersion is used to increase response.

11. A. J. Durelli and V. J. Parks. "Experimental Stress Analysis of Loaded Boundaries in Two-Dimensional Second Boundary Value Problems"--February 1967.
The pinching effect that occurs in two-dimensional bonding problems, noted in Reports 2 and 4 above, is analyzed in some detail.

12. A. J. Durelli, V. J. Parks, H. C. Feng and F. Chiang, "Strains and Stresses in Matrices with Inserts,"-- May 1967.
Stresses and strains along the interfaces, and near the fiber ends, for different fiber end configurations, are studied in detail.

13. A. J. Durelli, V. J. Parks and S. Uribe, "Optimization of a Slot End Configuration in a Finite Plate Subjected to Uniformly Distributed Load,"--June 1967.
Two-dimensional photoelasticity was used to study various elliptical ends to a slot, and determine which would give the lowest stress concentration for a load normal to the slot length.

14. A. J. Durelli, V. J. Parks and Han-Chow Lee, "Stresses in a Split Cylinder Bonded to a Case and Subjected to Restrained Shrinkage,"--January 1968.
A three-dimensional photoelastic study that describes a method and shows results for the stresses on the free boundaries and at the bonded interface of a solid propellant rocket.

15. A. J. Durelli, "Experimental Stress Analysis Activities in Selected European Laboratories"--August 1968.
This report has been written following a trip conducted by the author through several European countries. A list is given of many of the laboratories doing important experimental stress analysis work and of the people interested in this kind of work. An attempt has been made to abstract the main characteristics of the methods used in some of the countries visited.

16. V. J. Parks, A. J. Durelli and L. Ferrer, "Constant Acceleration Stresses in a Composite Body"--October 1968.
Use of the immersion analogy to determine gravitational stresses in two-dimensional bodies made of materials with different properties.

17. A. J. Durelli, J. A. Clark and A. Kochev, "Experimental Analysis of High Frequency Stress Waves in a Ring"--October 1968.
A method for the complete experimental determination of dynamic stress distributions in a ring is demonstrated. Photoelastic data is supplemented by measurements with a capacitance gage used as a dynamic lateral extensometer.

18. J. A. Clark and A. J. Durelli, "A Modified Method of Holographic Interferometry for Static and Dynamic Photoelasticity"--April 1968.
A simplified absolute retardation approach to photoelastic analysis is described. Dynamic isopachics are presented.

19. J. A. Clark and A. J. Durelli, "Photoelastic Analysis of Flexural Waves in a Bar"--May 1969.
A complete direct, full-field optical determination of dynamic stress distribution is illustrated. The method is applied to the study of flexural waves propagating in a urethane rubber bar. Results are compared with approximate theories of flexural waves.

20. J. A. Clark and A. J. Durelli, "Optical Analysis of Vibrations in Continuous Media"--June 1969.
Optical methods of vibration analysis are described which are independent of assumptions associated with theories of wave propagation. Methods are illustrated with studies of transverse waves in prestressed bars, snap loading of bars and motion of a fluid surrounding a vibrating bar.

21. V. J. Parks, A. J. Durelli, K. Chandrashekhara and T. L. Chen, "Stress Distribution Around a Circular Bar, with Flat and Spherical Ends, Embedded in a Matrix in a Triaxial Stress Field"--July 1969.
A Three-dimensional photoelastic method to determine stresses in composite materials is applied to this basic shape. The analyses of models with different loads are combined to obtain stresses for the triaxial cases.

22. A. J. Durelli, V. J. Parks and L. Ferrer, "Stresses in Solid and Hollow Spheres Subjected to Gravity or to Normal Surface Tractions"--October 1969.
The method described in Report No. 10 above is applied to two specific problems. An approach is suggested to extend the solutions to a class of surface traction problems.

23. J. A. Clark and A. J. Durelli, "Separation of Additive and Subtractive Moiré Patterns"--December 1969.
A spatial filtering technique for adding and subtracting images of several gratings is described and employed to determine the whole field of Cartesian shears and rigid rotations.

24. R. J. Sanford and A. J. Durelli, "Interpretation of Fringes in Stress-Holo-Interferometry"--July 1970.
Errors associated with interpreting stress-holo-interferometry patterns as the superposition of isopachics (with half order fringe shifts) and isochromatics are analyzed theoretically and illustrated with computer generated holographic interference patterns.

25. J. A. Clark, A. J. Durelli and P. A. Laura, "On the Effect of Initial Stress on the Propagation of Flexural Waves in Elastic Rectangular Bars"--December 1970.
Experimental analysis of the propagation of flexural waves in prismatic, elastic bars with and without prestressing. The effects of prestressing by axial tension, axial compression and pure bending are illustrated.

26. A. J. Durelli and J. A. Clark, "Experimental Analysis of Stresses in a Buoy-Cable System Using a Birefringent Fluid"--February 1971.
An extension of the method of photoviscous analysis is presented which permits quantitative studies of strains associated with steady state vibrations of immersed structures. The method is applied in an investigation of one form of behavior of buoy-cable systems loaded by the action of surface waves.

27. A. J. Durelli and T. L. Chen, "Displacements and Finite-Strain Fields in a Sphere Subjected to Large Deformations"--February 1972.
Displacements and strains (ranging from 0.001 to 0.50) are determined in a polyurethane sphere subjected to several levels of diametral compression. A 500 lines-per-inch grating was embedded in a meridian plane of the sphere and moiré effect produced with a non-deformed master. The maximum applied vertical displacement reduced the diameter of the sphere by 27 per cent.

28. A. J. Durelli and S. Machida, "Stresses and Strain in a Disk with Variable Modulus of Elasticity"--March 1972
A transparent material with variable modulus of elasticity has been manufactured that exhibits good photoelastic properties and can also be strain analyzed by moiré. The results obtained suggests that the stress distribution in the disk of variable E is practically the same as the stress distribution in the homogeneous disk. It also indicates that the strain fields in both cases are very different, but that it is possible, approximately, to obtain the stress field from the strain field using the value of E at every point, and Hooke's law.

29. A. J. Durelli and J. Buitrago, "State of Stress and Strain in a Rectangular Belt Pulled Over a Cylindrical Pulley"--June 1972.
Two- and three-dimensional photoelasticity as well as electrical strain gages, dial gages and micrometers are used to determine the stress distribution in a belt-pulley system. Contact and tangential stress for various contact angles and friction coefficients are given.

30. T. L. Chen and A. J. Durelli, "Stress Field in a Sphere Subjected to Large Deformations"--June 1972.
Strain fields obtained in a sphere subjected to large diametral compressions from a previous paper were converted into stress fields using two approaches. First, the concept of strain-energy function for an isotropic elastic body was used. Then the stress field was determined with the Hookean type natural stress-natural strain relation. The results so obtained were also compared.

31. A. J. Durelli, V. J. Parks and H. M. Hasseem, "Helices Under Load"--July 1973.
Previous solutions for the case of close coiled helical springs and for helices made of thin bars are extended. The complete solution is presented in graphs for the use of designers. The theoretical development is correlated with experiments.

32. T. L. Chen and A. J. Durelli, "Displacements and Finite Strain Fields in a Hollow Sphere Subjected to Large Elastic Deformations"--September 1973.
The same methods described in No. 27, were applied to a hollow sphere with an inner diameter one half the outer diameter. The hollow sphere was loaded up to a strain of 30 per cent on the meridian plane and a reduction of the diameter by 20 per cent.

33. A. J. Durelli, H. H. Hasseem and V. J. Parks, "New Experimental Method in Three-Dimensional Elastostatics"--December 1973.
A new material is reported which is unique among three-dimensional stress-freezing materials, in that, in its heated (or rubbery) state it has a Poisson's ratio which is appreciably lower than 0.5. For a loaded model, made of this material, the unique property allows the direct determination of stresses from strain measurements taken at interior points in the model.

34. J. Wolak and V. J. Parks, "Evaluation of Large Strains in Industrial Applications"--April 1974.
It was shown that Mohr's circle permits the transformation of strain from one axis of reference to another, irrespective of the magnitude of the strain, and leads to the evaluation of the principal strain components from the measurement of direct strain in three directions.

35. A. J. Durelli, "Experimental Stress Analysis Activities in Selected European Laboratories"--April 1975.
Continuation of Report No. 15 after a visit to Belgium, Holland, Germany, France, Turkey, England and Scotland.

36. A. J. Durelli, V. J. Parks and J. O. Bühler-Vidal, "Linear and Non-linear Elastic and Plastic Strains in a Plate with a Big Hole Loaded Axially in its Plane"--July 1975.
Strain analysis of the ligament of a plate with a big hole indicates that both geometric and material non-linearity may take place. The strain concentration factor was found to vary from 1 to 2 depending on the level of deformation.

37. A. J. Durelli, V. Pavlin, J. O. Bühler-Vidal and G. Ome, "Elastostatics of a Cubic Box Subjected to Concentrated Loads"--August 1975.
Analysis of experimental strain, stress and deflection of a cubic box subjected to concentrated loads applied at the center of two opposite faces. The ratio between the inside span and the wall thickness was varied between approximately 5 and 121.

38. A. J. Durelli, V. J. Parks and J. O. Bühler-Vidal, "Elastostatics of Cubic Boxes Subjected to Pressure"--March 1976.
Experimental analysis of strain, stress and deflections in a cubic box subjected to either internal or external pressure. Inside span-to-wall thickness ratio varied from 5 to 14.

39. Y. Y. Hung, J. D. Hovanesian and A. J. Durelli, "New Optical Method to Determine Vibration-Induced Strains with Variable Sensitivity After Recording"--November 1976.
A steady state vibrating object is illuminated with coherent light and its image slightly misfocused. The resulting specklegram is "time-integrated" as when Fourier filtered gives derivatives of the vibrational amplitude.

40. Y. Y. Hung, C. Y. Liang, J. D. Hovanesian and A. J. Durelli, "Cyclic Stress Studies by Time-Averaged Photoelasticity"--November 1976.
"Time-averaged isochromatics" are formed when the photographic film is exposed for more than one period. Fringes represent amplitudes of the oscillating stress according to the zeroth order Bessel function.

41. Y. Y. Hung, C. Y. Liang, J. D. Hovanesian and A. J. Durelli, "Time-Averaged Shadow Moiré Method for Studying Vibrations"--November 1976.
Time-averaged shadow moiré permits the determination of the amplitude distribution of the deflection of a steady vibrating plate.

42. J. Buitrago and A. J. Durelli, "On the Interpretation of Shadow-Moiré Fringes"--April 1977.
Possible rotations and translations of the grating are considered in a general expression to interpret shadow-moiré fringes and on the sensitivity of the method. Application to an inverted perforated tube.

43. J. der Hovanesian, "18th Polish Solid Mechanics Conference." Published in European Scientific Notes of the Office of Naval Research, in London, England, Dec. 31, 1976.
Comments on the planning and organization of, and scientific content of paper presented at the 18th Polish Solid Mechanics Conference held in Wisla-Jawornik from September 7-14, 1976.

44. A. J. Durelli, "The Difficult Choice,"--May 1977.
The advantages and limitations of methods available for the analyses of displacements, strain, and stresses are considered. Comments are made on several theoretical approaches, in particular approximate methods, and attention is concentrated on experimental methods: photo-elasticity, moiré, brittle and photoelastic coatings, gages, grids, holography and speckle to solve two- and three-dimensional problems in elasticity, plasticity, dynamics and anisotropy.

45. C. Y. Liang, Y. Y. Hung, A. J. Durelli and J. D. Hovanesian, "Direct Determination of Flexural Strains in Plates Using Projected Gratings,"--June 1977.
The method requires the rotation of one photograph of the deformed grating over a copy of itself. The moiré produced yields strains by optical double differentiation of deflections. Applied to projected gratings the idea permits the study of plates subjected to much larger deflections than the ones that can be studied with holograms.

46. A. J. Durelli, K. Brown and P. Yee, "Optimization of Geometric Discontinuities in Stress Fields"--March 1978.
The concept of "coefficient of efficiency" is introduced to evaluate the degree of optimization. An ideal design of the inside boundary of a tube subjected to diametral compression is developed which decreases its maximum stress by 25%, at the time it also decreases its weight by 10%. The efficiency coefficient is increased from 0.59 to 0.95. Tests with a brittle material show an increase in strength of 20%. An ideal design of the boundary of the hole in a plate subjected to axial load reduces the maximum stresses by 26% and increases the coefficient of efficiency from 0.54 to 0.90.

47. J. D. Hovanesian, Y. Y. Hung and A. J. Durelli, "New Optical Method to Determine Vibration-Induced Strains With Variable Sensitivity After Recording"--May 1978.
A steady-state vibrating object is illuminated with coherent light and its image is slightly misfocused in the film plane of a camera. The resulting processed film is called a "time-integrated specklegram." When the specklegram is Fourier filtered, it exhibits fringes depicting derivatives of the vibrational amplitude. The direction of the spatial derivative, as well as the fringe sensitivity may be easily and continuously varied during the Fourier filtering process. This new method is also much less demanding than holographic interferometry with respect to vibration isolation, optical set-up time, illuminating source coherence, required film resolution. etc.

48. Y. Y. Hung and A. J. Durelli, "Simultaneous Determination of Three Strain Components in Speckle Interferometry Using a Multiple Image Shearing Camera,"--September 1978
This paper describes a multiple image-shearing camera. Incorporating coherent light illumination, the camera serves as a multiple shearing speckle interferometer which measures the derivatives of surface displacements with respect to three directions simultaneously. The application of the camera to the study of flexural strains in bent plates is shown, and the determination of the complete state of two-dimensional strains is also considered. The multiple image-shearing camera uses an interference phenomena, but is less demanding than holographic interferometry with respect to vibration isolation and the coherence of the light source. It is superior to other speckle techniques in that the obtained fringes are of much better quality.

49. A. J. Durelli and K. Rajaiah, "Quasi-square Hole With Optimum Shape in an Infinite Plate Subjected to In-plane Loading"--January 1979. This paper deals with the optimization of the shape of the corners and sides of a square hole, located in a large plate and subjected to in-plane loads. Appreciable disagreement has been found between the results obtained previously by other investigators. Using an optimization technique, the authors have developed a quasi-square shape which introduces a stress concentration of only 2.54 in a uniaxial field, the comparable value for the circular hole being 3. The efficiency factor of the proposed optimum shape is 0.90. whereas the one of the best shape developed previously was 0.71. The shape also is developed that minimizes the stress concentration in the case of biaxial loading when the ratio of biaxiality is 1:-1.

50. A. J. Durelli and K. Rajaiah, "Optimum Hole Shapes in Finite Plates Under Uniaxial Load,"--February 1979.
This paper presents optimized hole shapes in plates of finite width subjected to uniaxial load for a large range of hole to plate widths (D/W) ratios. The stress concentration factor for the optimized holes decreased by as much as 44% when compared to circular holes. Simultaneously, the area covered by the optimized hole increased by as much as 26% compared to the circular hole. Coefficients of efficiency between 0.91 and 0.96 are achieved. The geometries of the optimized holes for the D/W ratios considered are presented in a form suitable for use by designers. It is also suggested that the developed geometries may be applicable to cases of rectangular holes and to the tip of a crack. This information may be of interest in fracture mechanics.

51. A. J. Durelli and K. Rajaiah, "Determination of Strains in Photoelastic Coatings,"--May 1979
Photoelastic coatings can be cemented directly to actual structural components and tested under field conditions. This important advantage has made them relatively popular in industry. The information obtained, however, may be misinterpreted and lead to serious errors. A correct interpretation requires the separation of the principal strains and so far, this operation has been found very difficult. Following a previous paper by one of the authors, it is proposed to drill small holes in the coating and record the birefringence at points removed from the edge of the holes. The theoretical background of the method is reviewed; the technique necessary to use it is explained and two applications are described. The precision of the method is evaluated and found satisfactory in contradiction to information previously published in the literature.

52. A. J. Durelli and K. Rajaiah, "Optimized Inner Boundary Shapes in Circular Rings Under Diametral Compression,"--June 1979.
Using a method developed by the authors, the configuration of the inside boundary of circular rings, subjected to diametral compression, has been optimized, keeping cleared the space enclosed by the original circular inside boundary. The range of diameters studied was $0.33 \leq ID/OD \leq 0.7$. In comparison with circular rings of the same ID/OD, the stress concentrations have been reduced by about 30%, the weight has been reduced by about 10% and coefficients of efficiency of about 0.96 have been attained. The maximum values of compressive and tensile stresses on the edge of the hole, are approximately equal, there are practically no gradients of stress along the edge of the hole, and sharp corners exhibit zero stress. The geometries for each ID/OD design are given in detail.

53. A. J. Durelli and K. Rajaiah, "Lighter and Stronger,"--February 1980.
A new method has been developed that permits the direction design of shapes of two-dimensional structures and structural components, loaded in their plane, within specified design constrains and exhibiting optimum distribution of stresses. The method uses photoelasticity and requires a large field diffused light polariscope. Several problems of optimization related to the presence of holes in finite and infinite plates, subjected to uniaxial and biaxial loadings, are solved parametrically.
Some unexpected results have been found: 1) the optimum shape of a large hole in a bar of finite width, subjected to uniaxial load, is "quasi" square, but the transverse boundary has the configuration of a "hat"; 2) for the small hole in the large plate, a "barrel" shape has a lower s.c.f. than the circular hole and appreciably higher coefficient of efficiency; 3) the optimum shape of a tube, subjected to diametral compression, has small "hinges" and is much lighter and stronger than the circular tube. Applications are also shown to the design of dove-tails and slots in turbine blades and rotors, and to the design of star-shaped solid propellant grains for rockets.

54. C. Brémond and A. J. Durelli, "Experimental Analysis of Displacements and Shears at the Surface of Contact Between two Loaded Bodies,"--July 1980.
The displacements which exist at the contact between two loaded bodies depend on the geometry of the surface of contact, the type of the loading and the property of the materials. A method has been developed to determine these displacements experimentally. A grid has been photographically printed on an interior plane of a transparent model of low modulus of elasticity. The displacements were recorded photographically and the analysis was conducted on the photographs of the deformed grids. Shears were determined from the change in angles. The precision of the measurements at the interface is estimated to be plus or minus 0.05mm. Examples of application are given for the cases of loads applied normally and tangentially to a rigid cylindrical punch resting on a semi-infinite solft plate. Important observations can be made on the zones of friction and of slip. The proposed method is three-dimensional and the distributions can be obtained at several interior planes by changing the position of the plane of the grid. The limitations of the method are pointed out. The possibility of using gratings (12 to 40 lpmm) is considered as well as the advantages of using moiré to analyze the displacements.

55. M. Erickson and A. J. Durelli, "Stress Distribution Around a Circular Hole in Square Plates, Loaded Uniformly in the Plane, on two Opposite Sides of the Square"--The complete stress distribution around a circular hole, located in the center of a square plate, has been determined photoelastically for the case of the plate loaded uniformly on two opposite sides. The study was conducted parametrically for a large range of the ratio of the side of the square to the diameter of the hole. The results obtained permit the determination of the stresses for any biaxial condition and verify a previous solution obtained for the case of the pressurized hole. The experimental procedure is briefly described.

56. A. J. Durelli, M. Erickson and K. Rajaiah, " "This paper presents the shapes that will optimize the stress distribution about central holes in square plates subjected to uniform load on two opposite sides of the plate. The study is conducted for a large range of hole to plate widths ratios (D/W) The stress concentration factor for the optimized holes decreased by as much as 21% when compared to the one associated with a circular hole. Simultaneously, the weight of the plate with optimized hole is reduced by as much as 36% as compared to the circular hole. Coefficient of efficiecy of around 0.92 is achieved for all D/W ratios. The geometry of the optimized holes are presented in a form suitable for use by designers.

57. K. Rajaiah and A.J. Durelli, "Optimization of Hole Shapes in Circular Cylindrical Shells under Axial Tension" -- Hole shapes are optimized in circular cylindrical shells subjected to axial load considering only the predominantly large membrane stresses present around the holes. Two-dimensional photoelastic isochromatics obtained with a special-purpose polariscope are utilized for the optimization process. The process leads to a significant decrease in the membrane stress-concentration factor and a modest decrease in weight, thus yielding a considerable increase in strength-to-weight ratio. This paper presents results for certain typical ratios of hole diameter to shell diameter. Previous theoretical and experimental studies for the circular hole have also been verified.

58. A.J. Durelli and K. Rajaiah "Quasi-Square Hole with Optimum Shape in an Infinite Plate Subjected to In-Plane Loading" - This paper deals with the optimization of the shape of the corners and sides of a square hole, located in a large plate and subjected to in-plane loads, with the object of minimizing stress concentrations. Appreciable disagreement has been found between the results obtained previously by other investigators. In this paper new tests have been conducted and discrepancies have been corrected. Using an optimization technique, the authros have developed a quasi square shape which introduces a stress concentration of only 2.54 in a uniaxial field, the comparable value for the circular hole being 3. The efficiency factor of the proposed optimum shape is 0.90 whereas the efficiency factor of the best shape developed previously was 0.71. The shape also is developed that minimizes the stress concentration in the case of biaxial loading when the ratio of biaxiality is 1:-1.

59. A.J. Durelli and K. Rajaiah, "Optimization of Inner and Outer Boundaries of Beams and Plates with Holes" - This paper presents optimized shapes of inner and outer boundaries for three specific problems: A long rectangular plate with a central hole subjected to uniaxial tension, a simply-supported slotted beam subjected to a load uniformly distributed over a small area at the centre, and a square plate with a central hole under uniaxial uniform pressure. The two-dimensional photoelastic method is used for optimization. The results indicate a significant reduction in stress concentration factor or in weight, or in both. The examples presented also include cases where the inner and outer boundary stresses are mutually dependent.

STRESS CONCENTRATIONS

Report No. 60

The scope of this work on "Stress Concentrations" includes critical studies of the presently available handbooks, geometrically non-linear problems, mixed boundary value problems, three-dimensional problems, dynamic stress concentrations and also deals with the advantages and limitations of the methods commonly used to determine stress concentration factors.

The work was conducted with the financial support of the Office of Naval Research. The author of the chapter dealing with dynamic stress concentration was Prof. W. F. Riley of Iowa state University. It is unfortunate that these acknowledgements did not find place in the printed text. The author is particularly grateful to Dr. N. Basdekas of ONR for continuing a financial support that permitted the publication of the 60th report of a series that started about 20 years ago. P. Baxter was in charge of several phases of the work reproduction.

Stress concentrations

A. J. Durelli

1.1 Introduction 1
1.2 Advantages and disadvantages of stress analysis methods used to determine stress concentrations 16
1.3 Compilation of results 24
1.4 Geometrically non-linear stress concentrations 43
1.5 Stress concentrations in mixed boundary value problems 67
1.6 Stress concentrations in some specific problems 94
1.7 Stress concentrations in three-dimensional problems 105
1.8 Dynamic stress concentrations 134
1.9 Unconventional approaches to the study of stress concentrations 146
References 155

1 Stress concentrations

1.1 Introduction

Stress is defined as a limiting process. It takes place at a mathematical point. It is a tensor. One of the components of the stress may have the same value at two neighboring points. In that case these points belong to the same contour or locus (for instance, all points on the same isochromatic line have the same value of maximum shear stress, all points on the same isobar have the same value of normal stress). In general, stress components change from point-to-point.

A uniform state of stress is usually illustrated by a straight column subjected to uniaxial load provided this load is applied also in a uniform manner at the ends of the column. A case like this is seldom if ever found in practice. In general, the state of stress changes from point-to-point and if any of the components of stress (or the resultants) are represented by a family of loci, peaks and valleys of the values appear. The stress is therefore distributed in a non-uniform manner and the not always precisely defined concept of stress concentration is associated with peaks, and gradients around the peaks, of the stress components.

The previous comments apply to an ideally continuous matter. They apply with even more reason if the material is made of discrete particles: inclusions, grains, crystals, atoms, etc. In general, the state of stress will not be uniform at the interface between discrete particles.

These considerations apply equally well to strain, strain components and strain concentrations. If the concept of stress concentration is more popular than the concept of strain concentration it is due to the fact that laws of failure are more commonly related to stress, and that historically, engineers found the computation of loads, and the stresses derived from loads easier to handle than the measurement of displacements, and the determination of their derivatives, which are necessary to obtain strains.

Stress Concentration Factors. The stress concentration factor is a means to evaluate quantitatively the stress concentration. Another means which is less commonly used but also has importance in fracture is the gradient of the stress.

The stress concentration factor can be defined as the ratio between the peak (or maximum) stress in the body and some other stress (or stress-like quantity) taken as reference. The reference stress is arbitrary. When the stress concentration is associated with the disturbance produced in the stress field by the presence of an inside boundary, the reference stress can be computed using elementary equations applied to either the gross or the net area of a cross-section through the point at which the peak stress takes place. When the stress concentration is associated with a change in the outside geometry of the body, the reference stress can be computed using elementary equations applied to a cross-section through the point at which the peak stress takes place, or alternatively the equations can be applied to a cross-section at some remote region of the body. In most cases it is convenient to give stress concentration factors taking as reference the stress computed over net areas rather than gross areas. Besides being intuitively preferable, this method avoids that the factors approach infinity when the net area is small Figure 1.1.

In some mixed boundary-value problems of the restrained shrinkage type (see Section 1.5) it is convenient to define the stress concentration factor as the ratio between the maximum normal, or shear, stress and the product of the free shrinkage of the body multiplied by the modulus of elasticity of the body.

In dynamic problems it is usually convenient to define the stress concentration factor as the ratio of a component of the stress at a point at which its value is maximum, to the same component at the same point of the body built without the geometric discontinuity. The body without the discontinuity may be subjected to the same dynamic load as the body with it, or to a static system of forces equivalent to the dynamic load. The stress concentration is then a function of time and may occur at different points, for different times.

Stress concentration factors are defined by Roark and Young [1] as the ratio of the true maximum stress to the stress calculated by the ordinary formulae of mechanics (flexure formula, torsion formula, etc.). Peterson [2] defines the factor in a similar way as the ratio of the maximum value of the stress to the nominal value obtained using linear distribution over the cross-section, and so does Griffel [3]. All these

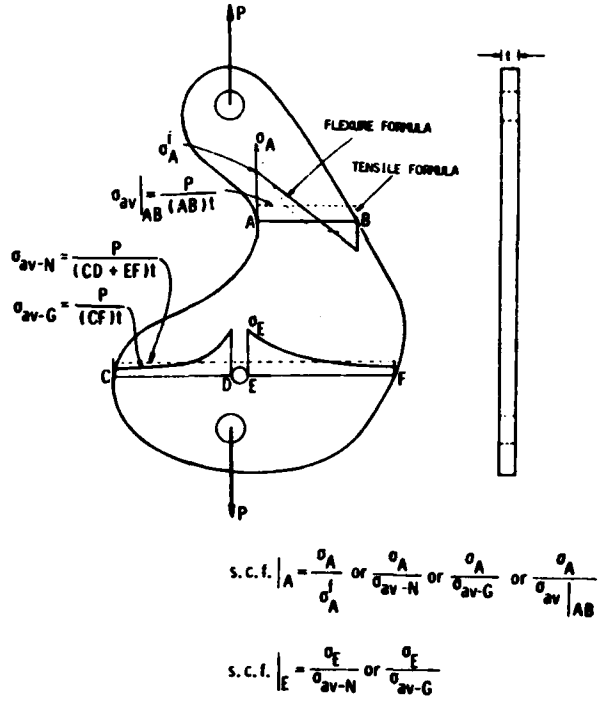

$$\text{s.c.f.}\Big|_A = \frac{\sigma_A}{\sigma_A^f} \text{ or } \frac{\sigma_A}{\sigma_{av\text{-}N}} \text{ or } \frac{\sigma_A}{\sigma_{av\text{-}G}} \text{ or } \frac{\sigma_A}{\sigma_{av}\Big|_{AB}}$$

$$\text{s.c.f.}\Big|_E = \frac{\sigma_E}{\sigma_{av\text{-}N}} \text{ or } \frac{\sigma_E}{\sigma_{av\text{-}G}}$$

Figure 1.1. Definitions of stress concentration factors.

definitions are convenient in many cases but not applicable in others, as those instances in which stresses associated with pressure (either on the surface of a shell or plate, or on the inside surface of hole) are given as related to the amount of that pressure. Peterson [2] in Figure 126 uses this convention which is inconsistent with his definition. It seems more reasonable to state that the factor takes as reference any quantity with the dimensions of a stress, as long as that reference is defined.

The lack of consistency in the use of the particular cross-section over which the stress is averaged for reference, may also introduce confusion. Tetelman and McEvily [4] define the elastic stress concentration factor as the ratio of the local stress near the discontinuity to the nominal stress acting across the gross cross-section, (p. 16). Few lines later the statement is made however that the maximum stress concentration factor decreases from 3 (for the case of the circular hole) as the ratio of the hole size to plate size increases. Actually, when the gross

area is taken as reference, the stress concentration factor increases toward infinity. It decreases when the net area is taken as reference [6] (p. 2.7).

Stress concentration factors are not always defined as the ratio of a peak stress to another stress taken as reference. Sometimes they are defined as the ratio of any stress in the perturbated region to a reference stress. See for instance Tetelman and McEvily [4] Equation (1.13) and Savin [5], figures IV-5 and IV-7. It seems less confusing to call 'stress ratio' the value of any stress referred to a convenient reference or nominal stress, and call "stress concentration factor" the ratio of the maximum stress referred to that reference stress. Both stress ratios and stress concentration factors are pure numbers.

Physical significance of stress concentrations. The theory of elasticity is based on the assumption of continuity of matter, indefinitely divisible, each particle retaining its original properties during the division.

The physical world, however, is more complicated than that idealized model. Materials are made of structural elements which may be crystals or molecules, both of which are combinations of atoms. At the dimensional level of these structural elements, matter is not uniform or homogeneous. Its properties change from point to point. They may also change with direction at a point. If a circular hole in an infinite homogeneous, isotropic plate, subjected to uniaxial load, develops a complicated stress field (Kirsch problem), it is easy to understand the difficulties which would be encountered in the rigorous solution of the stress distribution present in a material made of such a mosaic of elements. The following considerations may help in the understanding of the scope of the application of the theory of elasticity and of the stress concentrations factors obtained using its basic assumptions. They are obviously important in the study of problems related to fracture mechanics since in fracture mechanics the study of crack propagation and of stress distributions around cracks, are basic, and the order of the dimension of the crack tips may be the same as the order of the structural elements of matter.

Heterogeneity and discontinuity Figures 1.2 to 1.8 show a series of photographs of materials in which the range of dimensions of the structural elements varies from about one inch to about 10^{-7} inches. At one extreme of the range, the structural elements are visible to the bare eye, (in the case of some civil engineering structures like concrete

Figure 1.2. Actual grains fragmented from a titanium alloy ingot. XI 1/2 (W. Rostoker).

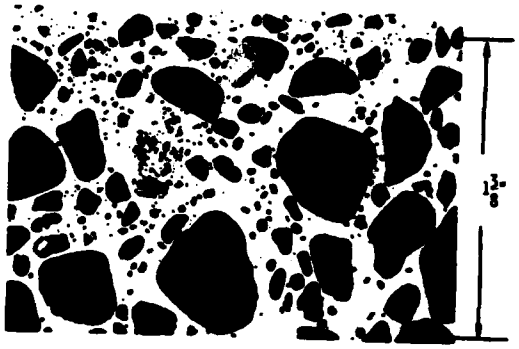

Figure 1.3. Structure of a concrete made of portland cement, water, sand and stones (Bureau of Reclamation).

dams, the structural elements may have dimensions of the order of feet), at the other end of the range, powerful microscopes are necessary to see the structural elements.

An ideal parallelepiped is introduced in the theory of elasticity to obtain the basic equations. It is assumed to be sufficiently small for the forces acting on its faces to be essentially uniform and represented in the first approximation by single average loads acting in the center of their areas of application. It is obvious, however, that this wording is relative and that the parallelepiped will be small or large by comparison.

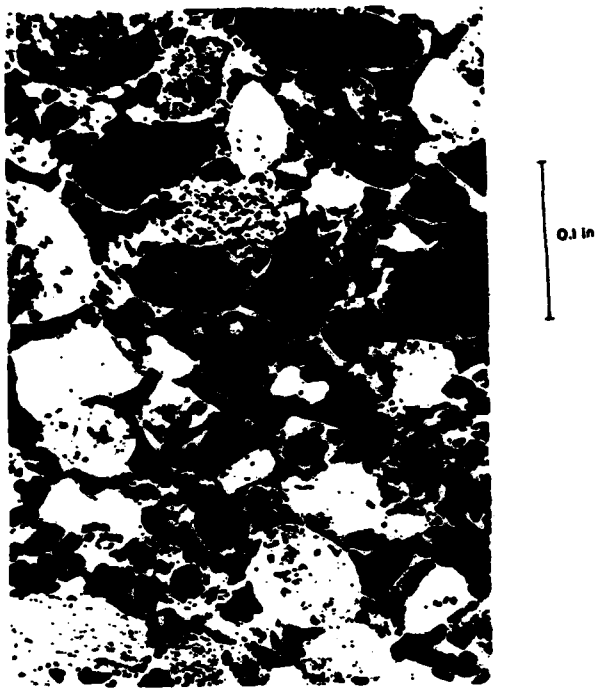

Figure 1.4. Structure of a mortar made of cement, water and sand. Many voids are present. (Portland Cement Association).

The grain size of 1020 steel is of the order of 10^{-4} inches, the grain size of 1045 steel is of the order of 10^{-5} inches.

In Figure 1.9 the cross-section of the structural elements of the solid propellant shown in Fig. 1.5 has been outlined. It will be assumed that the elements have, perpendicularly to the paper, dimensions of the same order as the ones shown in the paper. Uniform forces have been applied to the sides (about 0.05 in.) of the parallelepiped. The normal stress σ_z along a vertical cross-section will likely have a complicated distribution as shown, which will depend on the relative rigidity of the elements and of the embedding matrix. Because of equilibrium, however, the average has to be equal to the value of the stress applied to the side of the parallelepiped. A smaller parallelepiped (sides about 0.001 in.) as the one located in position 1 will be sufficiently small for the forces acting on its

Figure 1.5. Structure of a rocket solid propellant. X73 (K. Bills).

faces to be represented by a single average acting in the center. If the smaller parallelepiped is at position 2, it will still be too large for this approximation to be sufficiently accurate. A parallelepiped one tenth that size may be necessary.

Consider now the tungsten grains of Figure 1.7, which have been outlined in Figure 1.10. If a small parallelepiped of this material (sides about 0.015 in.) is taken from a loaded body, the distribution of the stresses on the sides of the parallelepiped may look as shown in Figure 1.10. The distribution is complicated and will depend on the relative rigidities of the structural elements and of the embedding matrix; but it should be noticed that these stresses are statically equivalent to the applied uniform stresses. The theory of elasticity developments would apply to this parallelepiped if the analysis is limited to the average stress over the face of the parallelepiped, the scatter about the average is neglected, and any other discontinuity present is of much larger size than the size of the elements. In the figure, only σ_y has been represen-

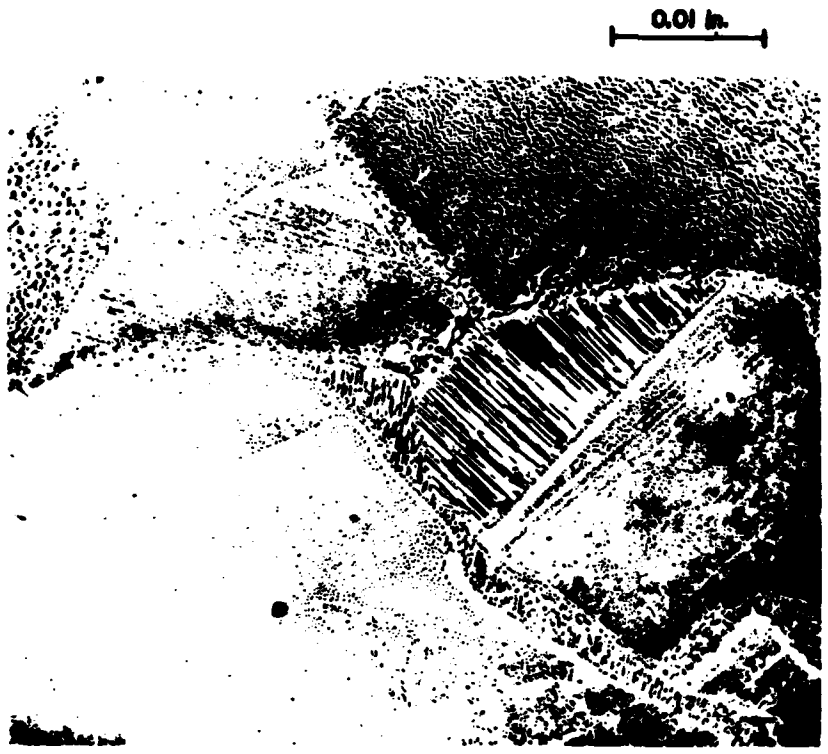

Figure 1.6. Structure of chromium–chromium carbide eutectic. X100 (W. Rostoker).

ted, for clarity; but the same reasoning applies to σ_x and τ_{xy}, and to the other three stress components.

So far the illustrations have been schematic. There are methods, however, which in some cases can illustrate the previous considerations, experimentally and with relatively good accuracy. Figure 1.11 shows the isochromatic pattern obtained from a photoelastic coating applied to a concrete block 3 in. × 3 in. × 3 in. This concrete is a mixture of sand, cement, water and gravel. The coating is a thin film of epoxy that follows faithfully at the interface the deformations of the surface of the block of concrete. The block was subjected to a uniform pressure on its vertical faces. If the assumptions of the theory were satisfied, the total surface would be uniformly light or uniformly dark. The fringes shown in the figure are loci of points of equal maximum shear strain

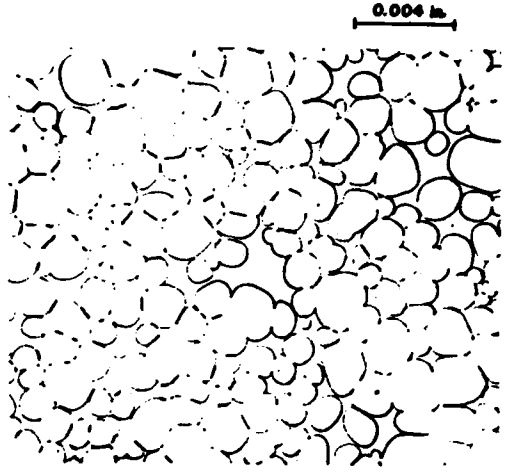

Figure 1.7. Duplex structure of tungsten grains in a nickel–iron envelope matrix. X250 (W. Rostoker).

neglecting the influence on the birefringence, of gradients of stresses in the direction of the light. The points indicated by letters correspond to the maxima of shear strain. The distribution is obviously extremely complicated.

The illustrations can also be obtained from transparent models photoelastically analyzed. Figure 1.12 shows the maximum shear stress distribution in a matrix shrunk around circular inserts much more rigid than the matrix. The loading condition is equivalent to a uniform biaxial-loading of biaxiality equal to unity. Figure 1.13 shows the distribution for the case of inclusions of different sizes, rigidities and shapes. Since the linear theory of the continuum applies to bodies irrespective of actual size, it can be visualized that the size of the inserts is of the order of a fraction of a thousandth of an inch. It can also be imagined that the inserts are not necessarily circular, nor regularly spaced, and that they may exhibit different rigidities. This would illustrate the stress distribution present, at that scale, in a material like the one shown Figures 1.5 and 1.7.

A circular hole in a heterogeneous medium. Suppose that a small hole (diameter about 0.001 in.) is drilled in a material like the chromium-chromium carbide represented in Figure 1.6 and suppose a unidimen-

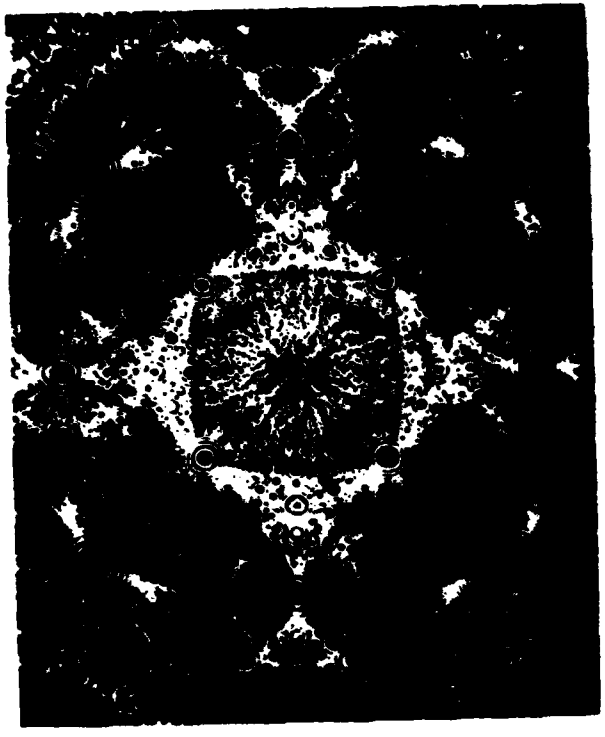

Figure 1.8. Platinum crystal hemisphere—Radius about 1900 Å. (Magnification: 530,000 times.) Each dot is a platinum atom. The circles are crystal facets. Erwin S. Mueller (No. 14254).

sional load is applied as indicated in Figure 1.14 If the hole is at position 1, the stress distribution will likely not be too for from the one predicted by Kirsch, unless anisotropy is very pronounced. Suppose, however, that the hole is slightly larger and located at position 2. It would be practically impossible to predict the stress distribution using theoretical means.

Suppose finally that the hole diameter is appreciably larger than the structural element size (about 10 times). This case is illustrated in Figure 1.15. With some scatter, the theoretical curve may represent approximately the actual stress distribution.

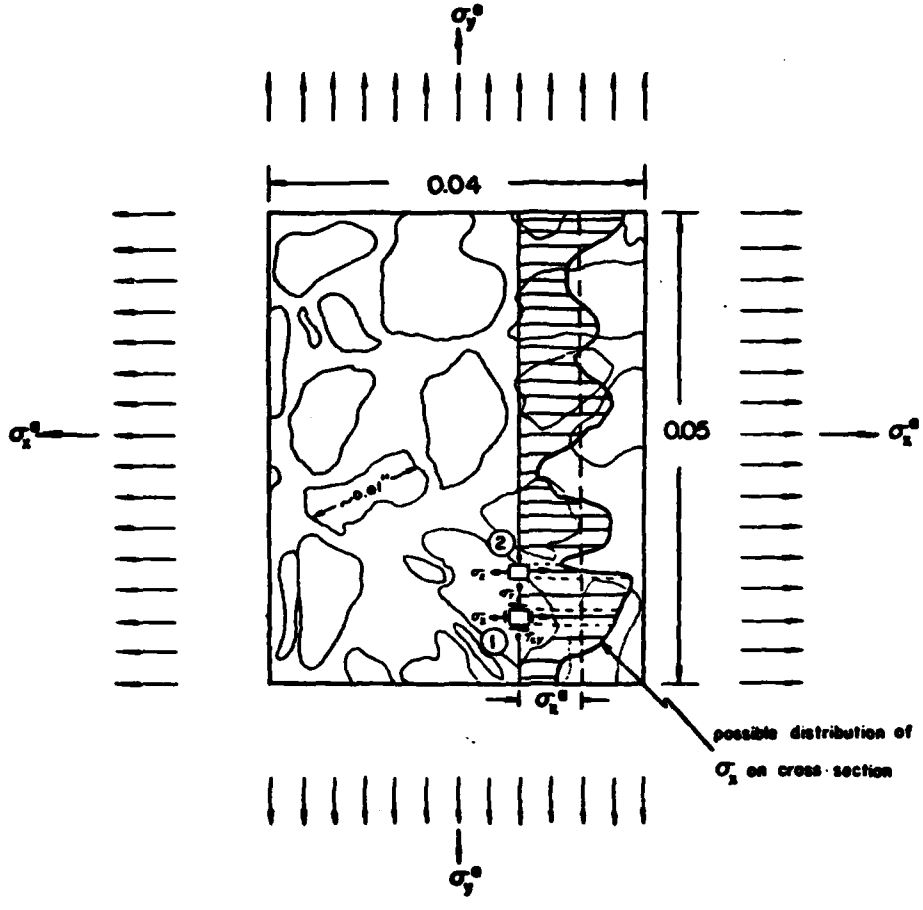

Figure 1.9. Portion of solid propellant (Figure 1.5), of 0.04 in. × 0.05 in., subjected to uniform loads on its sides. An ideal parallelepiped of 0.001 in. at position 1 will have forces about uniformly distributed on its sides. The same size parallelepiped at position 2 will not.

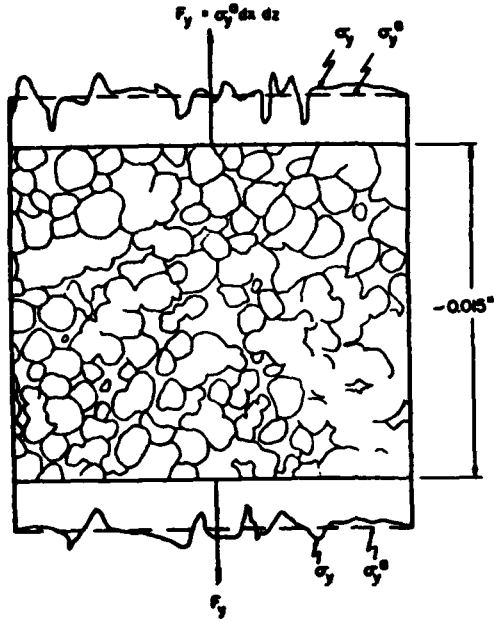

Figure 1.10. Structural elements of the tungsten shown in Figure 1.7. A parallelepiped of about 0.015 in. side, taken from the body, may have on its sides stresses distributed as shown. The theory of elasticity developments may still hold if applied to the average stress.

Concentrated loads. Frequently, in theoretical developments, loads are assumed to be concentrated on a point. An example is Boussinesq's problem of the concentrated load acting normal to the edge of a thin plate of large expanse. The elasticity solution gives an infinite stress at the point of contact.

Physically there is no such thing as an infinite stress, just like there is no such thing as a stress without a deformation, since no material is infinitely rigid. Any load transmitting member must have finite cross-section. And any material to which a narrow loading member is applied will show a deformed area under the load. Even for ideally homogeneous and isotropic materials no infinite stress would appear at the point of application of the concentrated load.

Sometimes a theoretical solution shows an infinite stress because the body exhibits a sudden change in geometry, as a reentrant corner. This is also physically impossible. First, no corner has a zero radius. Any corner observed under a sufficiently large magnification exhibits a finite

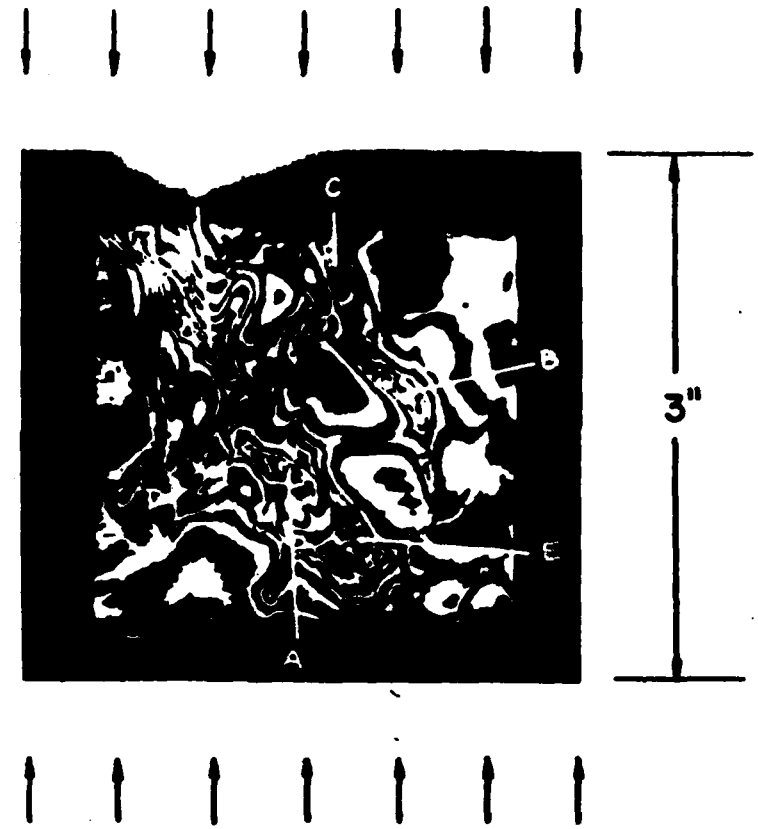

Figure 1.11. Isochromatics in a photoelastic coating cemented to the surface of a concrete block, subjected to uniform pressure on its top and bottom surfaces. Identified points exhibit zero shear. (G. U. Oppel).

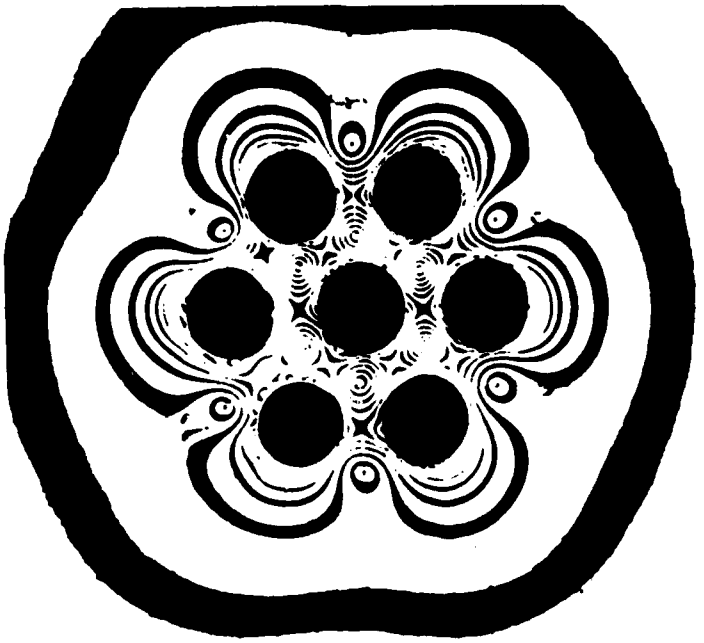

Figure 1.12. Isochromatic fringe pattern in Hysol 8705 with seven circular inclusions.

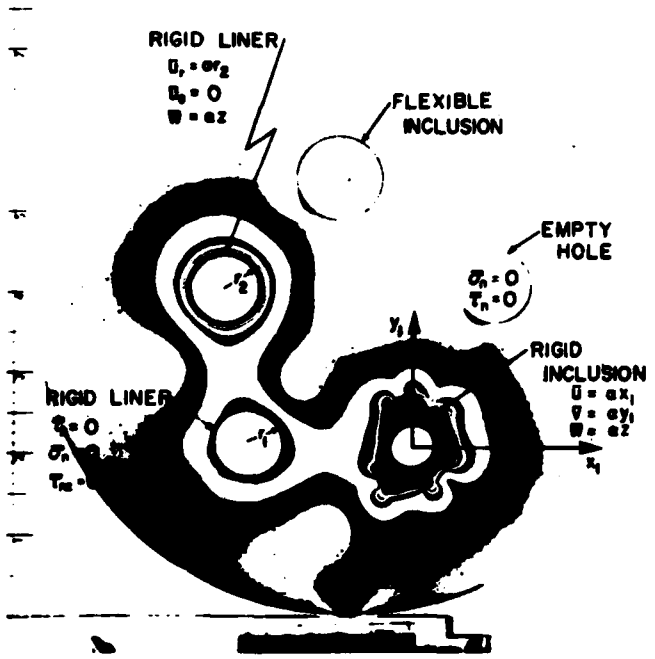

Figure 1.13. Isochromatics associated with restrained shrinkage around several inclusions of different kinds allowing free motion between inclusions.

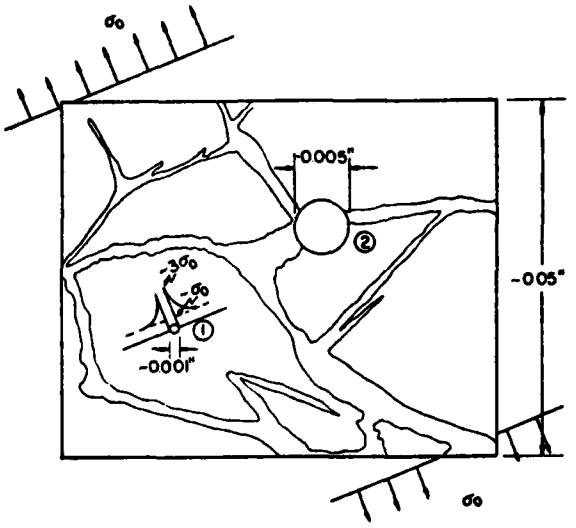

Figure 1.14. Small holes in a material like the chromium–chromium carbide eutectic (Figure 1.6). Stress distribution in hole at position 1 can be determined approximately. There is no available solution for stresses around hole at position 2.

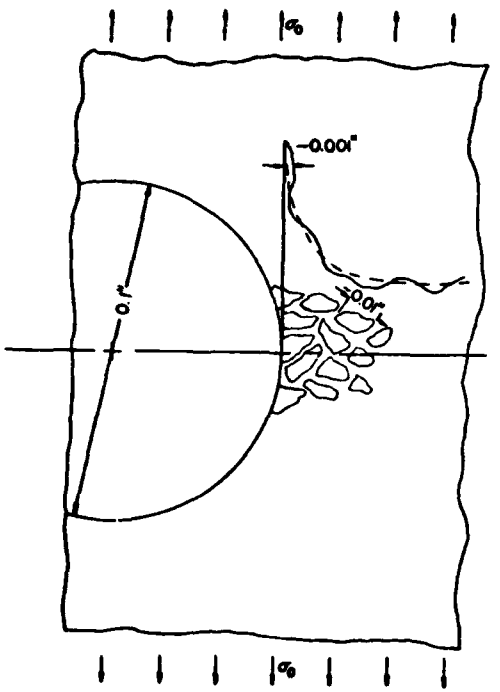

Figure 1.15. Possible stress distribution in the neighborhood of a relatively large hole in a plate of a material with relatively small structural elements.

radius. Second, the high stress associated with the sharp corner either produces a yielding in the material redistributing the stresses or distributes itself over some larger area of a finite size element. A third associated phenomenon is that even in theoretically isotropic, homogeneous and continuous materials, as soon as a stress acts on the boundary strains appear which deform the boundary and alter its radius of curvature.

1.2 Advantages and disadvantages of stress analysis methods used to determine stress concentrations

Many stress analysis methods are available to determine the stress distribution in loaded bodies of complicated shapes. Some of these methods use mathematical approaches based usually on the assumptions

of the theory of elasticity. Among these some are numerical methods replacing differential equations with difference equations or replacing the continuum by a system of finite elements.

Other methods are experimental and consist in measuring physical properties, or changes in physical properties, which can be related to stresses, strains, or displacements. Among these methods the most commonly used are two- and three-dimensional, static and dynamic photoelasticity, brittle coatings, photoelastic coatings, electrical strain gages using ohmic resistance or capacitance or inductance properties, mechanical and optical strain gages, grids, moiré, holography, speckle, etc.

The advantages and disadvantages of these methods to study stress and strain distributions in different kinds of bodies subjected to different kinds of loading conditions have been considered in previous publications [7, 8]. Here the emphasis will be put on the particular subject of the determination of stress and strain concentration factors using the above mentioned methods.

The fact that stress concentrations occur as peak values in a field and that the gradients around these peaks are usually steep, present particular problems in the evaluation of the strains and stresses and make certain methods more adaptable than others for the study of the concentrations.

Some mathematical approaches. Four theoretical approaches are frequently considered: (1) collocation (also called 'boundary collocation' or point 'matching'), (2) conformal mapping, (3) finite differences, and (4) finite elements.

The first two methods are, in general, combinations of analytical and numerical procedures, while the last two are essentially numerical.

When the collocation method is used it is simple to satisfy the boundary conditions. Once a series solution is established for the governing differential equation, the method requires that the boundary conditions be satisfied only at discrete points along the boundary [9]. The accuracy and the convergence of the solution obtained using this method are in general very much influenced by the choice of the collocation points.

In problems of stress concentration such as plates with holes or notches, the method is capable of yielding highly accurate results if the chosen function also satisfies exactly the boundary conditions around the discontinuity, as is the case in problems with circular or elliptical holes or semicircular notches. But in situations where this is not pos-

sible, the method would determine only approximate values of stress concentration factors, depending on the number and location of collocation points. The rate of convergence of the method can be improved when a least square criterion is added to the technique [10].

For problems governed by Airy's biharmonic equation, Mushkelishvili [11] has developed the conformal mapping method to obtain the exact solution if the mapping function is known (usually in polynomial form). In some cases the function can be approximated in a fairly simple fashion, but in general one must make use of an extensive numerical procedure to obtain it. In the case of a simply connected domain, finding the mapping function reduces to the solution of an integral equation [12–14] and for doubly-connected domains (the case of some rocket motor cross sections) a system of coupled integral equations must be solved [15].

The mapping function must be very accurate in the neighborhood of points where stress concentrations occur. When this method is used it is frequently difficult to reproduce the geometry of sharp corners. This is one of the significant limitations of the method.

Finite-difference methods reduce continuous systems to equivalent lumped-parameter systems. Instead of obtaining a continuous solution of the differential equation, the differential equation is replaced by a finite-difference equation and the approximate values of the solution are found at isolated points. The procedure leads to a system of n simultaneous linear algebraic equations when n discrete points are selected. A common way of solving this system of simultaneous equations is to use iteration or relaxation methods. When large stress gradients are present in the field, numerical instability and errors may take place. These methods have become more practical since the advent of digital computers.

The method that has taken the greatest advantage of the new development of digital computers is the finite-element method. When this method is used the continuous structure is replaced by a large number of small elements and equilibrium and compatability are applied to the whole of each of them. The method has found applications in many fields of mechanics and can be used when bodies have complicated boundaries and inhomogeneous anisotropic nonelastic properties. Smaller-size elements can be used where gradients are high and storage capacity can be made very large, but there is a practical limit to the number of elements in the matrix to be used. Some investigators [16] propose hybrid techniques in which the local concentration is separated from the regular field, permitting an appreciable reduction in the number

of elements. This technique has been introduced in some standard programs [17].

Depending on the type of problem to be solved, finite-difference methods may be more or less efficient than finite-element methods. Considerations on the subject have been made by Bushnell [18] who calls attention to some of the advantages of finite-difference energy methods. Key and Krieg [19] also compare both approaches and point out situations in which the finite-difference method may give better results. The introduction of arbitrary meshes in the finite-difference methods by Perrone [20] makes the method in many cases more competitive with finite-elements methods. General considerations on finite-element methods from a historical perspective and also in comparison with finite-difference methods have been presented by Zienkiewicz [21] and by Oden [22].

Photoelasticity. Measurements can be taken of changes in indices of refraction, most frequently changes in the difference between indices of refraction (relative retardation), and relate them to some components of the stress or strain tensor. Usually photoelastic determinations yield directly the maximum shear in the plane of observation. The method can be very sensitive and very precise and is self-sufficient for the determination of the magnitude and directions of maximum shear stresses, but requires supplementary information to determine the individual principal stresses. For the common cases of elasto-static small deformations at room temperature the calibration is easy. However, if the calibration has to be conducted for elevated temperatures, if the loads are applied rapidly or the deformations are large, or irreversible, then the calibration can be very complicated.

Photoelastic coatings can be applied to prototype surfaces of complicated shape. In general, they lack sufficient sensitivity, their maximum response being about one fringe when applied to structural steel subjected to elastic strains. Determination of individual principal stresses is complicated and lacks precision.

It is frequently forgotten that a low shear in the plane of observation may be associated at the same point with a large shear in a plane perpendicular to the plane of observation. In plane stress problems the isochromatic observation is frequently limited to free boundaries and the analysis for a stress concentration factor is then complete. However when the photoelastic coating is applied to a structural member of complicated shape stress concentrations may exist that are not detected.

Photoelasticity is very well-suited to the determination of stress

concentration factors in two- and three-dimensional problems (the points of interest are usually subjected to one-dimensional or two-dimensional states of stress). Photoelastic coatings, because of thickness effects, may give appreciable errors.

Grids. Grid methods are not commonly used. They lack sensitivity for the determination of small strains, but they are very well suited for the determination of large strains in rubber-like materials, in plastics, or in metals undergoing plastic deformation. Grids can be applied to the surface of practically any prototype, but like moiré, are more often used on models.

Grids have the advantage of giving a direct geometric representation of the body. A limitation is the level of error associated with the measurement of the geometric transformation. The precision of the determinations will depend on the sharpness of the marks, the recording method (photograph, etc.) and the precision of the measuring instrument. (Indices of precision are usually associated with the standard deviation of the repeated measurements). The location of each point of the grid is determined by means of two readings on the instrument scale, the one corresponding to the zero point (or origin) and the one corresponding to the point of interest. Displacement components are obtained from the difference in position of points before and after deformation and so will have a somewhat lower degree of precision than the one of the values of the coordinates of the points.

Strains or strain-like quantities are obtained by further treatment of the measurements in the form $l_f - l_i/l_i$, $\Delta l/l$, $\Delta u/\Delta x$, $\partial u/\partial x$, etc. operations which further reduce the degree of precision. For a given grid line sharpness and measuring system, the error in the strain depends on the magnitude of Δl. This change in length of a segment can be increased by increasing the strain or increasing the base length. The base length l, however, has to be relatively short since the determined strain is assumed to be uniform over its length. A typical base length is $l = 0.4$ in. and a typical standard deviation is about 0.001 in. Thus

$$\varepsilon = \frac{\Delta l + 0.001}{0.4 + 0.001} \tag{1.1}$$

For a given Δl it is seen that the strain will have a standard deviation of the order of 0.002. The overall curves presented will be more accurate due to the averaging effect of drawing a smooth curve through the points.

A disadvantage of grids is the laborious point-by-point analysis. An attempt to reduce the time required to evaluate grid patterns has been described in [23].

Grids can be drawn or printed representing any desired coordinate system (polar or elliptical for instance) which may be difficult using other methods. In certain cases this may be an important advantage.

The main limitation of grids methods for the determination of stress concentrations is the relatively large base length over which the strain is averaged [7]: The accuracy, however, can be appreciably improved if the displacement curve is drawn, as suggested by Fischer [24, 25], and a graphical differentiation of the curve is conducted, giving a better estimate of the maximum strain.

Moiré. Moiré directly yields components of displacement without the need for an intermediate physical property. To obtain strains the displacement data must be differentiated.

The strain tensor at every point is then completely determined. The use of moiré on prototypes for the solution of two-dimensional static-elastic problems, despite the techniques of fringe multiplication available today, is limited in general in its application by the 40 *lpmm maximum* density of the available gratings. Without multiplication the maximum response of moiré is about one fringe per inch when applied to a structural steel subjected to elastic strains.

Multiplication and differentiation techniques are becoming more practical. Up to now, in-plane moiré in general cannot be applied to curved surfaces except when they are developable, or the radius of curvature is large. Projected gratings and shadow-moiré are, however, very practical to determine deflections in plates and shells.

Moiré-of-moiré patterns are approximate in the sense that they represent the average of the partial derivative over the shifted interval [7]. When the shift takes place normally to a boundary, the boundary value of the partial derivative has to be estimated by extrapolation from the recorded pattern. Otherwise it should be obtained by graphical differentiation of the displacement field. More detailed discussion of these points can be found in [26].

The standard deviation of the moiré grating pitch is probably less than 0.00001 and so the standard deviation in strain for a shift of 0.03 will be the order of

$$\varepsilon = \frac{0.00001}{0.03} \simeq 0.0003 \tag{1.2}$$

The moiré grating is so dense that the fringes are the average of a large number of grating line intersections. This averaging effect increases the precision beyond the one indicated above.

The same comment made about the base length for stress concentration determinations using grids applies also to moiré, but less critically, because the length of measurement is much shorter.

Brittle coatings. Principal stress trajectories can be obtained easily and with good precision using brittle coatings. The determination of the value of the principal stresses is subjected to larger errors and requires more skill in the operator. Even for this purpose, the method is very practical when the temperature is about room temperature and does not change abruptly. It can be applied to the actual prototypes, or components, without requiring the manufacture of a model [7]. The upper limit on strains is about 0.01. The method is less practical when several loading conditions are applied to the same body since a new coating will be necessary for each loading condition. (Photoelastic coatings and strain gages are not subjected to this limitation.) The sensitivity of brittle coatings is of the order of 500×10^{-6}, but with refrigerating techniques, and some sacrifice of precision, it can be as low as 100×10^{-6}.

For the solution of dynamic problems the coating should be properly calibrated. The techniques of application to dynamic problems are appreciably more complicated than for static work, and one of the difficulties to be overcome is the 'closing-up' of cracks at stress levels lower than the ones at which cracks close under static load. In respect to photoelastic coatings, brittle coatings have the important advantage of being much thinner.

The main limitation of brittle coatings to determine stress concentrations is the step-wise method used to apply loads. The value of the stress producing the failure of the coating is associated with a load that falls within the interval between the last load that does not produce a crack, and the first load producing the crack. The estimate can be improved by drawing a curve representing stresses, through the point of maximum stress, but the location of this point may also be subjected to error [25].

Holography. Holography [27] yields whole-field displacement information but it is easier to obtain the out-of-plane displacements than the in-plane displacement. This constitutes a serious limitation. In addition, the need for high stability and darkness during recording (when using a

cw laser) also limit its applicability. A great advantage is the very high sensitivity of the method and that measurements can be made on diffusely reflecting prototypes requiring no special preparation. It has found so far few applications in the determination of stress concentration factors, but it has found a wide field of application as an inspection of materials methods since flaws in materials produce an appreciable disturbance in the hologram.

Speckle. Methods based on laser speckle are a fairly recent development. Techniques have been developed to measure out-of-plane deflection and slopes, and in-plane displacements and strains. As of this time the technique for in-plane strains is not as practical as the others [28].

In general speckle methods, like holography, have the advantages of being noncontacting and requiring no surface preparation, which makes easier the application to prototypes. Depending on which technique is being used, speckle can yield either point-by-point or whole-field information. Some techniques also have the advantage of being able to vary the sensitivity over a large range. In contrast to holography (with which its shares many features), there is no problem with fringe localization and thus, evaluation of specklegrams is a much less ambiguous and simpler process. The main drawback of the speckle techniques is the generally poor quality of the fringe patterns. In addition, similar to holography, the out-of-plane measurements are easier and more precise than in-plane measurements. As is the case of holography it has so far been seldom used for stress concentration determination.

Strain gages. Electrical resistance strain gages are very sensitive, easy to apply and frequently have very small base lengths. They can be used on models or on prototypes. One of their main advantages is their ability to respond correctly to high-frequency strains since their rise time is of the order of 0.1×10^{-6} second [29]. They have the following limitations: (1) the temperature should usually be lower than 400°F and relatively steady; (2) the time of observation should usually be less than a few days; (3) the strain should not be larger than about 0.02; and (4) changes in moisture may affect the output. Special gages do, however, exist which can accommodate up to 20 percent strain and, independently, 800°F. The output can be recorded several convenient ways [7].

Mechanical strain gages (of the Huggenberger type, or using dial gages) have longer base lengths, cannot be used for dynamic ap-

plications, and their output has to be recorded visually. However, they are not subjected to the time, temperature, and humidity limitations of electrical resistance strain gages. Capacitance strain gages are better suited for determinations at elevated temperatures and are more stable as function of time, but their base length is usually longer than the base length of resistance type gages.

All these gages give point-by-point and unidirectional information. When 'rosettes' are used two or three of them are combined. Gages are very practical when the location of the point of stress concentration is known. The information obtained is an average over the base length of the gage and should therefore be relatively small. This is particularly true when the determination of the stress concentration factor is desired.

Interferometry. Interferometric techniques can be applied to a large class of problems. In some cases they provide all the necessary data while in others they are used in conjunction with other techniques.

In general, interferometric techniques have the advantage of high sensitivity, being able to measure on the order of the wavelength of light. The main drawbacks are that generally they require high stability, are difficult to zero, and are affected by rigid body motions. In addition, they require high-quality model surfaces for both reflection and transmission applications. They have been used few times to determine stress concentrations.

1.3 Compilation of results

The object of this section is to list and describe, and in some cases critically analyze, the most important handbooks published with compilations of stress concentration factors. It was thought useful to include the equations obtained by Neuber, for a large number of geometries and boundary conditions, since they deal with many of the most important cases of interest in fracture, and they are not easily available in English.

The circular and elliptical holes. Two problems are of basic importance in engineering design and in fracture prevention and analysis. They are the problems of the stress distribution around a circular hole and the problem of the stress distribution around an elliptical hole, in infinite plates. The solution to these problems have been obtained by Kirsch [30] and by Inglis [31] respectively. These solutions are important sometimes by themselves, sometimes by comparison with the solution of similar

problems. And of course the solution for the circular hole is a particular case of the solution for the elliptical hole.

The solution of the problem of stress distribution around a circular empty hole in a thin plate of infinite width subjected to unidimensional uniformity distributed load is:

$$\sigma_r = \frac{\sigma_{\infty G}}{2}\left(1-\frac{a^2}{r^2}\right)+\frac{\sigma_{\infty G}}{2}\left(1-\frac{4a^2}{r^2}+\frac{3a^4}{r^4}\right)\cos 2\theta \tag{1.3a}$$

$$\sigma_\theta = \frac{\sigma_{\infty G}}{2}\left(1+\frac{a^2}{r^2}\right)-\frac{\sigma_{\infty G}}{2}\left(1+\frac{3a^4}{r^4}\right)\cos 2\theta \tag{1.3b}$$

$$\tau_{r\theta} = -\frac{\sigma_{\infty G}}{2}\left(1+\frac{2a^2}{r^2}-\frac{3a^4}{r^4}\right)\sin 2\theta \tag{1.3c}$$

$$\sigma_z = \tau_{zx} = \tau_{xy} = 0 \tag{1.3d}$$

At the edge of the hole:

$$\sigma_\theta = \sigma_{\infty G}(1-2\cos 2\theta); \quad \sigma_r = \tau_{r\theta} = 0 \tag{1.4}$$

For the cross-section through the center and perpendicular to the x axis, along which the load is applied:

$$\sigma_\theta = \frac{\sigma_{\infty G}}{2}\left(2+\frac{a^2}{r^2}+\frac{3a^4}{r^4}\right) \tag{1.5}$$

A detailed representation of loci of stress components can be found in [32].

Consider the case of a circular hole in a biaxial stress field. The solution may be obtained by superposition. Calling $\sigma^{(1)}$ and $\sigma^{(2)}$ the two perpendicular uniform fields, $k=(\sigma_1/\sigma_2)$ and $c=(a/r)$ the maximum shear stresses (isochromatics) are given by:

$$\begin{aligned}\sigma_1-\sigma_2 = \sigma^{(2)}[&(k-1)^2(9c^8-12c^6-2c^4+4c^2+1)\sin 2\phi + \\ &+c^4(1+k)^2+(1-k)^2(9c^8-12c^6+10c^4-4c^2+1)\cos^2 2\phi + \\ &+c^2(1-k^2)(2+6c^4-4c^2)\cos 2\phi]^{1/2}\end{aligned} \tag{1.6}$$

at the edge of the hole:

$$(\sigma_1-\sigma_2)_{c=1} = \sigma^{(2)}[(1+k)+2(1-k)\cos 2\phi] \tag{1.7}$$

and the sum of the principal stresses anywhere in the field is given by:

$$\sigma_1 + \sigma_2 = \sigma^{(2)}[(1+k) + 2c^2(1-k)\cos 2\phi] \tag{1.8}$$

The individual values of $\sigma^{(1)}$ and $\sigma^{(2)}$ can be obtained by successive addition and subtraction of the isochromatics and isopachics.

For the case of the elliptical hole Inglis [31] used elliptical coordinates α and β such that:

$$x = C\cosh\alpha\cos\beta \tag{1.9a}$$

$$y = C\sinh\alpha\sin\beta \tag{1.9b}$$

and for α = constant:

$$\frac{x^2}{C^2\cosh^2\alpha} + \frac{y^2}{C^2\sinh^2\alpha} = 1 \tag{1.10}$$

and for β = constant

$$\frac{x^2}{C^2\cos^2\beta} - \frac{y^2}{C^2\sin^2\beta} = 1 \tag{1.11}$$

The three components of the stresses at the generic point are given in the form of infinite series, rather cumbersome to compute, but the particular case of the edge of the hole, which is in general the one of greatest interest, is relatively simple. It has been evaluated for the case of combined loading $\sigma^{(1)}$ and $\sigma^{(2)}$, perpendicular to each other. Calling 2a and 2b the lengths of the major and minor axes of the ellipse; α_0 the elliptical coordinate which is constant along the edge of the hole; ϕ the angle between the 2a axis and the directions of loading $\sigma^{(1)}$; and $k = \sigma^{(1)}/\sigma^{(2)}$ the stresses at the boundary of the elliptical hole are given by:

$$\sigma_\alpha = \tau = 0 \tag{1.12a}$$

$$\sigma_\beta = \frac{(\sigma^{(1)} + \sigma^{(2)})\sinh 2\alpha_0 + (\sigma^{(1)} - \sigma^{(2)})[\cos 2\phi - e^{2\alpha_0}\cos 2(\phi - \beta)]}{\cosh 2\alpha_0 - \cos 2\beta} \tag{1.12b}$$

When the directions of loading (1) and (2) coincide with the axes b and

a, respectively, of the ellipse then $\phi = \pi/2$ and

$$\sigma_\beta = \frac{(\sigma^{(1)} + \sigma^{(2)})\sinh 2\alpha_0 + (\sigma^{(1)} - \sigma^{(2)})[e\,2\alpha_0\cos 2\beta - 1]}{\cosh 2\alpha_0 - \cos 2\beta} \tag{1.13}$$

At the ends of the major (point B) and minor (point A) axes of the ellipse the stresses are:

$$\sigma_A = \sigma^{(2)}\left(1 + 2\frac{b}{a}\right) - \sigma^{(1)} \tag{1.14a}$$

$$\sigma_B = \sigma^{(1)}\left(1 + 2\frac{a}{b}\right) - \sigma^{(2)} \tag{1.14b}$$

Since at the apex of the major axis $2a$ of the ellipse, the radius of curvature is $\rho = b^2/a$, the above expression for the stress concentration factor can be given in terms of ρ. For the case of uniaxial loading, p:

$$\sigma_{max} = p\left[1 + 2\left(\frac{a}{\rho}\right)^{1/2}\right] \tag{1.15}$$

The stress concentration factors for a typical elliptical hole a/b = 2, and for a circular hole, subjected to biaxial loading conditions, are shown in Figure 1.16. The solution for the elliptical hole has been found independently by Kolosov [33].

Isida [34] gave a great deal of attention to the stress concentrations present at the edge of elliptical holes. He obtained solutions in the form of power series for the case of finite strips. Results of an experimental systematic study [35] on finite strips are shown in Figures 1.17 to 1.19.

All these developments refer to very small, or 'infinitesimal' strains. When the strains are 'finite,' sufficiently large to change appreciably the shape of the hole, the results may be considerably different from the ones recorded above. The analysis for finite strains is reported in Section 1.4.

Coker and Filon's 'Treatise on Photo-elasticity'. This classic work [36] not only on photoelasticity, but on many aspects of the theoretical treatment of elasticity problems, contains the first systematic treatment of stress concentrations around holes, fillets, notches, cracks and numerous machine components. The integration of the theoretical and

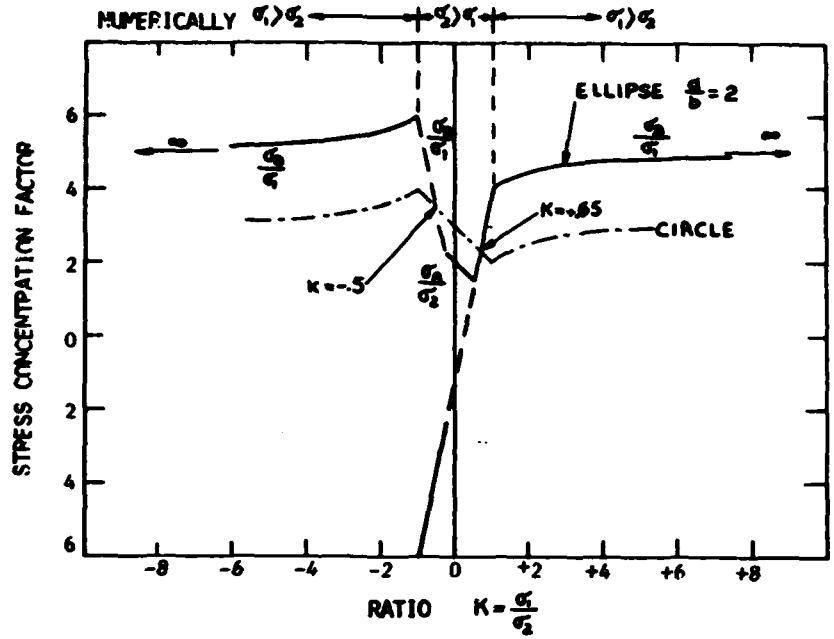

Figure 1.16. Stress concentration factor for an elliptical hole $a/b = 2$, and a circular hole, in an infinite plate, subjected to biaxial loading.

the experimental developments and their applications to engineering problems is unique.

Problems like the determination of stresses in eccentric hollow cylinders, or in cylinders with outer contour of square form (both under pressure) and problems like the determination of stresses in cutting tools, in spline shafts and in nuts and bolts have not only historic interest but permanent value. The same should be said of the study of concentrations in circular and elliptical chain links. The chapter on holes and cracks includes the treatment of eyebars and is fundamental.

Lehr's 'Distribution of Stresses in Elements of Construction'. Lehr's book [37] was probably the first of all the treatises dealing with the experimental analysis of strain and including all the information available at the time (1934), on stress concentrations. These concentrations are defined as the ratio of the peak stresses to the 'nominal' stresses, which are the ones obtained using the elementary formulae. Six main

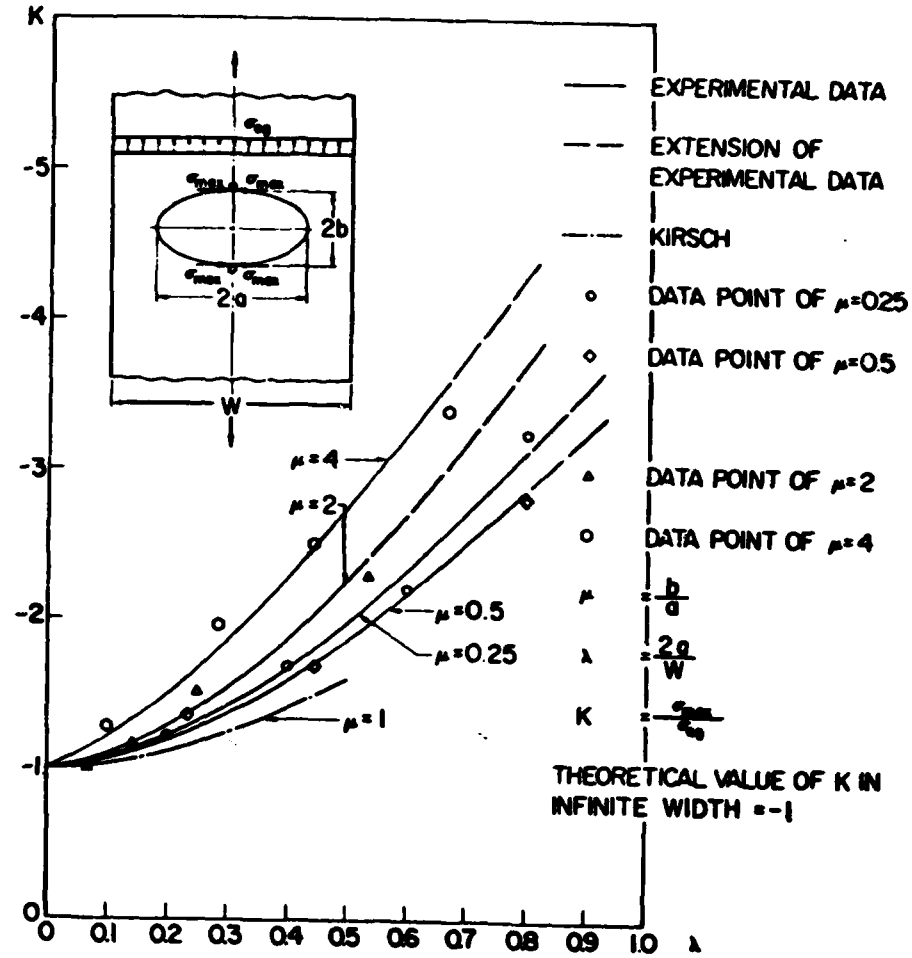

Figure 1.17. Stress concentration factors (K) for the points under maximum compression in a finite width plate with an elliptical hole.

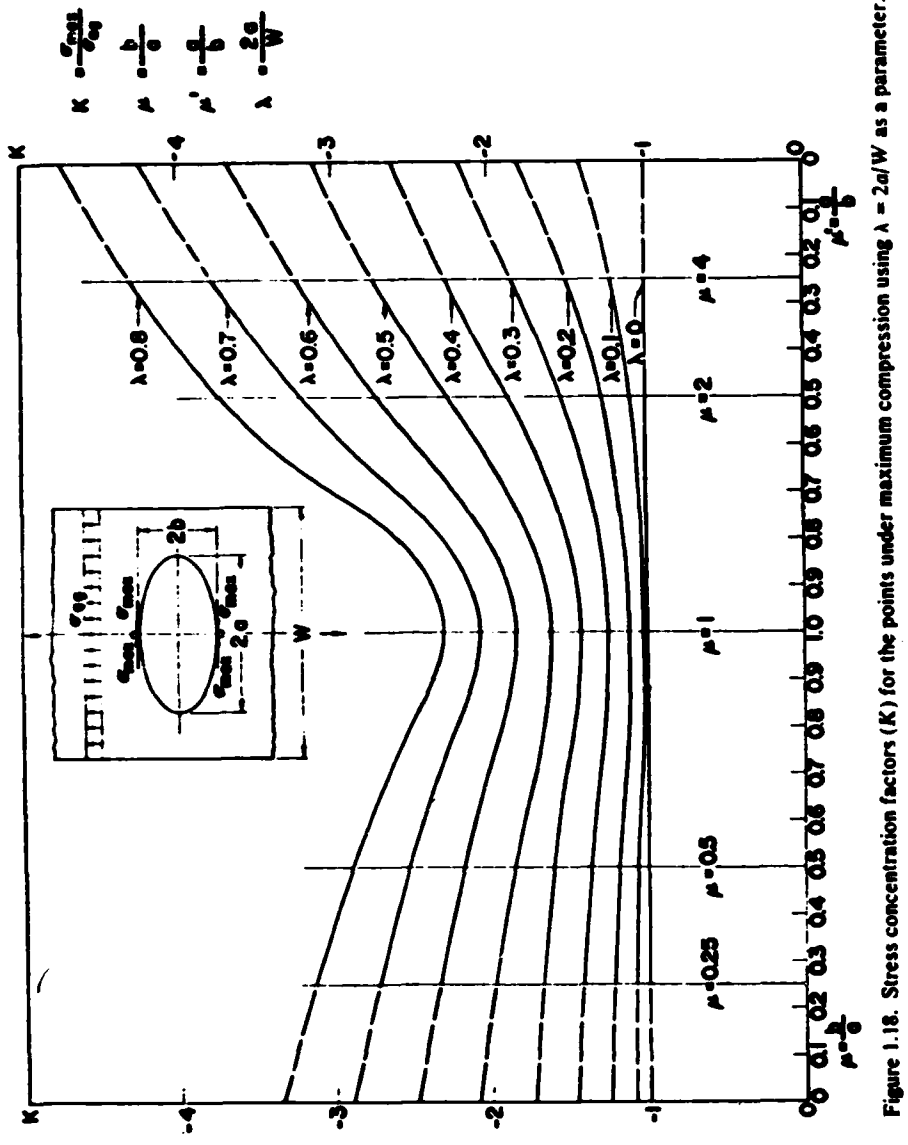

Figure 1.18. Stress concentration factors (K) for the points under maximum compression using $\lambda = 2a/W$ as a parameter.

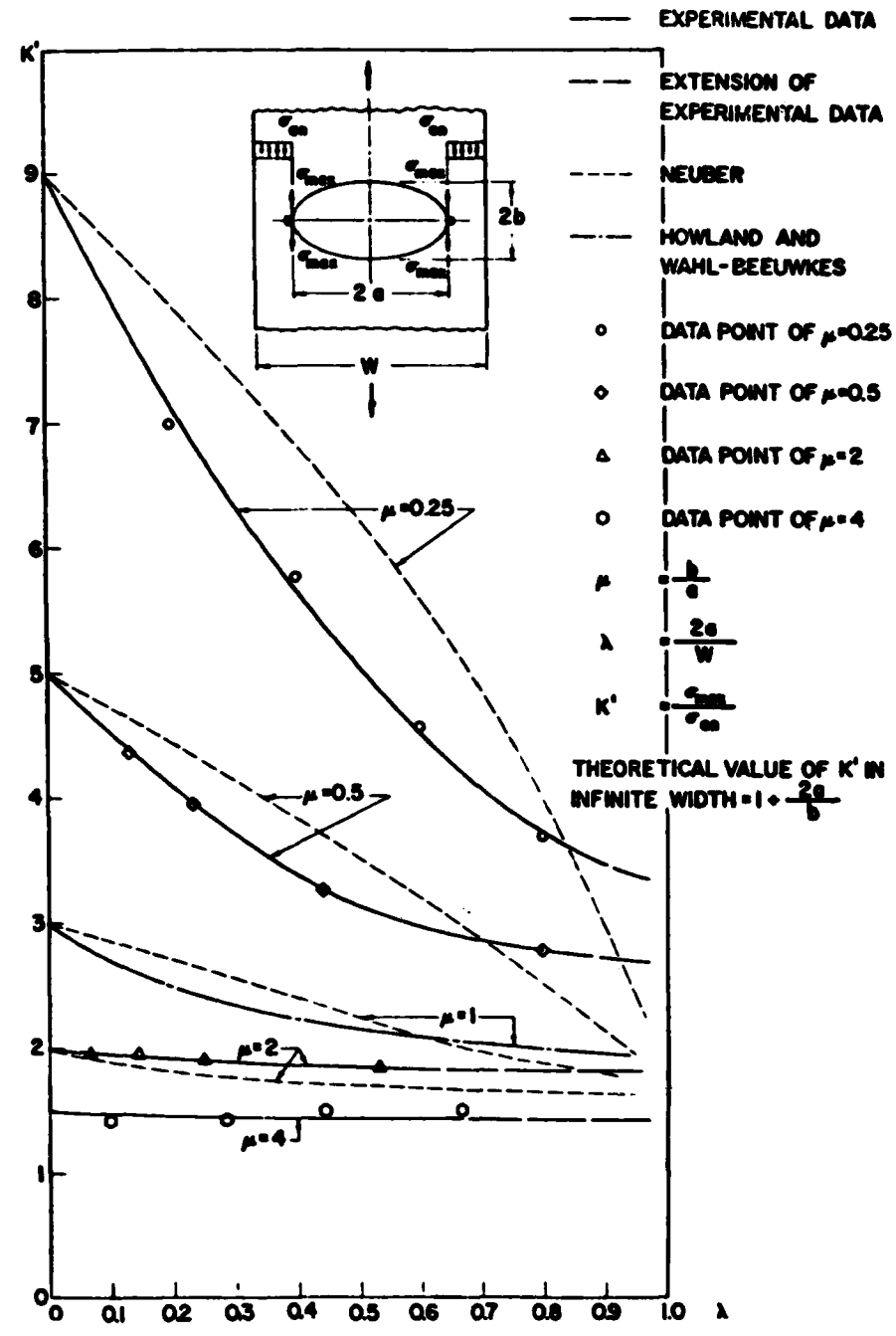

Figure 1.19. Stress concentration factors (K') for the points under maximum tension in a finite plate with an elliptical hole.

groups of geometries are considered: empty holes, holes with pins, shafts with grooves, frames, fillets and keyholes. The information is presented parametrically and the author evaluated the available results using his judgment to interpolate and extrapolate results obtained by other investigators. Results are also included for several machine components like crankshafts, gears and pressure vessels.

Neuber's approach. A book [38] of fundamental importance was published by Neuber in 1937. The determination of stress concentrations was simplified appreciably by: (1) reducing the number of cases to a few typical ones, (2) deciding that the curvature at the base of the notch is of primary importance while the effect of the flank angle at the ends of the notch is of secondary importance, (3) solving for the two limiting cases of shallow and deep notches, and (4) obtaining results from interpolation between the results corresponding to the two limiting cases. Other simplifying assumptions are introduced in the development of particular cases. Neuber calls his approach 'principles for exact calculation' but it obviously is only a useful approximation. Final results are summarized in a nomograph that permits the solution of a very large number of stress concentration problems in plates, rods and tubes, with shallow or with deep notches, subjected to axial load, to torsion, or to bending. The equations developed for the limiting cases (and which are not easily available in English literature) are the following:

(a) Deep external notches on both sides of a bar subjected to axial load (bars referred to in items (a) to (i) have rectangular cross-section)

$$\alpha_1 = \frac{\sigma_{max}}{p} = \frac{2\left(\frac{a}{\rho}+1\right)\sqrt{\frac{a}{\rho}}}{\left(\frac{a}{\rho}+1\right)\operatorname{arctg}\sqrt{\frac{a}{\rho}}+\sqrt{\frac{a}{\rho}}} \tag{1.16}$$

calling ρ the radius of curvature at the base of the notch, a half the width of the narrowest cross-section and p the average stress over the neck of thickness d, which is given by:

$$p = \frac{P}{2ad} \tag{1.17}$$

(b) Deep external notches on both sides of a bar subjected to pure bending:

$$\alpha_2 = \frac{\sigma_{max}}{p} = \frac{4\frac{a}{\rho}\sqrt{\frac{a}{\rho}}}{3\left[\sqrt{\frac{a}{\rho}}+\left(\frac{a}{\rho}-1\right)\operatorname{arctg}\sqrt{\frac{a}{\rho}}\right]} \tag{1.18}$$

where $p = \frac{3M}{2da^2}$.

(c) Deep external notches on both sides of a bar subjected to pure shear:

$$\frac{\tau_{max}}{p} = \frac{\frac{a}{\rho}\sqrt{\frac{a}{\rho}}}{\sqrt{\frac{a}{\rho}+1}\left[\left(\frac{a}{\rho}+1\right)\operatorname{arctg}\sqrt{\frac{a}{\rho}}-\sqrt{\frac{a}{\rho}}\right]} \tag{1.19a}$$

$$\frac{\sigma_{max}}{p} = \frac{\frac{a}{\rho}\sqrt{\frac{a}{\rho}+1}}{\left(\frac{a}{\rho}+1\right)\operatorname{arctg}\sqrt{\frac{a}{\rho}}-\sqrt{\frac{a}{\rho}}} \tag{1.19b}$$

where $p = V/2ad$ and V is the shearing force.

(d) Deep external notches on one side of a bar subjected to axial load:

$$\frac{\sigma_{max}}{p} = \frac{\alpha_1 - 2C}{1-\frac{C}{\sqrt{\frac{a}{\rho}+1}}} \tag{1.20}$$

where

$$C = \frac{\alpha_1 - \sqrt{\frac{a}{\rho}+1}}{\frac{4}{3\alpha_2}\sqrt{\frac{a}{\rho}+1}-1} \tag{1.21}$$

(e) Deep external notch on one side of a bar subjected to bending:

$$\frac{\sigma_{max}}{p} = \frac{2\left(\frac{a}{\rho}+1\right)-\alpha_1\sqrt{\frac{a}{\rho}+1}}{\frac{4}{\alpha_2}\left(\frac{a}{\rho}+1\right)-3\alpha_1} \tag{1.22}$$

(f) Deep external notch on one side of a bar subjected to shear: same equations as in (e) but with

$$p = \frac{V}{ad} \tag{1.23}$$

(g) Shallow external notch on one side, or shallow external notches on two sides, of a bar subjected to axial load:

$$\frac{\sigma_{max}}{p} = 3\sqrt{\frac{t}{2\rho}} - 1 + \frac{4}{2 + \sqrt{\frac{t}{2\rho}}} \tag{1.24}$$

where

$$p = \frac{P}{bd} \quad \text{or} \quad p = \frac{P}{2bd} \tag{1.25}$$

depending on whether there is notch on one side or both sides.

(h) Shallow external notch on one side, or shallow external notches on two sides, of a bar subjected to bending:
Same equations as for (g) with

$$p = \frac{6M}{b^2 d} \quad \text{and} \quad p = \frac{3M}{2b^2 d} \tag{1.26}$$

for one side notch or two sides notches respectively.

(i) Shallow external notch on one side, or shallow external notches on two sides, of a bar subjected to shear:

$$\tau_{max} < 1.5p. \tag{1.27}$$

where

$$p = \frac{V}{bd} \quad \text{or} \quad p = \frac{V}{2bd} \tag{1.28}$$

for one side or two sides notches respectively.

(j) Deep external circumferential notch in a round bar subjected to

axial load

$$\frac{\sigma_{max}}{p} = \frac{1}{N}\left[\frac{a}{\rho}\sqrt{\frac{a}{\rho}+1} + \left(0.5 + \frac{1}{m}\right)\frac{a}{\rho} + \left(1 + \frac{1}{m}\right)\left(\sqrt{\frac{a}{\rho}+1} + 1\right)\right] \tag{1.29}$$

where

$$N = \frac{a}{\rho} + \frac{2}{m}\sqrt{\frac{a}{\rho}+1} + 2; \quad p = \frac{P}{\pi a^2} \tag{1.30}$$

$1/m$ Poisson's ratio and a the radius at the neck.

(k) Deep external circumferential notch in a round bar subjected to bending:

$$\frac{\sigma_{max}}{p} = \frac{1}{N}\frac{3}{4}\left(\sqrt{\frac{a}{\rho}+1} + 1\right)\left[3\frac{a}{\rho} - \left(1 - \frac{2}{m}\right)\sqrt{\frac{a}{\rho}+1} + 4 + \frac{1}{m}\right] \tag{1.31}$$

where

$$p = \frac{4M}{\pi a^3} \tag{1.32}$$

and

$$N = 3\left(\frac{a}{\rho}+1\right) + \left(1 + \frac{4}{m}\right)\sqrt{\frac{a}{\rho}+1} + \frac{1 + \frac{1}{m}}{1 + \sqrt{\frac{a}{\rho}+1}} \tag{1.33}$$

(l) Deep external circumferential notch in a round bar subjected to shear:

$$\frac{\sigma_{max}}{p} = \frac{\left(\frac{a}{\rho}+1\right)\left(\frac{a}{\rho}+2\sqrt{\frac{a}{\rho}+1}+2\right)\left(\frac{a}{\rho}+2+\frac{2}{m}\right)}{2\sqrt{\frac{a}{\rho}}\left(\sqrt{\frac{a}{\rho}+1}+\frac{1}{m}\right)\left(\frac{a}{\rho}+2\right)^{3/2}} \tag{1.34}$$

where

$$p = \frac{V}{\pi a^2} \tag{1.35}$$

(m) Deep external circumferential notch in a round bar subjected to torsion:

$$\frac{\tau_{max}}{p} = \frac{3\left(1+\sqrt{\frac{a}{\rho}+1}\right)^2}{4\left(1+2\sqrt{\frac{a}{\rho}+1}\right)} \tag{1.36}$$

where

$$p = \frac{2M}{\pi a^3} \tag{1.37}$$

(n) Shallow circumferential internal notch in a round bar subjected to axial load:

$$\frac{\sigma_{max}}{p} = \frac{1}{N}\left\{2\left(\frac{t}{\rho}\right)^2 - \left(1.5-\frac{1}{m}\right)\frac{t}{\rho}+1-\frac{1}{m}+\left[-\left(1.5+\frac{1}{m}\right)\frac{t}{\rho}+\frac{1}{m}\right]\frac{t}{\rho}c\right\} \tag{1.38}$$

where

$$c = \frac{\operatorname{arctg}\sqrt{\frac{t}{\rho}-1}}{\sqrt{\frac{t}{\rho}-1}}, \quad \text{if } \frac{t}{\rho} > 1 \tag{1.39a}$$

$$c = \frac{\ln\left(1+\sqrt{1-\frac{t}{\rho}}\right)-\frac{1}{2}\ln\frac{t}{\rho}}{\sqrt{1-\frac{t}{\rho}}}, \quad \text{if } \frac{t}{\rho} < 1 \tag{1.39b}$$

and

$$N = \frac{t}{\rho}+1-\frac{1}{m}+\left(\frac{t}{\rho}-2+\frac{2}{m}\right)\frac{t}{\rho}c-\left(1+\frac{1}{m}\right)\left(\frac{t}{\rho}\right)c^2 \tag{1.40}$$

and where t is the depth of the notch, b the radius of the bar, and

$$p = \frac{P}{\pi b^2} \tag{1.41}$$

(o) Shallow circumferential internal notch in a round bar subjected to bending:

$$\frac{\sigma_{max}}{p} = \frac{1}{N}\left\{g[g(10t^2-2\alpha)-36t^2+16-4\alpha]-16t^2\right\} \tag{1.42}$$

where

$$g = \frac{\frac{t}{\rho}}{\left(\frac{t}{\rho}-1\right)^2}\left[3\frac{t}{\rho}c-2\frac{t}{\rho}-1\right] \tag{1.43}$$

(p) Shallow circumferential internal notch in a round bar subjected to shear:

$$\frac{\sigma_{max}}{p} = \frac{1}{N}2\sqrt{\frac{t}{\rho}-1} \tag{1.44}$$

where

$$p = \frac{3m+2}{2m+2}\frac{V}{\pi b^2} \tag{1.45a}$$

$$N = \left(\frac{t}{\rho}-1\right)^{-3/2}\left\{\left[\left(2-\frac{1}{m}\right)\frac{t}{\rho}+1+\frac{1}{m}\right]\left[\frac{t}{\rho}c-1\right]-2\frac{t}{\rho}+2\right\} \tag{1.45b}$$

and c is given by equations (1.39a) and (1.39b).

(q) Shallow circumferential internal notch in a round bar subjected to torsion:

$$\frac{\tau_{max}}{p} = \frac{2\left(\frac{t}{\rho}-1\right)^2}{3\left(\frac{t}{\rho}\right)^2 c-5\frac{t}{\rho}+2} \tag{1.46}$$

where

$$p = \frac{2Mt}{\pi b^4} \tag{1.47}$$

(r) Circular and elliptical hole in a very wide bar, subjected to axial load:

$$\frac{\sigma_{max}}{p} = 1 + 2\sqrt{\frac{t}{\rho}} = 1 + 2\frac{t}{s} \tag{1.48}$$

t being half the axis of the ellipse, in the direction perpendicular to the applied load, and s half the axis in the direction parallel to the applied load.

(s) Circular and elliptical hole in a very wide bar, subjected to bending

$$\frac{\sigma_{max}}{p} = 1 + \sqrt{\frac{t}{\rho}} \tag{1.49}$$

(t) Circular and elliptical hole in a very wide bar, subjected to pure shear:

$$\frac{t_{max}}{p} = 3\frac{\left(\frac{t/\rho + 2}{3}\right)^{3/2} - \sqrt{\frac{t}{\rho}}}{\left(\sqrt{\frac{t}{\rho}} - 1\right)^2} \tag{1.50a}$$

$$\frac{\sigma_{max}}{p} = \frac{3}{2}\left(\sqrt{\frac{t}{\rho}} + 2 + \frac{1}{\sqrt{\frac{t}{\rho}}}\right) \tag{1.50b}$$

This monumental work of great imagination showing the unusual mastery that the author has of the theory of elasticity equations ends with a sheet in which three nomographs summarize the whole book. All stress concentrations factors can be computed with two or three motions of the pencil. This is a unique accomplishment in the literature of stress concentrations. In the second edition an extension was made to account also for the influence of nonlinear stress-strain relationships. Experimental work, conducted mainly after the publication of the book, shows in some cases appreciable differences with the values obtained from Neuber's nomographs (see for instance Figure 1.19). These differences are frequently due to the approximate method Neuber uses to interpolate between results corresponding to shallow and deep notches. Although they should be a warning to the scientist using the nomographs, the differences do not detract from the overall value of Neuber's attempt at giving a unified presentation of the field.

Roark and Young's 'Formulas for Stress and Strain'. Roark and Young's book [39] on formulae for stresses and strains is organized like a regular treatise on advanced strength of materials, but with little description of principles and methods, and great emphasis on the presentation of problems already solved. Large number of tables contain the problems described schematically. Next to them are listed the equations necessary to solve them and all the necessary auxiliary data. Frequently the most important values for design are given directly. In many of the tables coefficients to solve the problem parametrically are included. The components analyzed are beams (straight and curved), bars under torsion, plates, columns, shells and pressure vessels. Analysis of contact stresses, buckling, dynamic and thermal stresses are also included.

A chapter at the end of the book deals specifically with stress concentrations. The material is presented for 23 geometric shapes in the same format of the rest of the book. Results are not given in graphical form as in Peterson's handbook, nor in the form of more or less general equations to be frequently worked out, as in Savin's book, but by means of simple algebraic equations, with reference to the sources which report mostly experimental work.

The matter of the definition of stress concentrations should be mentioned again. Some stress concentration factors are listed in the body of the book, which are not listed in the table dealing with stress concentration factors. An instance is the large stress present in rectangular beams of great depth, when subjected to uniform loads, or to concentrated loads. Stresses twenty times larger than those obtained using elementary formulae may appear. The fact that the boundaries are straight does not seem good enough reason not to call this situation a concentration of stress. Another example is the case of contact stresses.

Lipson, Noll and Clock's 'Handbook on Stress and Strength'. In this book [40], 45 charts have been assembled giving in graphical form the stress concentration factors for holes, fillets and grooves in solid and hollow circular shafts subjected to tension, bending and torsion. The information was obtained from theoretically and experimentally obtained data. The main emphasis of the book however is in the presentation of almost 100 charts for so-called 'fatigue' stress concentration factors K_f, corresponding to annealed and to quenched steel. Most of these have been derived from the 'theoretical' stress concentration factor K_t and values of notch sensitivity q obtained averaging

experimental data obtained by several investigators, and using the expression:

$$K_f = 1 + q(K_t - 1). \tag{1.51}$$

The book has been written for designers and many of the results given are only a first approximation to the solution.

Savin's 'Stress Distribution Around Holes'. Although G. N. Savin's book [41] does not deal with discontinuities at outside boundaries, it is a unique treatise on stress distributions around inside discontinuities. The treatment of all kinds of holes is dealt in an exhaustive manner. It includes any number of holes of any shape, in linear and nonlinear materials, subjected to small or large deformations, and also when the materials behave plastically or viscoelastically. It also includes analysis of cases in which the materials with the holes are anisotropic and when the equations of equilibrium include moments. Most of the problems have been solved in an approximate manner using the method which consists in finding two analytical functions of a complex variable, the complex potentials of Kolosov and Muskhelishvili and of Cauchy-type integrals. In some cases the method of perturbation of the form of the boundaries has been used.

A great amount of information has been assembled in this book, each chapter of which contains a very large number of bibliographic references. The main limitations seem to be the approximate character of the solutions obtained, the fact that by conformal mapping not always the desired geometry is obtained and that the mapping function must be very accurate in the neighborhood of points where stress concentrations occur. References to experimental work are much less numerous than the references to theoretical contributions and do not seem to be up-to-date. It may be added that by contrast with engineering design handbooks, the graphic results are difficult to use because of the small size of the reproduction, or because some of the necessary information is not directly available. In some cases sketches in the figures are misleading like the ones representing infinite plates with holes as if they were finite plates. On the other hand, the number of equations assembled to approach mathematically the solution of stress distributions around holes is enormous.

Foeppl and Sonntag's 'Tables for Strength of Materials'. This book [42] presents the subject in a manner similar to the one used by Roark.

In a schematized way most problems in strength of materials are dealt with profusion of tables and graphs, and equations ready to be used by the designer. Chapters deal with bending of straight and curved bars, torsion, two-dimensional problems, three-dimensional problems, plates and shells. Stress concentrations are studied with more detail than by Roark and follow to a large extent Neuber's approach.

The problems of thick curved beams of variable height, and stress concentrations associated with protuberances are included.

The lack of reference to the work of Coker and Filon, and the very few references to experimental results are surprising.

Peterson's 'Stress Concentration Factors'. Whereas Savin's treatise is the result of the theoretical work of a school of investigators using a few particular methods, Peterson's handbook [43] is the compilation of the results obtained by hundreds of investigators using any available methods. And whereas Savin most of the time details the methods used and the step-by-step procedure to obtain the results, Peterson compiles the results with little or no reference to the methodology. Few of Savin's graphs have been prepared with enough precision to be used directly for measurements. All of Peterson's graphs have been prepared with this purpose in mind, and most of them present the information parametrically. Although conformal mapping methods are approximate methods, Savin's work emphasizes theoretical precision. In Peterson's handbook the emphasis is on usefulness to designers and judgment is expected in the application of the information to give answers to designers' problems.

The scope of Peterson's handbook is larger than the scope of Savin's treatise. It includes notches and grooves, shoulder fillets, holes in two and in three-dimensional bodies, and an appreciable number of structural components: shafts with key seats, splined shafts, gear teeth, shrink-fitted members, bolts and nuts, springs, crankshafts, hooks, box sections, rotating disks, rings, pressure vessels, etc. Considerations on fatigue are numerous, reflecting the experience of the author on this subject, but viscolasticity, plasticity and large deformations are not considered.

Strangely enough only two minor references to Savin's work can be found in Peterson's handbook and little advantage seems to have been taken from the sizable amount of information accumulated by Savin.

Griffel's 'Handbotk for Formulas for Stress and Strain'. The book [44] assembles the usual formulae for the bending of straight and curved

beams, the bending of plates, the design of pressure vessels and the vibration frequencies of plates. A large part of the book deals with properties related to the geometry of cross-sections of components. A chapter is included dealing with stress concentration factors in beams and plates with holes. Several of the results are taken from Savin's book. Here again sketches are misleading showing finite plates with very large holes as if they were infinite plates. More serious, however, are statements like: 'the data can certainly be applied with assurance to cases where the hole diameter is three-fifths the total width of the plate. . . .' (p. 246). For the case of the circular hole the stress concentration factor in the finite plate is 5.2 when referred to the gross area, and 2.1 when referred to the net area. The value given in the graph is 3. This and similar approximations do not seem acceptable.

Nisitani's approach. Using a socalled body force method Nisitani has determined a large number of stress concentration factors for fillets and notches in two- and three-dimensional problems. Some have been included in Peterson's handbook. Others, with particular emphasis on solutions for crack problems have been published in [45]. These include elliptical holes and notches with cracks at the apexes and the interaction between a crack and an elliptical notch. The results are given graphically and in tables and the relation between stress concentration factors and stress intensity factors is frequently pointed out.

Bibliographic sources. With the exception of Neuber's, the nine handbooks mentioned above have large numbers of bibliographic references. Savin's has more than 700, Coker more than 400, Peterson about 380, and Roark about 360. Another important source of references is one of the books by Heywood [46] with more than 1000 references.

Two reviews of the literature should be mentioned, a survey by Hogan with particular interest in holes and pressure vessels [47] with about 500 references, and another, very general, by Neuber and Hahn [48], with 250 references. Also related to the problem is a review by Sternberg [49] and a comparative evaluation of experimental methods by Durelli [50]. Sternberg confined his survey to the 'analytical treatment of three-dimensional stress concentrations within the linear equilibrium theory of homogeneous and isotropic, elastic media.' The papers surveyed used 'exact' methods to solve the homogeneous displacement equations of equilibrium in terms of stress functions. The problems include spherical, spheroidal and elliptical cavities and inclusions, cracks and notches, with 57 references.

1.4 Geometrically non-linear stress concentrations

Few studies have been conducted to determine the influence of non-linearities on stress concentration factors. Important contributions have been made by Neuber [51] who for certain cases of loading investigated theoretically the influence of material non-linearities, and by Savin [41] following Green and Adkins, who studied geometric non-linearities in circular and elliptical holes in finite plates. Some results obtained experimentally, using linear materials, after the original shape changes appreciably, will be reported here. The subject is certainly relevant to the study of cracks since their shape will likely deform appreciably before fracture.

Geometric non-linearity. Stress concentration factors obtained when deformations are infinitesimal, in materials behaving linearly, are applicable to any material behaving linearly, and subjected to any level of deformation, provided this level is within the proportional limit of the material. When geometric non-linearities are involved the stress concentration factor changes with the deformation level, and factors are applicable only to the particular level for which they have been obtained.

The definition of stress concentration also may change. In some instances, it has been found convenient to use:

$$\frac{\bar{\sigma}_{max}}{E} \tag{1.52}$$

where $\bar{\sigma}$ is a 'natural' stress defined as the integral of instantaneous, or incremental, stresses, each of them computed using the area corresponding to the particular incremental load level:

$$\bar{\sigma} = \lim_{\Delta P \to 0} \sum \frac{\text{instantaneous change in load}}{\text{instantaneous area}} (\Delta P) \tag{1.53a}$$

$$\bar{\sigma} = \int_{m=i}^{m=f} \frac{\Delta P}{A_m} \tag{1.53b}$$

where m is used to represent the increment. P is the load on the area A, and ΔP is the increase in load in the area A_m.

Use is also made of the concept of natural strain:

$$\bar{\varepsilon} = ln \frac{1}{1 - \varepsilon^E} \tag{1.54}$$

and of the two classic definitions of strain: the Lagrangian, or conventional engineering strain:

$$\epsilon^L = \frac{\text{total change in length}}{\text{initial length}} = \frac{l_f - l_i}{l_i} \tag{1.55}$$

and the Eulerian strain:

$$\epsilon^E = \frac{\text{total change in length}}{\text{final length}} = \frac{l_f - l_i}{l_f} \tag{1.56}$$

Besides the 'natural' stress definition mentioned above, the two classic definitions of stress, Lagrangian or engineering:

$$\sigma^L = \frac{P}{A_i} \tag{1.57}$$

referred to the undeformed area, and Eulerian:

$$\sigma^E = \frac{P}{A_f} \tag{1.58}$$

referred to the deformed area are used:

The materials used for all the experimental determinations reported in this section are several varieties of polyurethane rubbers, all of them behaving linearly and elastically to high levels of strain, of order of 80% in the natural representation.

Stress concentration around elliptical holes in finite plates subjected to uniform load producing finite strains. In Section 1.3 results of the analysis conducted using the infinitesimal theory were reported. Here the case of the elliptical holes in plates subjected to loads producing finite strains will be considered [52].

Figure 1.20 shows the change in the shape of the boundary of an elliptical hole $a_i/b_i = 2.0$ as the load is applied, for different ratios of the major axis of the hole to the width of the plate. Subscript i stands for 'initial' values as subscript f for 'final' values.

Figure 1.21 shows the stress distribution at the boundary of the hole for a very large plate: $\eta = a_i/w = 0.112$ where w is the width of the plate. Figure 1.22 shows the corresponding distribution for the case of a

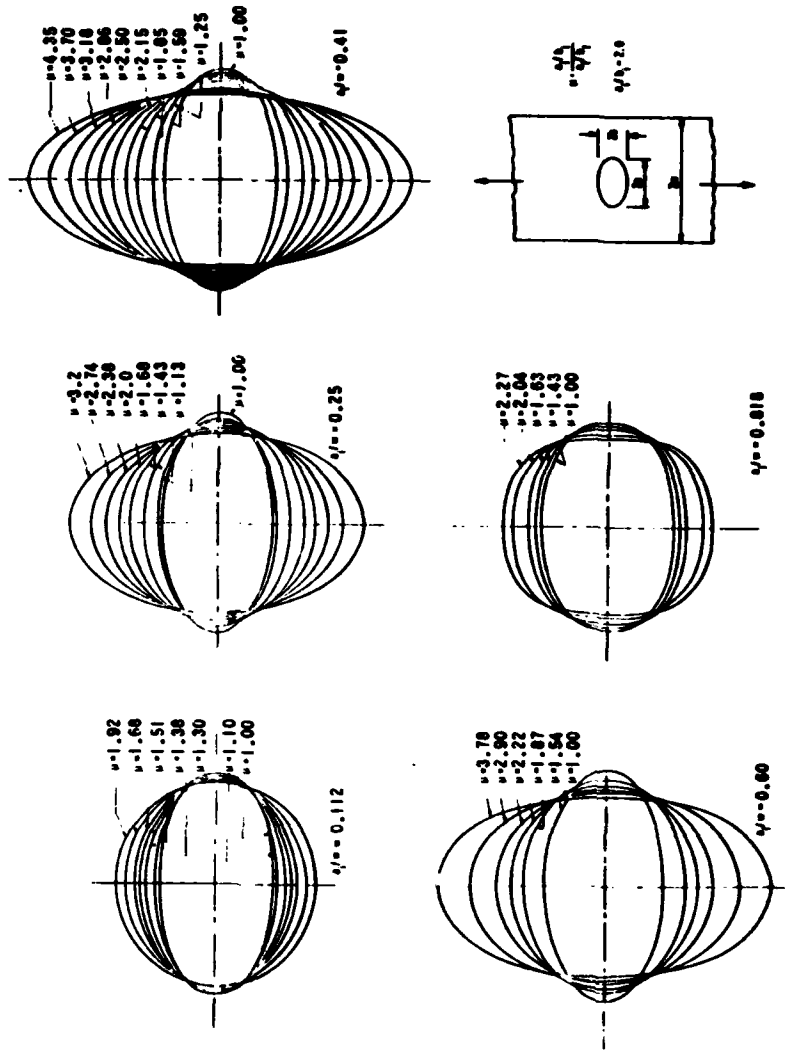

Figure 1.20. Metamorphosis of an elliptical hole in a plate subjected to deformation.

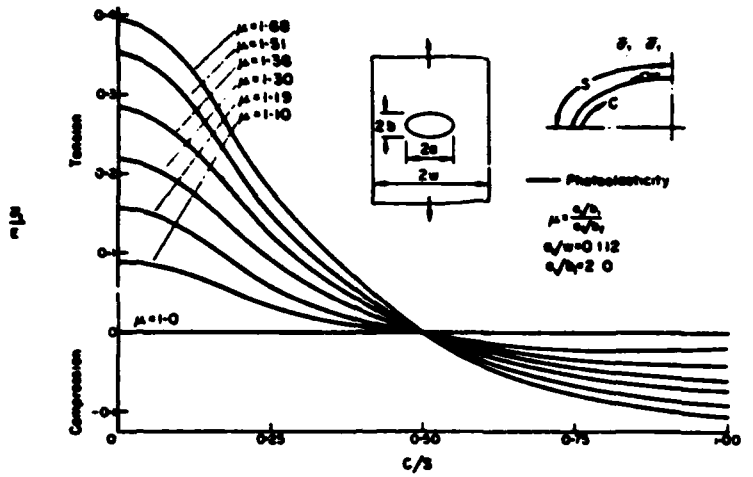

Figure 1.21. Normalized stress distribution at the undeformed boundary of the elliptical hole in a large plate ($\eta = 0.112$) for a linear material subjected to several levels of in-plane axial load.

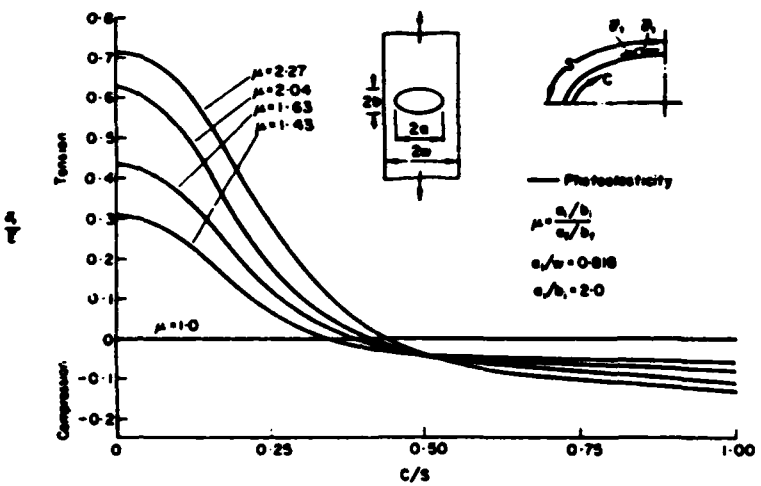

Figure 1.22. Normalized stress distribution at the undeformed boundary of the elliptic hole in a finite plate ($\eta = 0.818$) for a linear material subjected to several levels of in-plane axial load.

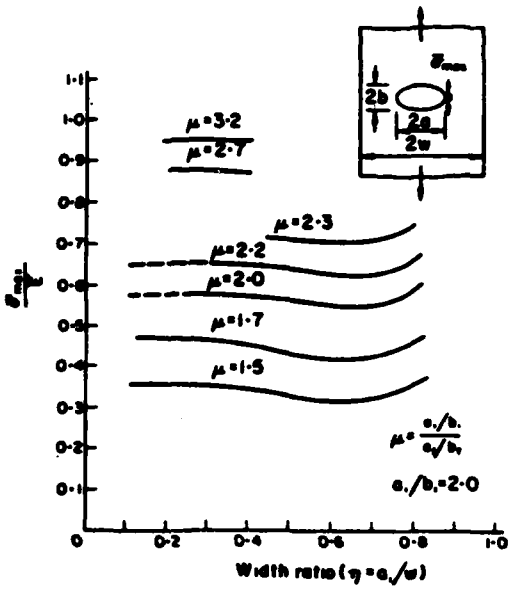

Figure 1.23. Normalized stress ratios as a function of width for a linear material subjected to in-plane axial loading.

narrow plate ($\eta = 0.818$) and Figure 1.23 shows the maximum stresses, parametrically, for all the cases investigated. The results indicate that the maximum stress is primarily a function of the shape of the hole in its deformed state. The investigation was conducted using photoelasticity, grids and moiré effects on a polyurethane rubber plate.

In the previous figures the normalization was obtained by dividing stresses by the modulus of elasticity. This is a correct but unconventional way. The following figures [53] use the more common method of dividing the stresses by some average stress, which requires knowledge of the load. The first method indicates the relationship of the stress to the deformed shape, the second emphasizes the stress-load relationship. Figure 1.24 shows the stress concentration factor, using the load as parameter, Figure 1.25 the change in shape and Figure 1.26 the stress concentrations factor using the hole shape as parameter.

Stress and strain concentrations in spheres diametrically loaded and subjected to finite strains. The values of the stresses and strains, at the center of a solid sphere, as the level of deformations increases, are of

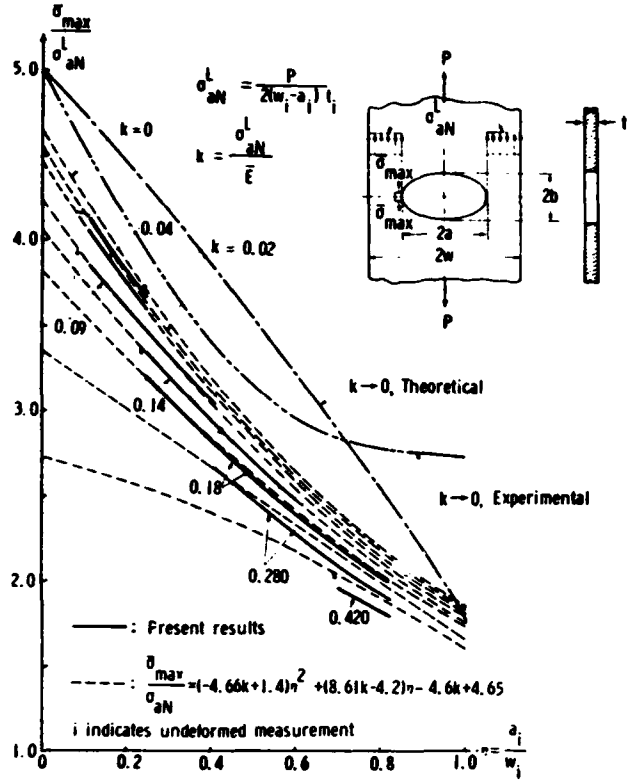

Figure 1.24. Stress concentration factor at the boundary of an elliptic hole in a plate of linear material, subjected to several levels of in-plane axial load, using normalized load as a parameter.

general interest [54] (Figure 1.27). They have been obtained using embedded gratings and moiré effects from a material with a strain energy function

$$W = C_1(I_1 - 3) + C_2 \ln\left(\frac{I_2}{3}\right) \tag{1.59}$$

where $C_1 = 17$ psi and $C_2 = 25$ psi.

The Eulerian vertical stresses on the horizontal axis of the sphere when subjected to several load levels of diametral vertical compression are shown in Figure 1.28. Further results can be found in [54].

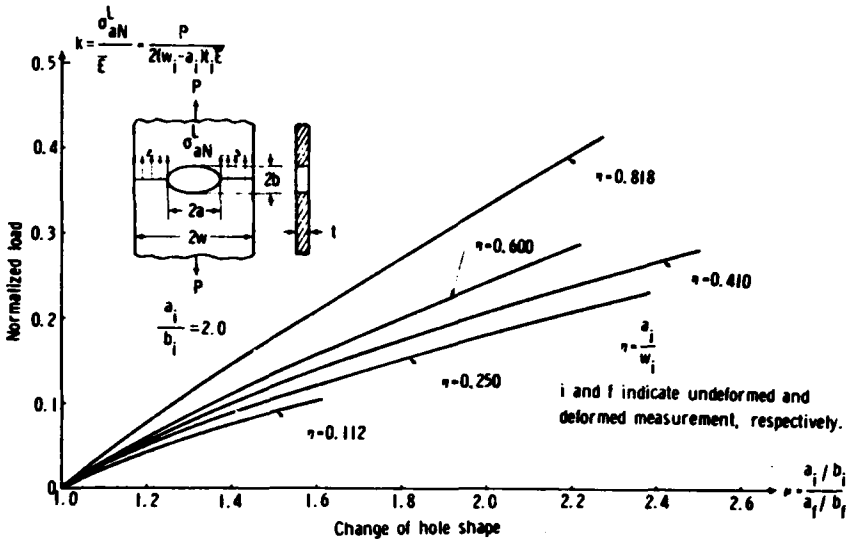

Figure 1.25. Change of shape of an elliptic hole in a finite plate subjected to several levels of in-plane axial load as a function of normalized load.

When the sphere is hollow ($OD/ID = 2$) the strain concentration factor, as shown in Figure 1.29 is amazingly close to constant, as function of the amount of load, despite very large changes in shape [55]. Figure 1.30 gives the complete distribution of principal strains on the inner boundary. Further results can be found in [57].

Stress and strain concentrations in a disk subjected to diametral load producing finite strains. It is important to know, mainly for problems related to fracture, the change in the position and value of the stress concentration factors in a disk, subjected to diametral compression, when deformations are large, but the material behaves in a linear manner [56].

The most striking feature of the influence of the level of deformation on the stress concentration factor, is that the location of the maximum in-plane shear, which takes place at, or near the point of load application when deformations are small, moves in toward the center of the disk, very appreciably Figure 1.31. At the same time the values of the maximum normal stresses decrease, also appreciably. The information is given in Figure 1.32 where $\bar{E}$ = Young's modulus based on true stress

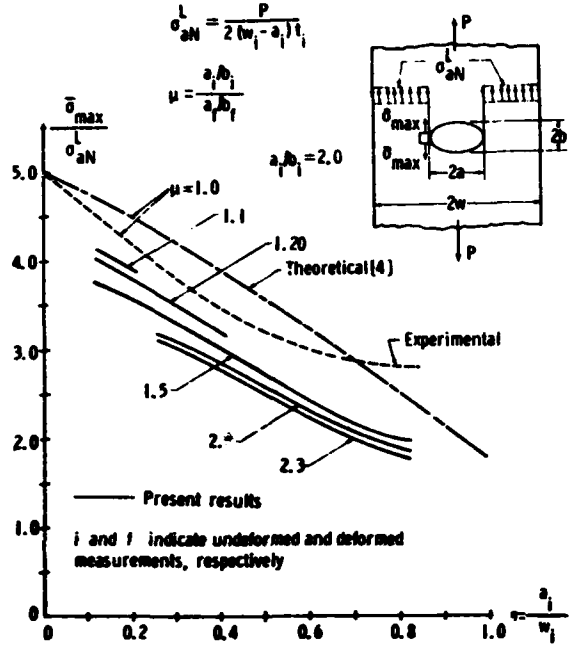

Figure 1.26. Stress concentration factor at the boundary of an elliptic hole in a plate of linear material, subjected to several levels of in-plane axial load, using change of the hole shape as a parameter.

versus natural strain, t_0 = thickness of undeformed disk, r_0 = radius of undeformed disk; $\bar{\sigma}_x$ and $\bar{\sigma}_y$ = Lagrangian true stresses, $\bar{\varepsilon}_x$, $\bar{\varepsilon}_y$, $\bar{\varepsilon}_z$ = Cartesian natural strains and n = photoelastic fringe order which gives the maximum natural shear stress.

The stress results shown are applicable to any disk, of any size, of any linear material. The strains are given for a material with a Poisson's ratio $\nu = 0.48$.

Stress and strain concentrations in a circular ring subjected to diametral compression producing finite strains. Using grids, moiré and photoelasticity and a polyurethane rubber as model material, strains and stresses have been determined in a ring subjected to eight levels of deformations [57, 58]. The ratio of the outside diameter to the inside

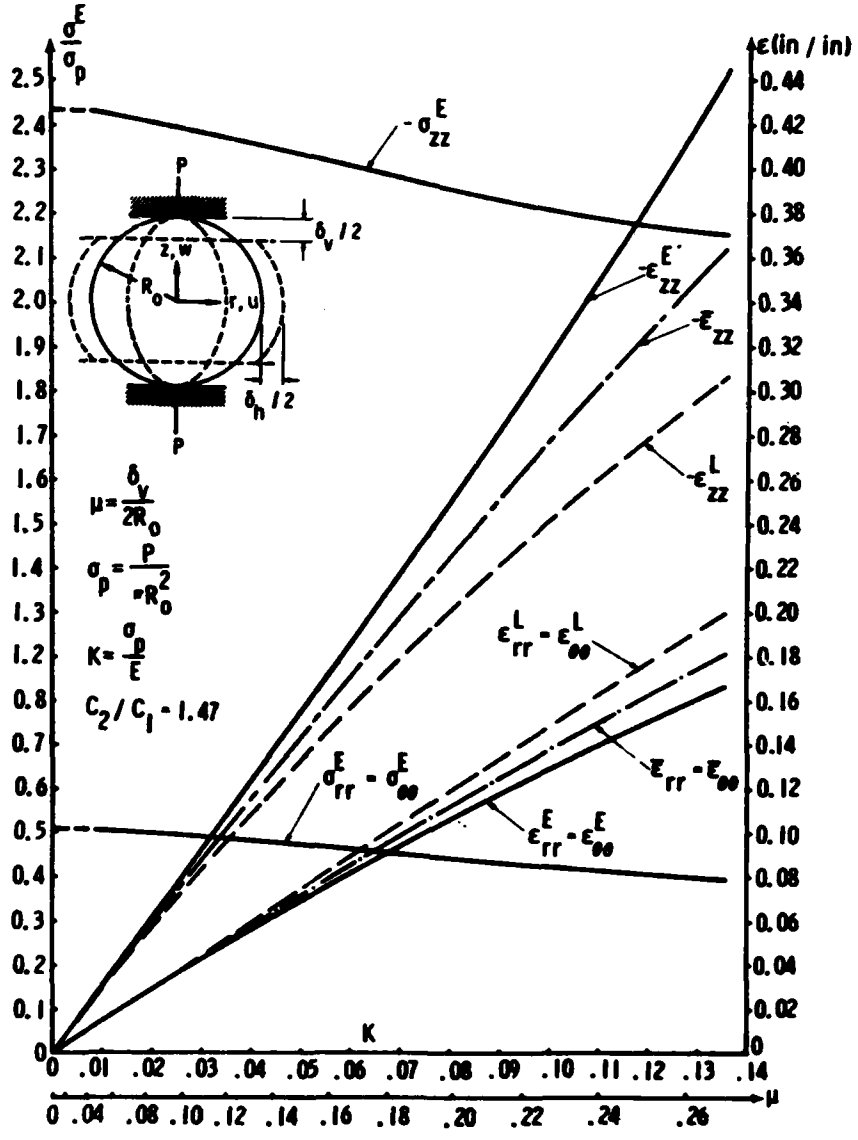

Figure 1.27. Stresses and strains, as a function of load, at the center of a sphere subjected vertically to several levels of diameteral compression.

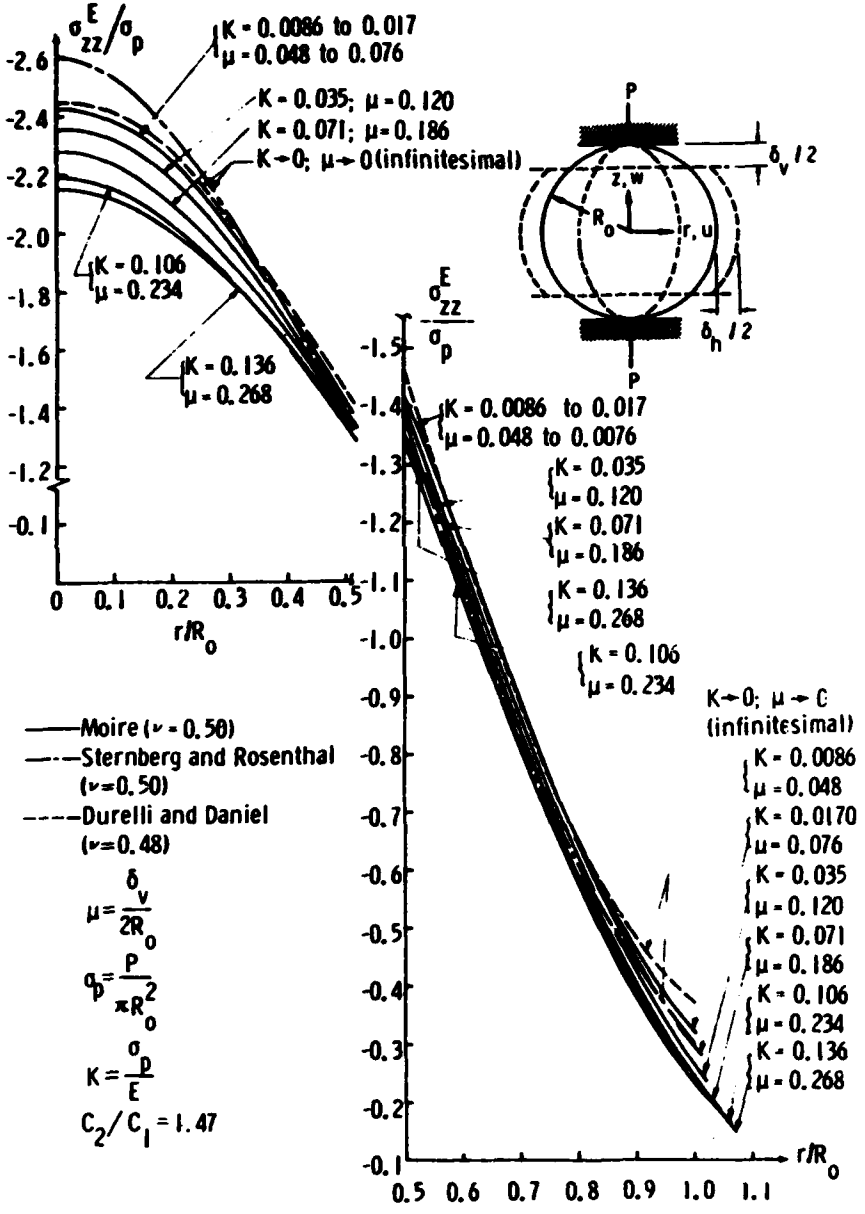

Figure 1.28. Eulerian vertical stress on the horizontal axis of a sphere subjected vertically to several load levels of diametral compression.

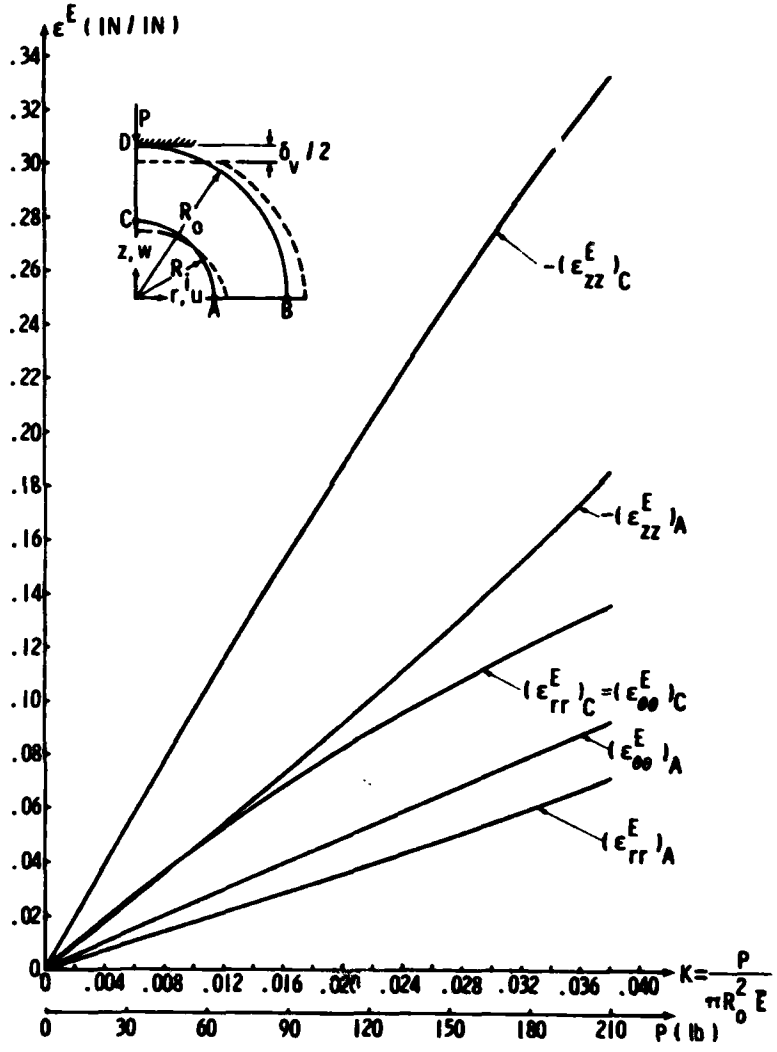

Figure 1.29. Strains at the intersection of the axes and the inner boundary sphere (*OD/ID*) = 2 subjected vertically to several load levels of diametral compression.

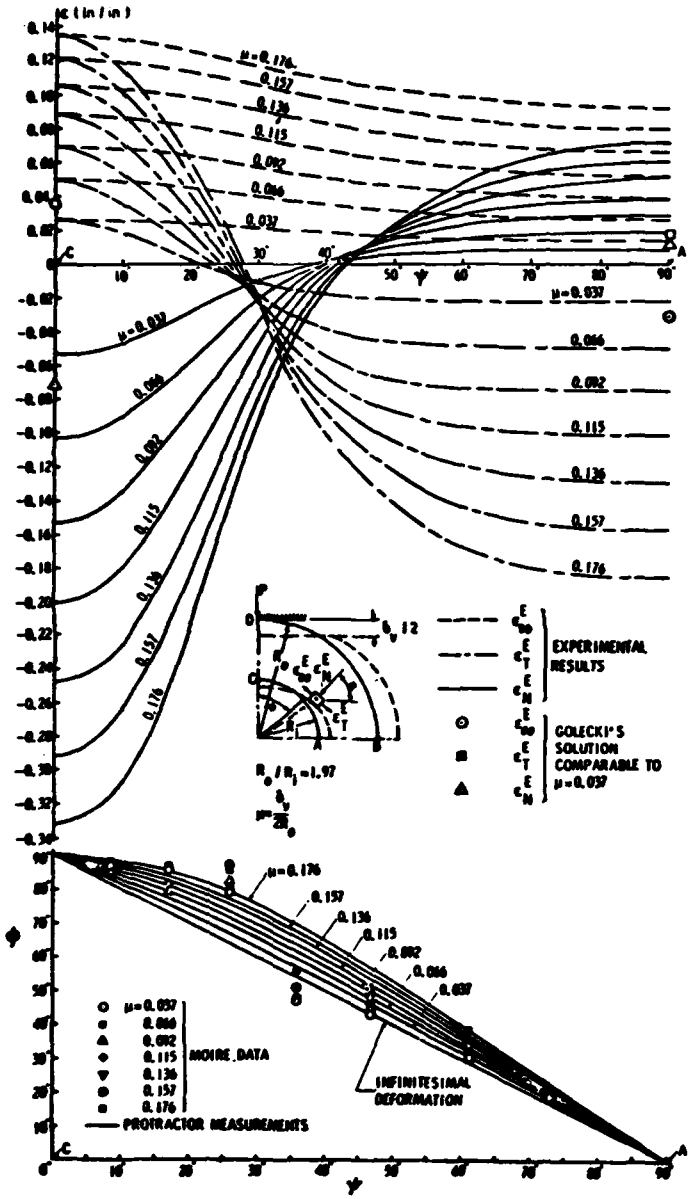

Figure 1.30. Principal strains $\varepsilon^E_{\theta\theta}$, ε^E_N and ε^E_T and their orientation on the inner boundary of a hollow sphere subjected vertically to seven levels of diametral compression in lagrangian description.

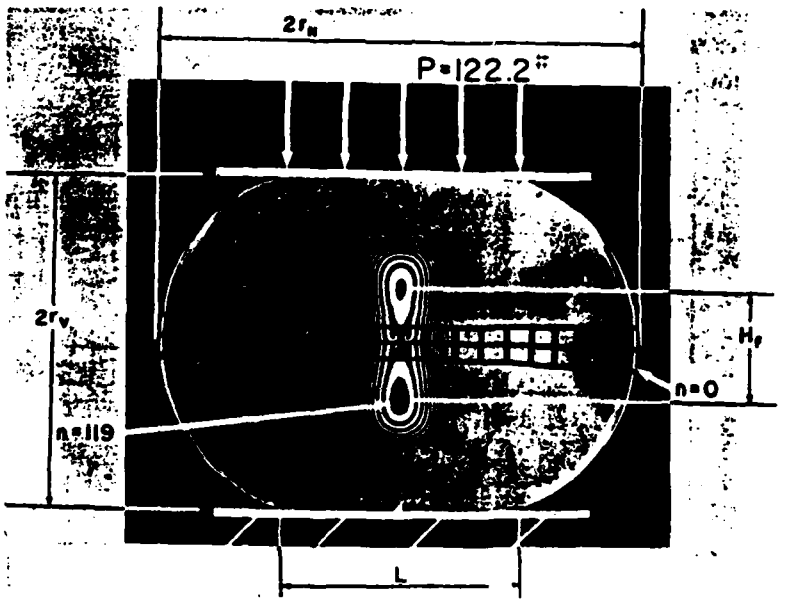

Figure 1.31. Isochromatics and grids in a polyurethane disk (solithane 113) subjected to diametral loading ($P = 122.2$ lbs., $K = 0.155$).

diameter of the ring is approximately 1.5., and the level of deformation is given by the parameter $\lambda = \delta_v/OD$, δ_v being the change in length of the loaded diameter. Some of the more significant results are shown in the figures. Figures 1.33 and 1.34 show the distorted grids and the Lagrangian strains tangential to the inner boundary, Figure 1.35 the Eulerian horizontal strains on the vertical axis, Figure 1.36 the Eulerian horizontal strains in the horizontal axis, Figure 1.37 the Eulerian vertical strains on the horizontal axis and Figure 1.38 the Eulerian principal strains and their orientations on the inner boundary. Typical record of the physical evidence is shown in Figure 1.39.

Linear and non-linear elastic and plastic stress concentration in a plate with a large circular hole loaded axially in its plane. The stress concentration at the edge of the circular hole, in a finite plate loaded axially

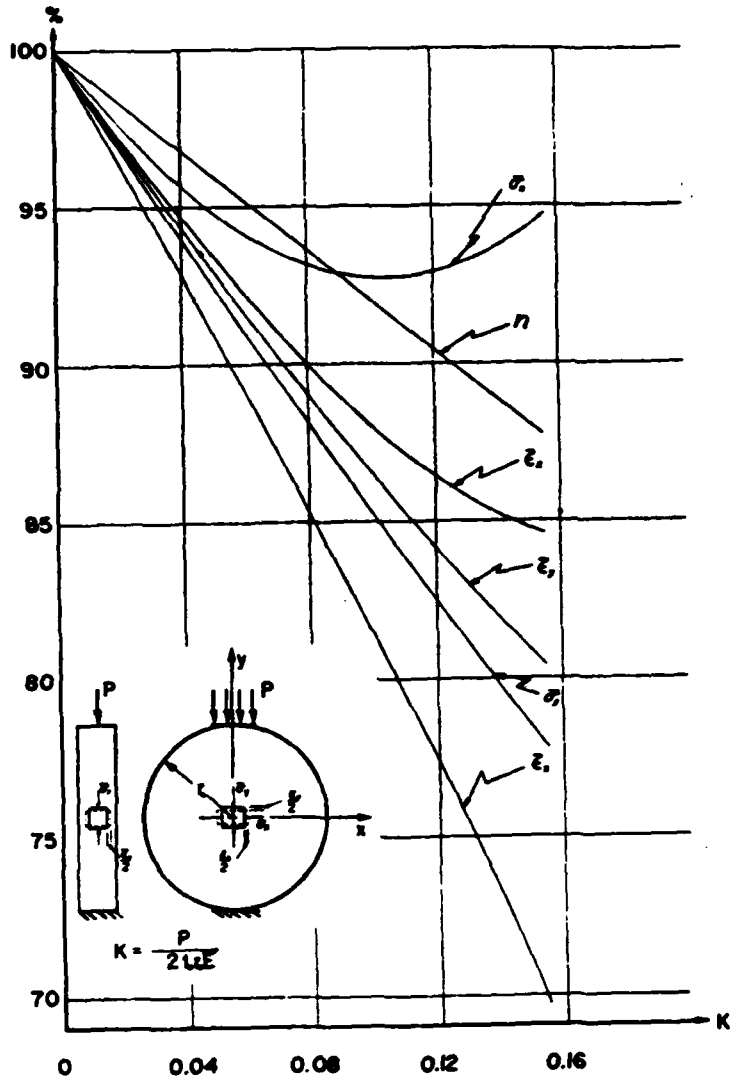

Figure 1.32. Stresses and strains, as function of load, at the center of a disk diametrically loaded, given as percent of the values obtained from the small strain theory.

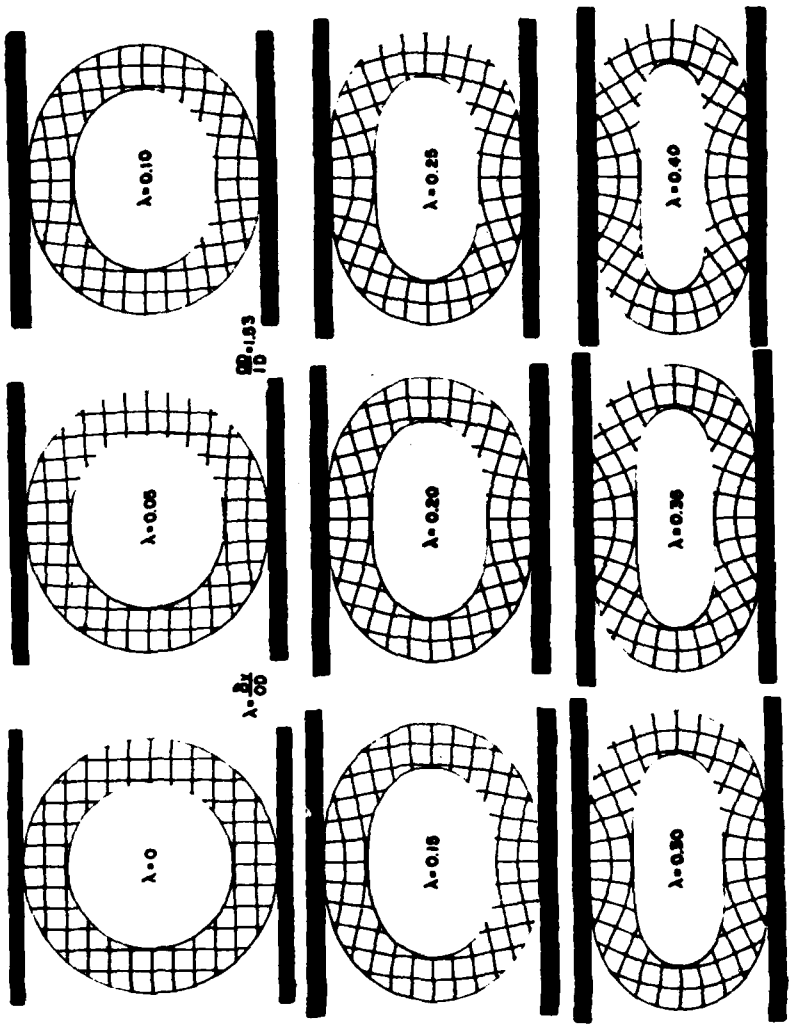

Figure 1.33. Cartesian grid on a circular ring subjected to several levels of diametral compression.

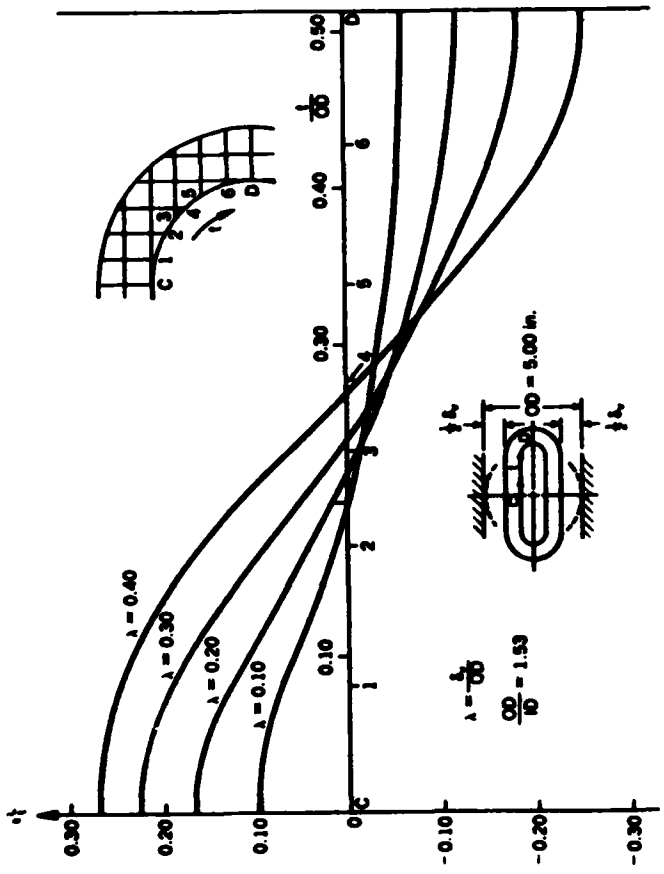

Figure 1.34. Lagrangian strain e_t^t tangential to the inner boundary of a circular ring subjected to several levels of diametral compression.

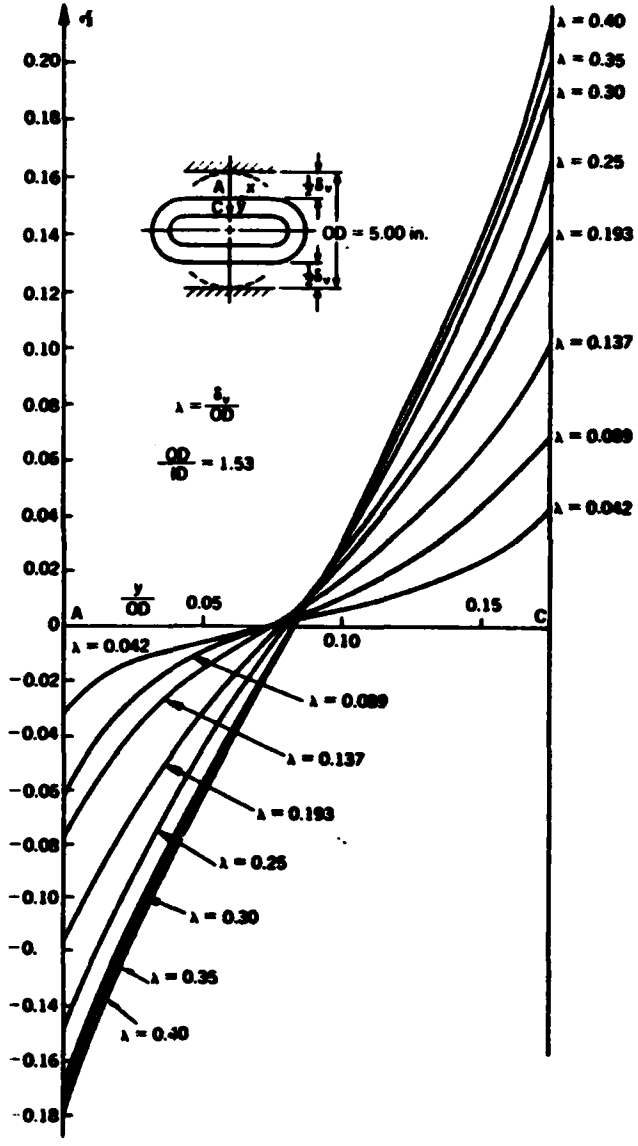

Figure 1.35. Eulerian horizontal strain e_x^x on the vertical axis of a circular ring subjected to several levels of diametral compression.

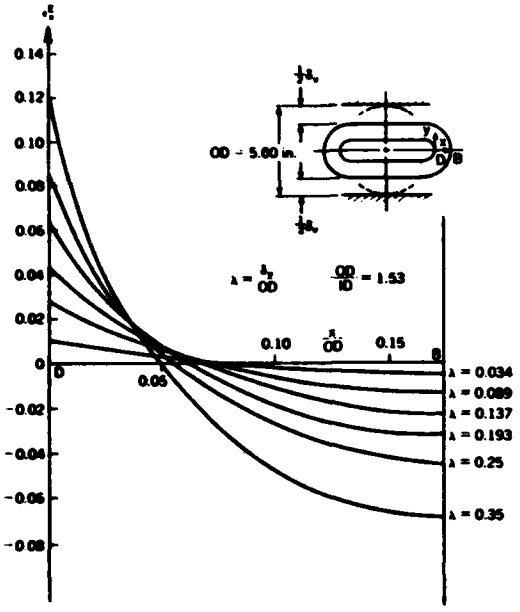

Figure 1.36. Eulerian horizontal strains ε_x^E on the horizontal axis of a circular ring subjected to several levels of diametral compression.

in its plane, is given in Figure 1.40 as function of D/W. As the hole becomes larger and it approaches the edge of the plate, large deformations may take place and the phenomenon is non-linear. Inconsistencies between results obtained by several investigators are probably due to the fact that their determinations were obtained at different load levels.

The matter was investigated [59] using the geometry shown in Figure 1.41 and the two materials the behavior of which is shown in Figure 1.42.

The strain concentration factor is given as a function of the level of deformation, expressed by ε_{av}, across the ligament or net area (Figure 1.43). The results obtained are particularly interesting in two respects: (1) the strain concentration factor varies from about 2 to 1, whether there is or not material non-linearity, and (2) there seems to be little variation between the strain concentration factor in the aluminum and the rubber, until the whole width of the aluminum ligament reaches the yield point. At this load, the strain concentration factor in the aluminum very quickly drops to unity.

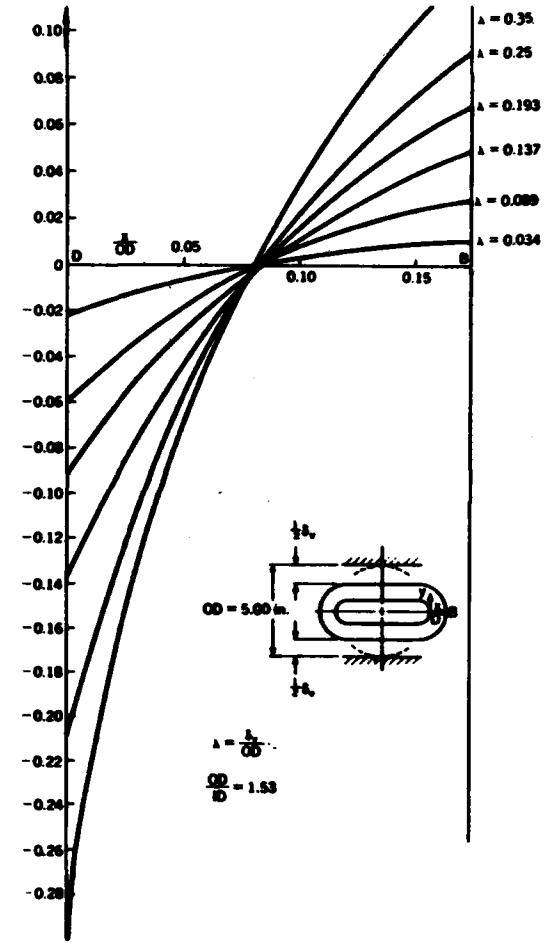

Figure 1.37. Eulerian vertical strain ε_y^E on the horizontal axis of a circular ring subjected to several levels of diametral compression.

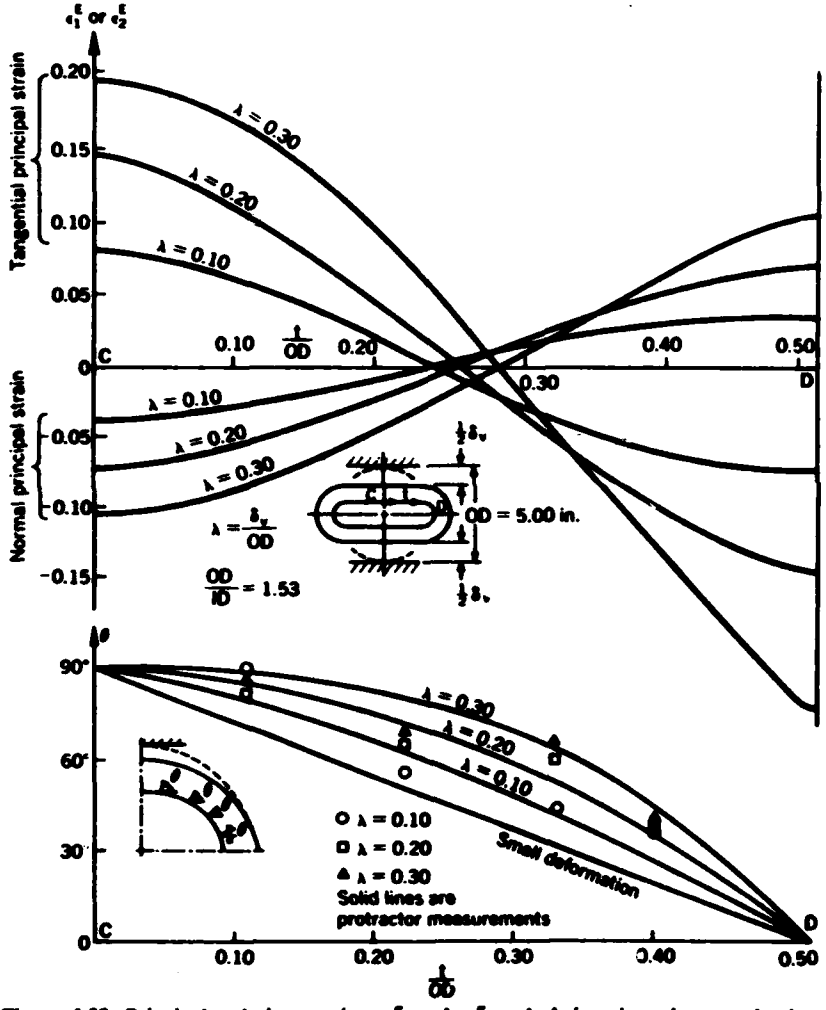

Figure 1.38. Principal eulerian strains e_1^E and e_2^E and their orientation on the inner boundary of a circular ring subjected to several levels of diametral compression.

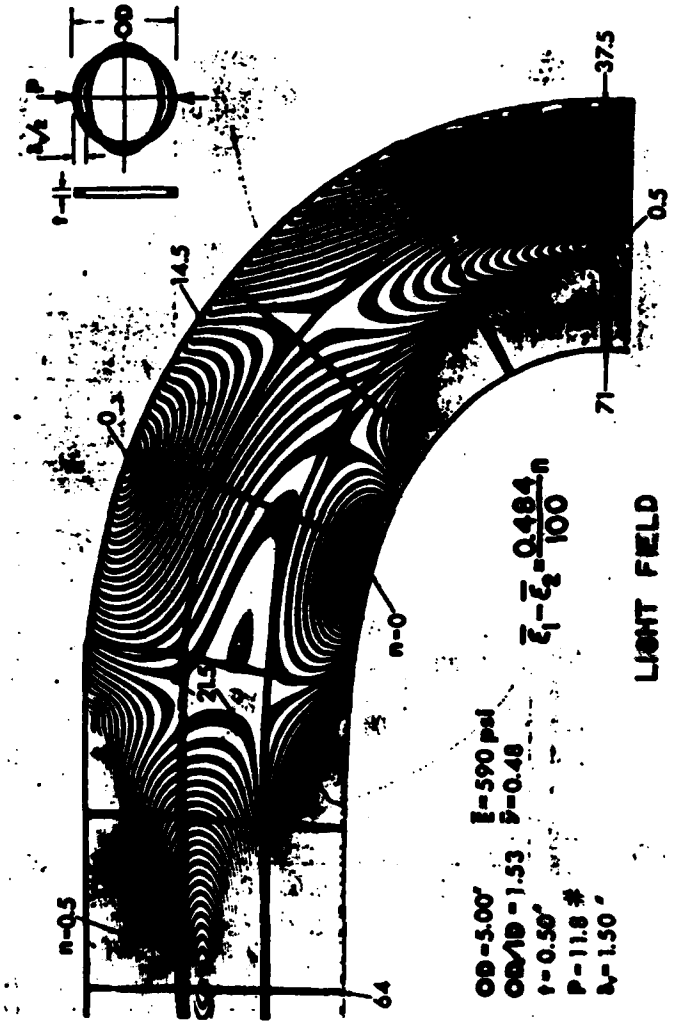

Figure 1.39. Isochromatics in a circular ring subjected to large diametral compression (obtained photoelastically).

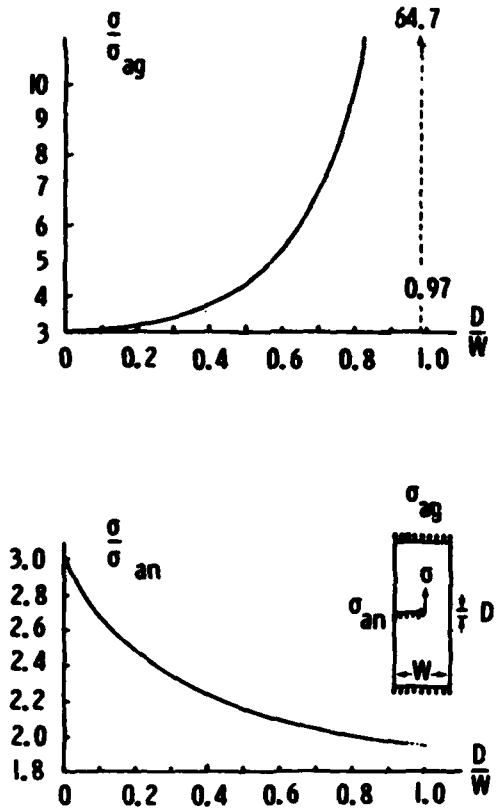

Figure 1.40. Stress concentration factors in an in-plane axially loaded finite plate with a circular hole, as function of the size of the hole.

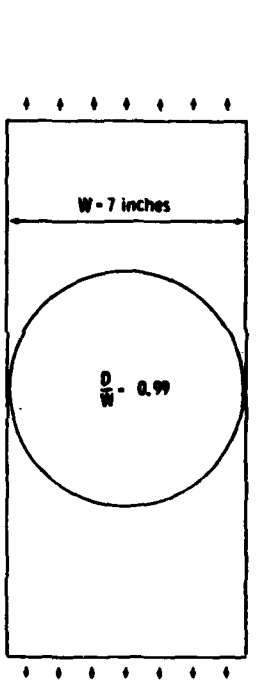

Figure 1.41. Geometry of the in-plane axially loaded plate with a big circular hole.

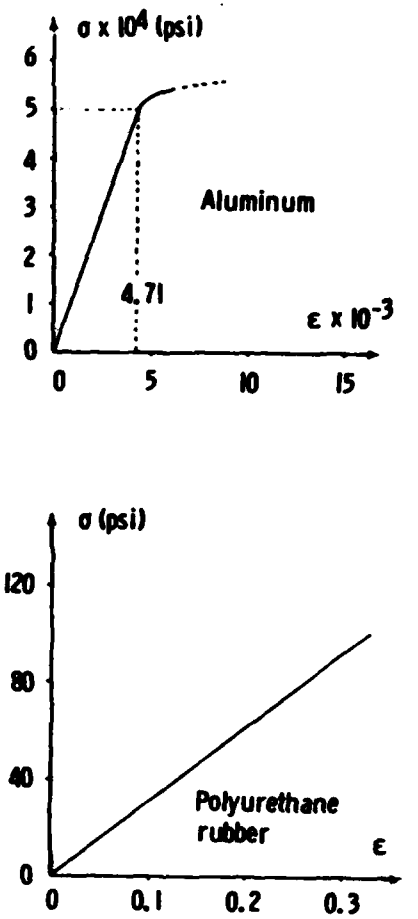

Figure 1.42. Mechanical properties of the materials used to determine the non-linear s.c.f.

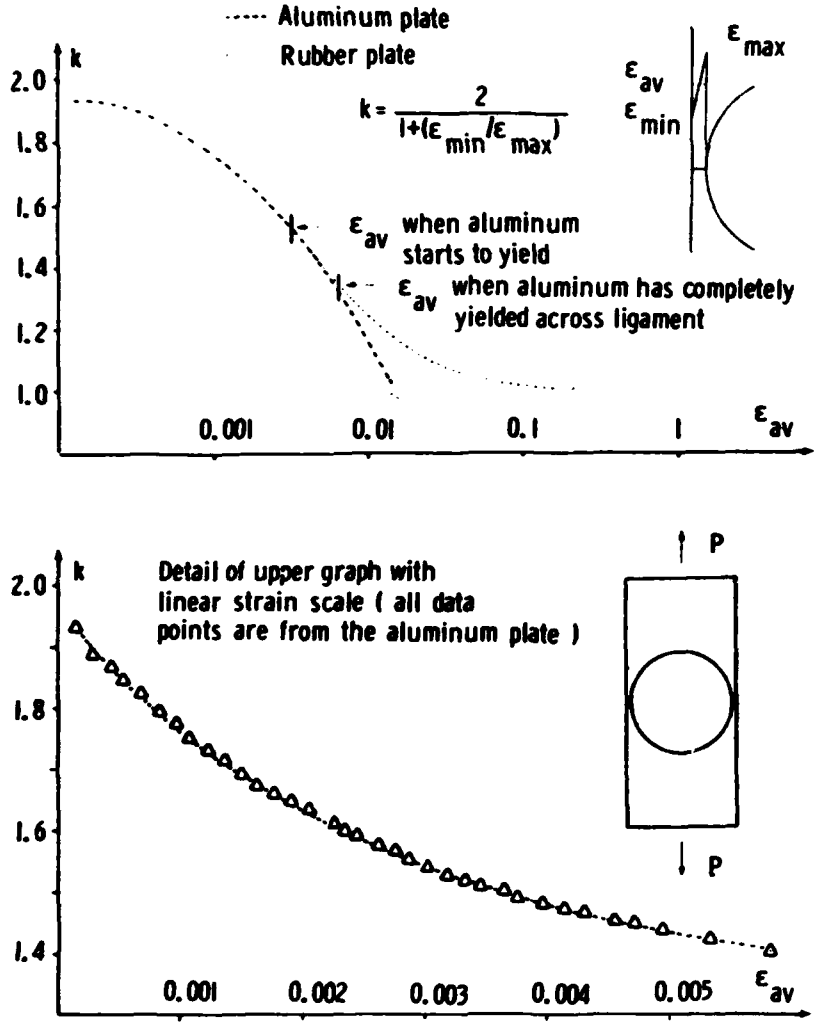

Figure 1.43. Stress concentration in a plate with a big hole, axially loaded in its plane, as a function of the level of deformation.

1.5 Stress concentrations in mixed boundary value problems

Most of the stress concentration factors listed in catalogs and easily available in the literature correspond to first boundary value problems and deal with notches and fillets. In this section some results will be shown of studies conducted to analyze concentrations in mixed-boundary value problems, and in particular at or near corners. The loading is the 'restrained shrinkage' produced by the difference in the free contraction or expansion of two bodies bonded to each other. Several thermal problems fall in this category. Restrained shrinkage can also develop in the process of curing or by absorption (or loss) of moisture. Applications are numerous in solid propellant rocket grains, composite materials, weldments, etc. Only the results obtained for two-dimensional problems are summarized in this section. Results corresponding to three-dimensional problems can be found in Section 1.7.

Stress concentration on the bonded interface of a strip with different end configurations. The long edge of the strip is bonded to a rigid bar. Loading is produced by the restrained shrinkage of the strip. The short ends of the strip have fillets of different configurations [60]. An illustration of the principal stresses at the interface is given in dimensionless manner in Figure 1.44 referred to α, free shrinkage of the strip, and E its modulus of elasticity. The stress concentration factor is shown in Figure 1.45.

Stress concentrations at variously shaped corners in rectangular bars bonded on two long edges, and subjected to restrained shrinkage. This problem arises when flat bars are bonded, cemented or welded on their top and bottom surfaces to other bodies of different mechanical or thermal characteristics. The free shrinkage of the bar is called α. The restraint in the longitudinal and the transverse direction of the bar could be the same in all directions, or have two perpendicular components α and $k\alpha$, where k a number smaller than unity is the ratio between the transverse and the longitudinal restraint. Restraint may be in only one direction, the direction of the length of the plate ($k = -\nu$, Poisson's ratio). By subtraction of one from the other of these loading conditions a variety of other biaxial conditions can be obtained [62, 63], Figure 1.46. The geometry of the corners investigated is shown in Figure 1.47.

The distributions of maximum shear stresses, and the distribution of

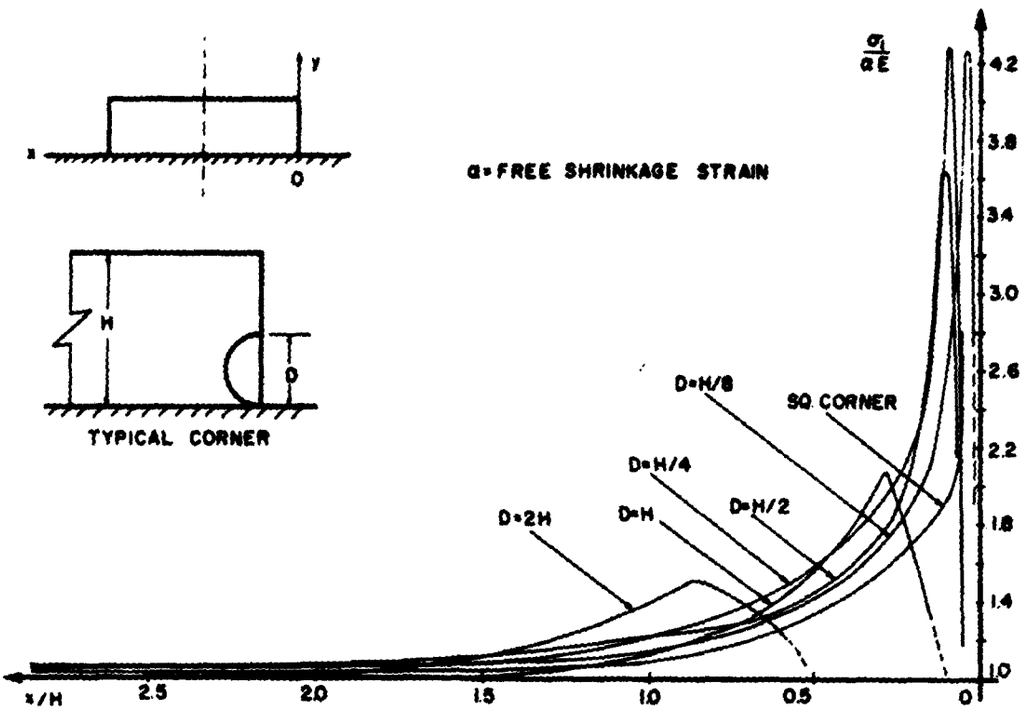

Figure 1.44. Principal stress σ_1 along the bonded edge of plates subjected to shrinkage.

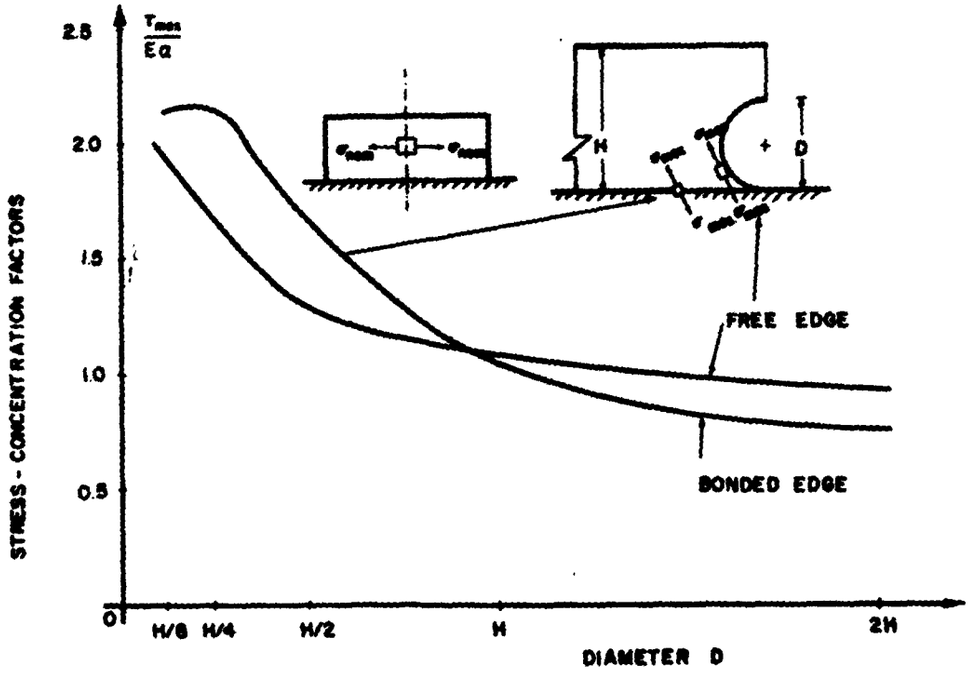

Figure 1.45. Stress-concentration factor in plates bonded along one edge.

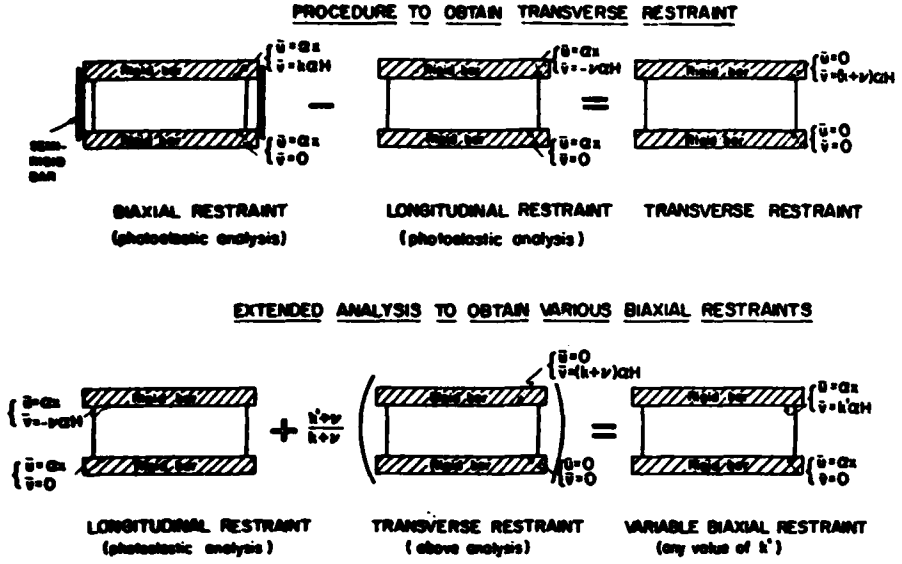

Figure 1.46. Schematic diagram indicating the procedure to obtain any ratio of biaxial restrained shrinkage.

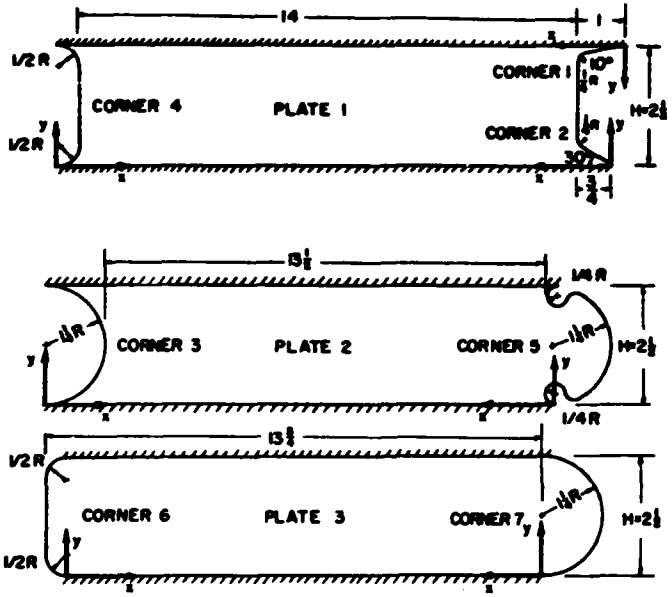

Figure 1.47. Dimensions of the three models used to analyze the strains associated with 7 different geometries of junctions of bonded and free boundaries.

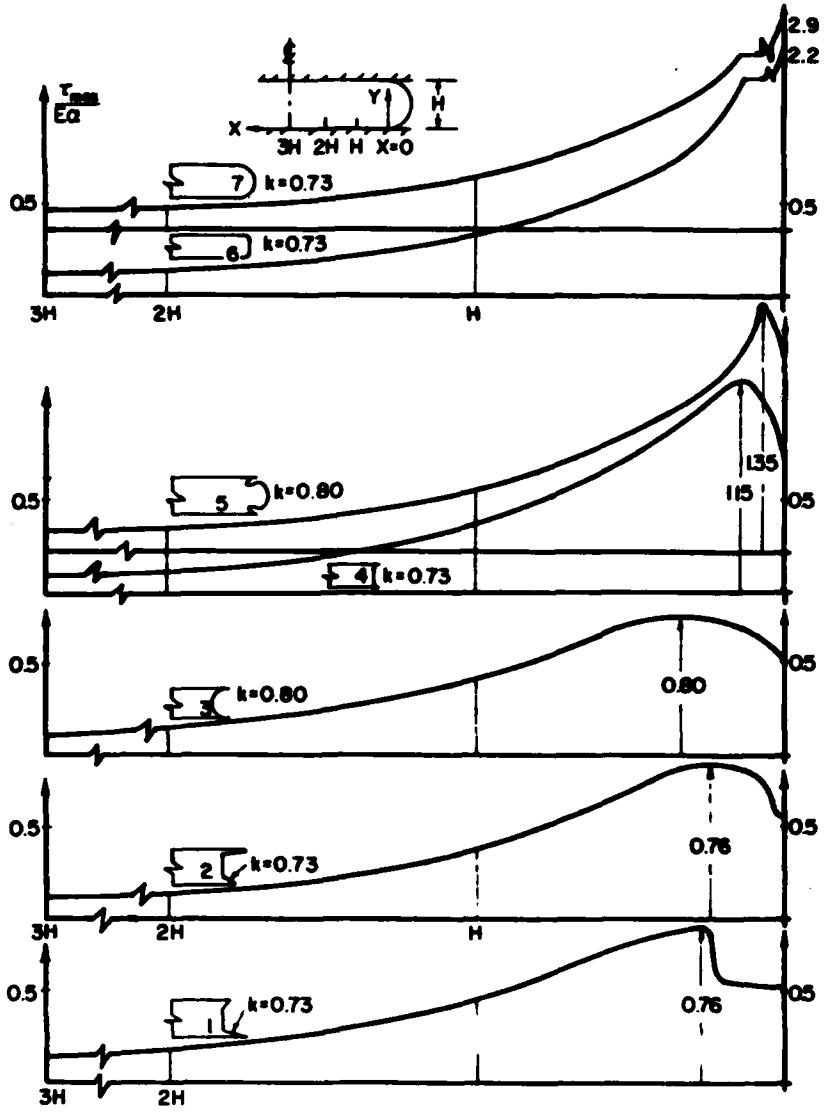

Figure 1.48. Maximum shear stresses along bonded edges of the shrunk plates subjected to biaxial restraint.

the cartesian shear stresses along the interface for both longitudinal and biaxial restraints have been obtained. An illustration is shown in Figure 1.48.

A summary of the stress concentrations factor (in terms of maximum shear, and also in terms of maximum cartesian shear) is shown in Figures 1.49 and 1.50.

These analyses of stresses are obviously very important in the study of crack propagation at interfaces. More information can be found in [61, 62].

CORNERS WITH PEAK τ_{max} ON INTERFACE			
TYPE OF CORNER $k = \frac{\text{transv. restraint}}{\text{longit. restraint}}$	k	PEAK VALUE OF $\tau_{max}/E\alpha$	PEAK VALUE OF INTERFACE SHEAR $\tau_{xy}/E\alpha$
⑦	0.73	2.9	2.7
⑥	0.73	2.2	2.1

CORNERS WITH PEAK τ_{max} ON FREE BOUNDARY		
TYPE OF CORNER	k	PEAK VALUE OF $\tau_{max}/E\alpha$
⑤	0.80	1.9
①	0.73	1.8
②	0.73	1.5
④	0.7	1.4
③	0.80	1.0

α = free shrinkage

Figure 1.49. Comparison of stresses in the neighborhood of corners (plates subjected to biaxial restraint).

CORNERS WITH PEAK τ_{max} ON INTERFACE		
TYPE OF CORNER	PEAK VALUE OF $\tau_{max}/E\alpha$	PEAK VALUE OF INTERFACE SHEAR $\tau_{xy}/E\alpha$
⑦	1.6	1.0
⑥	1.7	1.4

CORNERS WITH PEAK τ_{max} ON FREE BOUNDARY	
TYPE OF CORNER	PEAK VALUE OF $\tau_{max}/E\alpha$
⑤	1.0
①	0.9
②	0.8
④	1.0
③	0.8

α = free shrinkage

Figure 1.50. Comparison of stresses in the neighborhood of corners (plates subjected to longitudinal restraint).

Stress concentrations at corners of slabs with different edge geometries, when bonded on one face and shrunk. The situation is found when flat surfaces of two bodies are bonded, cemented or welded to each other and subjected to thermal or mechanical differential shrinkage [63]. The boundary conditions are illustrated in Figure 1.51. The stress concentration factors for five different geometries are shown in Figure 1.52. Typical distribution of normalized stresses are shown in Figures 1.53 to 1.55.

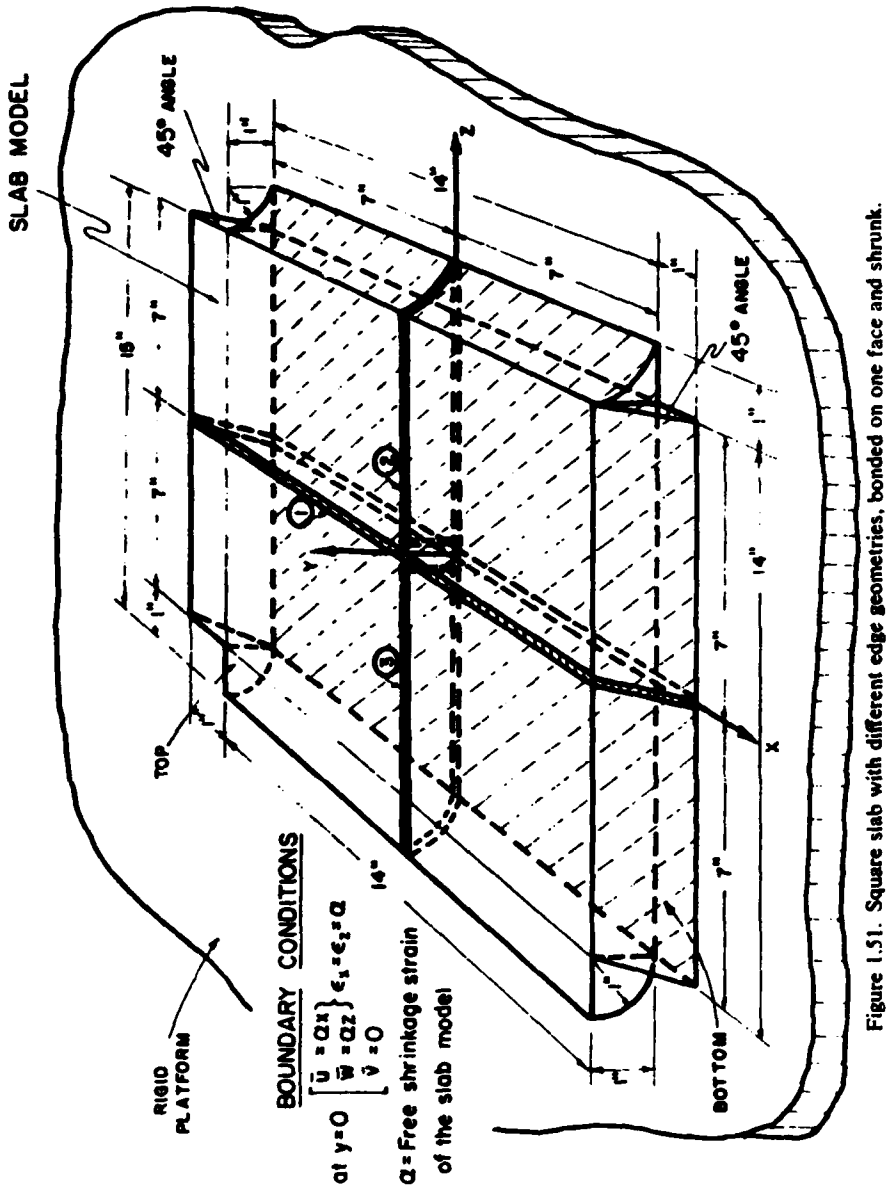

Figure 1.51. Square slab with different edge geometries, bonded on one face and shrunk.

GEOMETRY	K = max $\tau_{max}/E\alpha$
Max. concentration	3.4
45° Max. conc.	3.3
Max. conc.	3.0
60° Max. conc.	1.9
90° Max. conc.	1.7

Figure 1.52. Stress concentration factors for five different edge geometries.

Considerations on analysis at corners. The corner at the intersection of the bonded and free edges is particularly difficult to analyze. The free edge requires that $\sigma_n = 0$ and $\tau_n = 0$. If it is assumed that on the bonded edge $\varepsilon_x = a$, for a square corner Hooke's law then requires a negative tangential stress and strain on the free boundary, $\sigma_y = -Ea/\nu$ and $\varepsilon_y = -a/\nu$. Analysis of the isochromatics along the free edge shows the fringes to represent a positive σ_y everywhere at the free boundary (increasing to a high positive value as the free boundary approached the bonded boundary). This discrepancy (between a negative and a positive

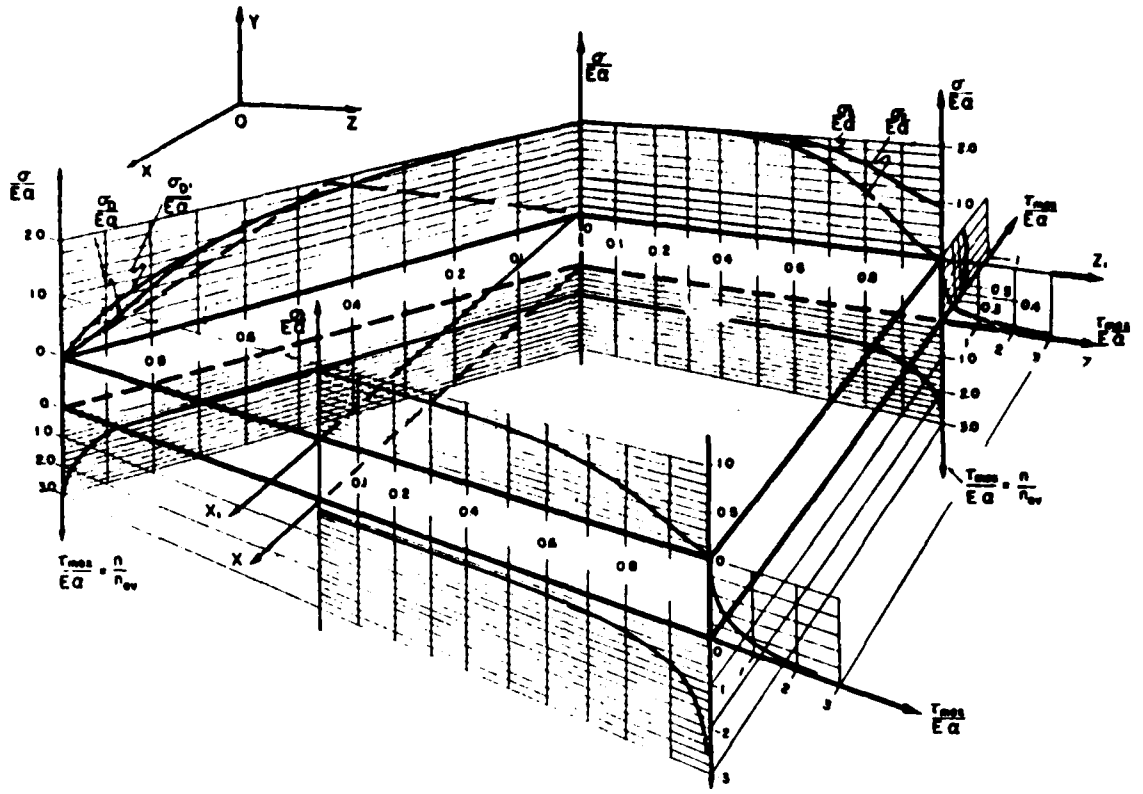

Figure 1.53. Normalized stresses at the principal planes of the top and bottom faces of the square slab bonded on one face and shrunk.

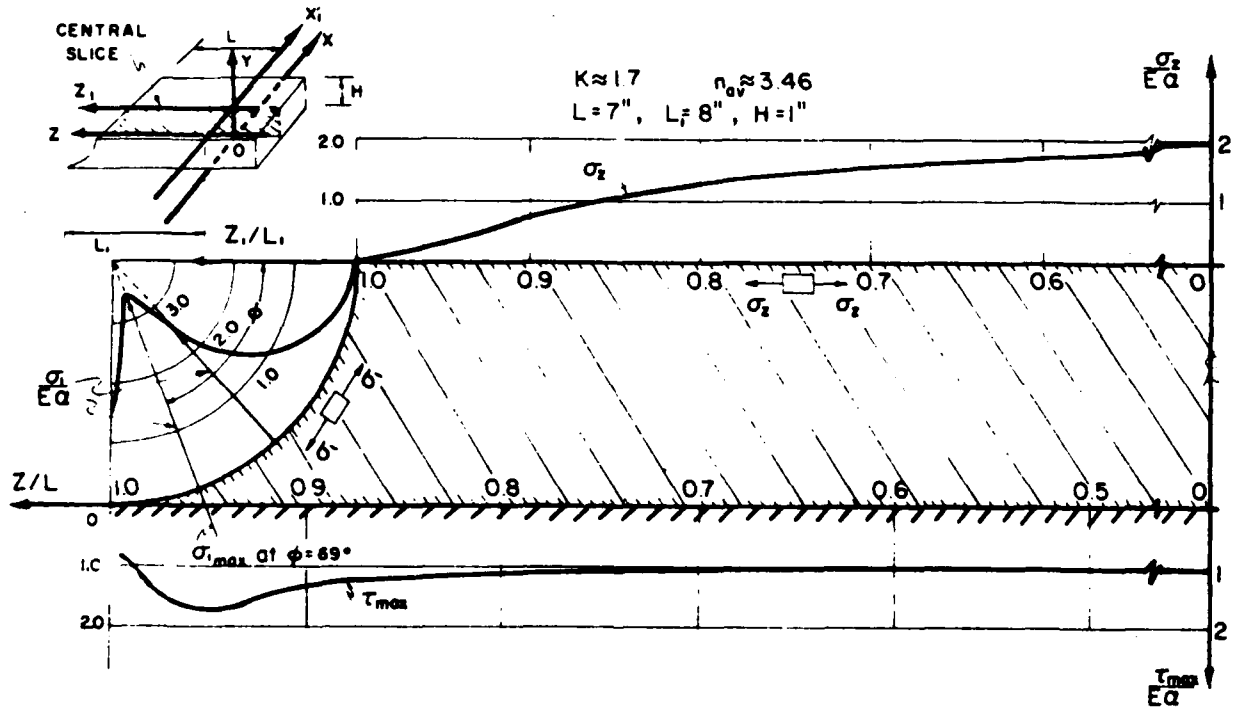

Figure 1.54. Normalized stresses at the boundaries of the central slice of a slab, bonded on one face and shrunk. (Geometry: concave corner).

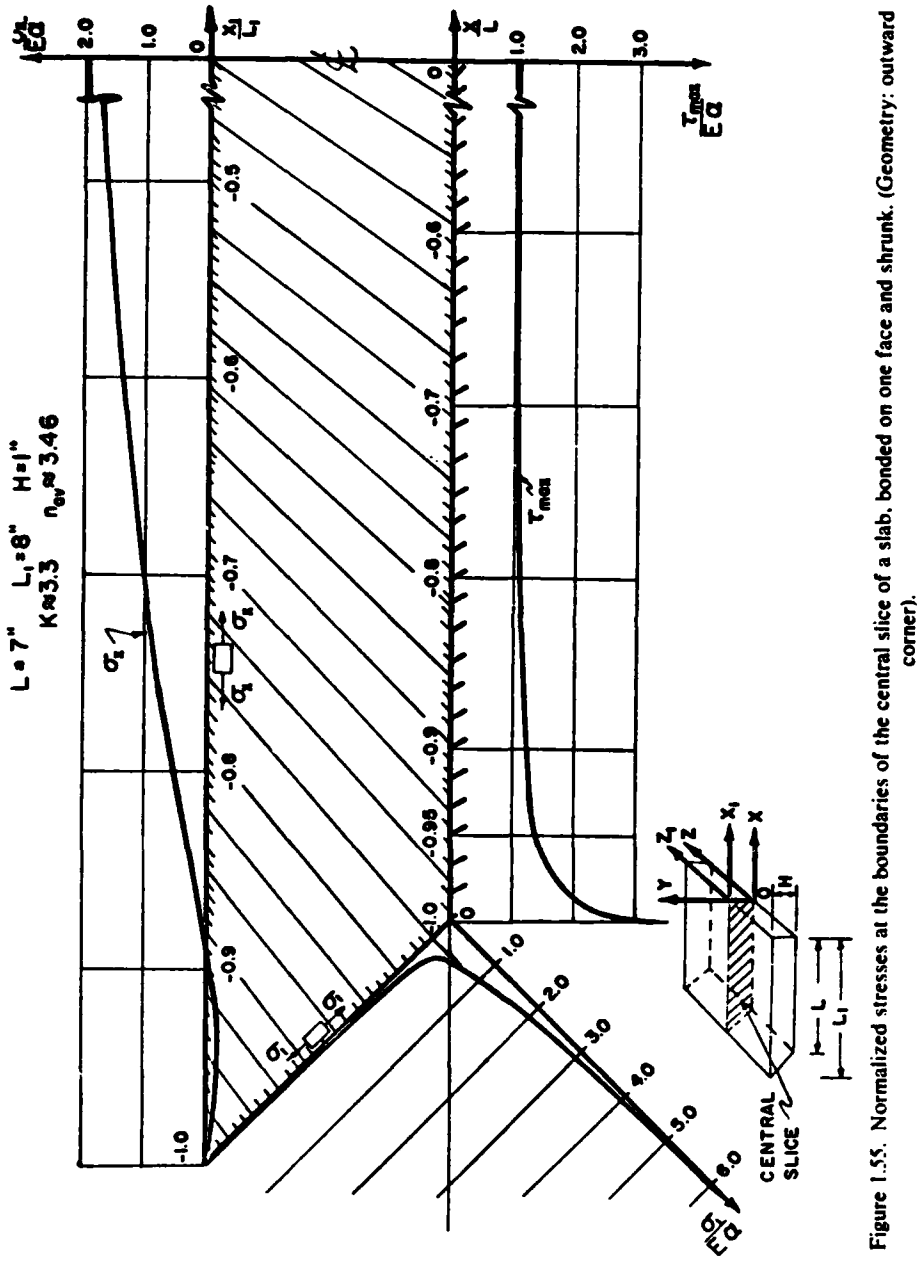

Figure 1.55. Normalized stresses at the boundaries of the central slice of a slab, bonded on one face and shrunk. (Geometry: outward corner).

value for σ_y) suggests that very near the corner a complicated situation develops. Thus, for example, if on the free boundary within less than a thousandth of an inch of the corner, σ_y changes to negative, there would be an isotropic point which may be very difficult to detect.

The following comments should also be considered: (1) the corner geometry cannot be ideally square and probably had a radius of the order of 0.001 in., (2) the optical and photographic techniques used do not permit a higher resolution than 0.001 in., (3) the thickness of the plate used was 0.125 in. In the neighbourhood of the corner (closer than 0.125 in.) the elastic phenomenon is probably three-dimensional and only an approximate analysis can be conducted with the two-dimensional techniques. Results obtained using three-dimensional methods (Fig. 1.54) are more representative in this respect.

It is also possible that the boundary condition $\varepsilon_x = \alpha$ is not valid all the way up to the corner. To satisfy the condition of a positive tangential stress, it is necessary that ε_x be compressive; however, the existence of a compressive ε_x at the corner could not be substantiated by a moiré analysis using 1000 lines per inch along the bonded edge. Again, as with photoelasticity, it is possible that very near the corner the sensitivity of the methods used may not be sufficiently high to record the phenomenon.

The theoretical solutions do not appear helpful in this respect. Solutions given by Duffy [64] and Theocaris and Dafermos [65] show the corner as a singular point at which all the stresses approach infinity, which is physically impossible. In particular, the tangential stress, σ_t is shown to have an unbounded positive value. One theoretical solution by Aleck [66] shows a finite positive value of σ_t, but does not satisfy the condition $\varepsilon_x = \alpha$ near the corner.

It is recognized that there is a considerable distortion at the corner. This suggests another possible explanation of the difficulty. The distortion at the corner may be sufficient to produce a geometry that *does* allow positive values of tangential stress with positive values of ε_x. To see what the geometric relation of the free boundary to the bonded boundary would have to be for resolving the difficulty, consider the combined Mohr circle of stress and strain (plane-stress) shown in Figure 1.56.

The tangential stress and normal stress on the free boundary are given as σ_t and σ_n ($\sigma_n = 0$). Circles of strain are drawn for $v = 1/2$ and $v = 1/3$. It can be seen that to obtain positive values of strain along the bonded edge, the angle β between the bonded edge and the free edge can be no greater than 55° for the $v = 1/2$ or 60° for $v = 1/3$.

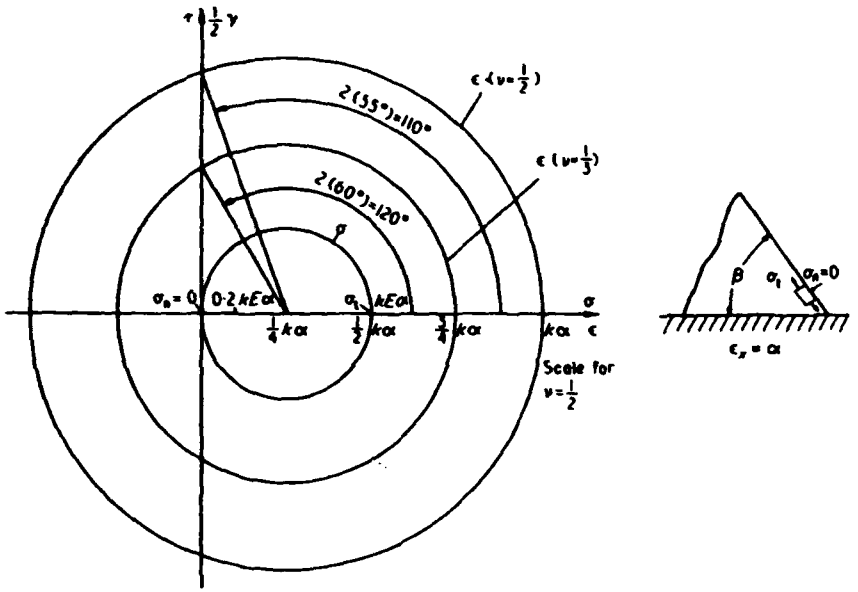

Figure 1.56. Mohr's circle to relate stresses and strains at a corner of a bonded and a free edge.

If the value of $\sigma_t = 10\,E\alpha$, for $v = 1/2$ the angle needed to produce $\epsilon_x = \alpha$ on the bonded edged is about 50°. If the reasoning were correct, however, this angle should appear as soon as any amount of shrinkage is applied to the restrained boundary.

Stress concentrations associated with notches in a restrained shrinking disk. Stress concentrations associated with notches in infinite, semi-infinite and finite plates have been studied with great detail, as shown in some of the sources reviewed in Section 1.4. Few systematic studies have been conducted however when the plates have more complicated boundary conditions. Here results are given for the case of a circular disk with a diametral slot of variable length, and of variable radius at the notch end [67]. The outer perimeter is subjected to a restrained shrinkage α, as when bonded materials with different thermal coefficients of expansion are subjected to a change in temperature. The problem was solved using photoelasticity and Figure 1.57 shows the geometry of the several cases investigated. All the results obtained are shown

CUT	1	2	3	4	5	6	7	8	9	10	11	12	13	14	15	16	17
L/D	.086	.167	.333	.333	.333	.417	.417	.500	.500	.583	.583	.667	.667	.833	.833	.940	.940
W/D	.086	.048	.048	.048	.144	.048	.144	.048	.144	.048	.144	.048	.144	.048	.144	.048	.144

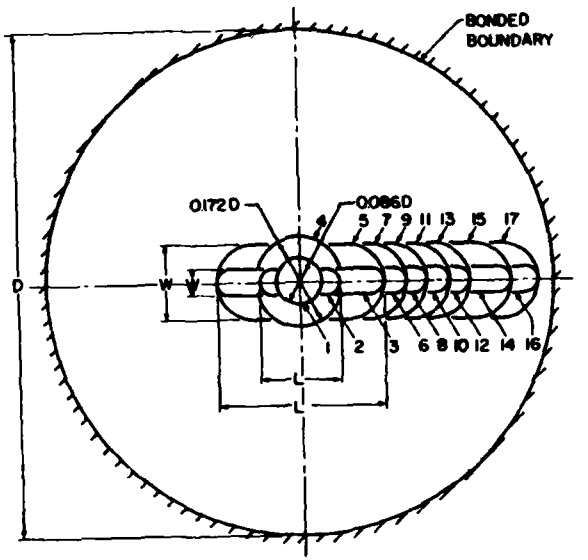

Figure 1.57. Cutting plan to obtain a series of isochromatics patterns from a single urethane rubber disk bonded to a rigid ring.

parametrically in Figure 1.58. It is interesting to note that, as is the case for the cracks usually considered in fracture mechanics, the isochromatics axis do not follow the axis of the slot. The maximum values are on either side of the tip.

Stress concentrations around elliptical holes in shrunk plates with bonded boundaries and discontinuities in bond. If the boundaries of a plate are bonded partially or totally to a rigid frame and the plate is then shrunk, a biaxial stress field is set. The plate may have straight or semicircular boundaries. If a hole is cut tangent to the boundary, a stress concentration will be induced along the free boundary of the hole, and the plate will fail in this region when the shrinkage becomes too large. In specimen 1 all plate boundaries were bonded, and one elliptical hole was located longitudinally at one apex of the plate and another was located

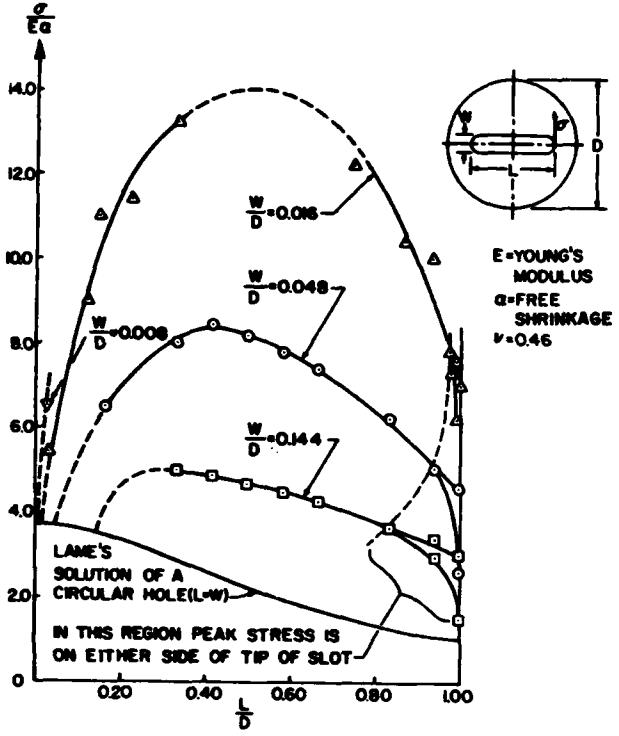

Figure 1.58. Stress concentration factors for slots with semi-circular ends in a disk restrained at its outer boundary and shrunk.

transversely at the other apex. In specimen II the plate was bonded only along the straight boundaries, and the circular boundaries were free. Two elliptical holes were located longitudinally at the point of discontinuity between bonded and unbonded boundaries at one end of the plate, and two more were located transversely at similar points on the other end. The sizes of the holes were varied systematically. All elliptical holes had a 2:1 ratio of major axis a to minor axis b (Figure 1.59).

Figure 1.60 shows typical isochromatic patterns near elliptical holes located longitudinally and transversely at the point of discontinuity between bonded and unbonded boundaries [68]. The stress concentration factor $K = \sigma_{max}/E\alpha$ obtained in this study is restricted to locations at the free boundaries of the holes. Here σ_{max} is the maximum tangential stress at the free boundary, E is Young's modulus, and α is the free shrinkage.

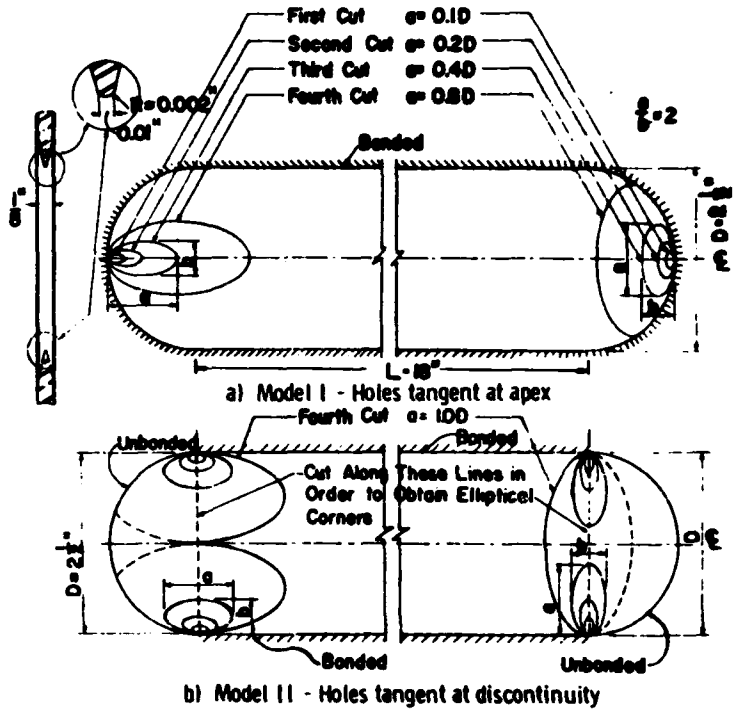

Figure 1.59. Geometry of plates with bonded boundaries and with discontinuities in bond.

Figure 1.61 shows the results for the two photoelastic models made with an incompressible material. For specimen I, Figure 1.61*a* the maximum stress associated with elliptical holes with major axes parallel to the transverse direction exceeds that for holes with major axes parallel to the longitudinal direction. In both cases, the peak K occurs at $a/D = 0.3$. For model II Figure 1.61*b* the relative values of K for the two orientations of the holes was opposite to the previously mentioned result.

If the semicircular ends in the second model were cut straight along its diameter, as indicated in Figure 1.59 the plate would become a long rectangular plate with free, short, straight edges. The maximum stresses at the elliptical corners obtained in this case have values very close to those of the original model with a maximum deviation of 6%. Therefore, the results given in Figure 1.61 can be also used for such cases.

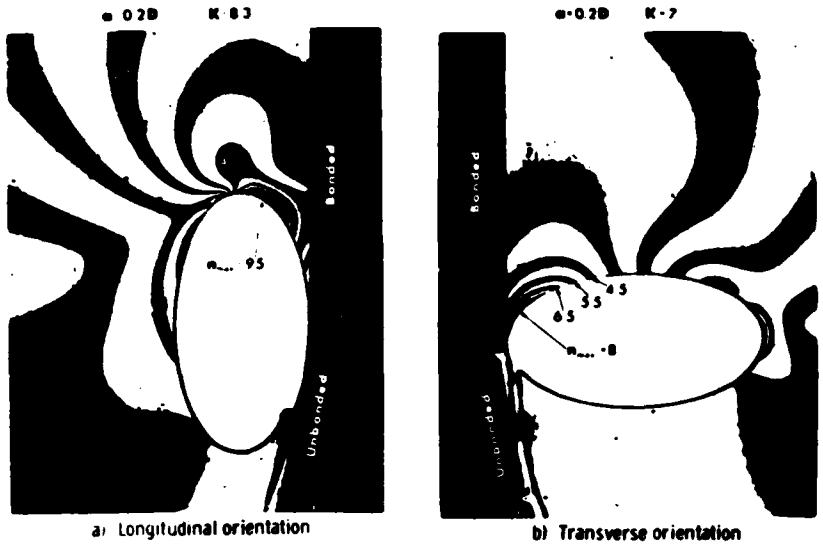

Figure 1.60. Enlargements of isochromatics in neighborhood of elliptical holes at discontinuity of bond.

Curves for circular holes ($a = b$) also were obtained and are incorporated in Figures 1.61 and 1.62. Figure 1.62 shows K vs A/A_0, the ratio of hole area ($A = \pi ab/4$) to equivalent cross-sectional area ($A_0 = \pi D^2/4$), which may be significant in cases of cylinders. Finally, Figure 1.63 shows k vs a/b for various values of A/A_0. All curves seemed to have minimum values near $a/b = 1$ (a circular hole).

Thermal stress concentration at the interfaces in three-ply laminates. The middle layer of the laminate is made of a material which differs from that of the top and the bottom layers, and may tend to expand or shrink, when the temperature changes, to an amount different from the amount of expansion or shrinkage of the exterior layers. The geometry of the laminate used for the photoelastic tests and the stress distribution are shown in Figure 1.64. Fracture starts at small regions of the interface, and at a short distance from the corner. The location of these regions correlates well with the position of the stress concentration. More information can be found in [69].

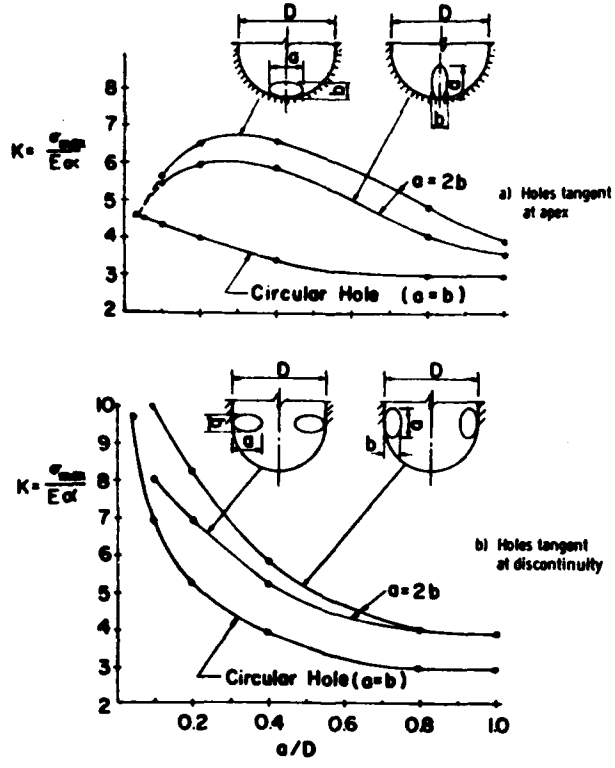

Figure 1.61. Parametric stress concentration factors (k vs a/D) for various elliptical holes in plates with bonded boundary, subjected to restrained shrinkage.

Stress concentration at the angular corners of long strips bonded on one end and shrunk. The configuration of the strip used for the tests is shown Figure 1.65. One end of the strip is a plane inclined at different angles ϕ with respect to the longitudinal axis and has a radius R at the corner. Three different corners with radius $R = \frac{1}{8}$ in., $\frac{1}{32}$ in. and a radius of less than $\frac{1}{10,000}$ in. were used. While the first two were formed by using $\frac{1}{4}$ and $\frac{1}{16}$ in. diam routers, respectively, the last one was obtained using a stainless-steel plastic-coated razor blade. The end angle $\phi = 0$ deg (equivalent to a crack) was obtained by forcing the blade into the rubber along the knife edge of the bonding bar.

The configuration of the tip of the cut made with the razor blade is

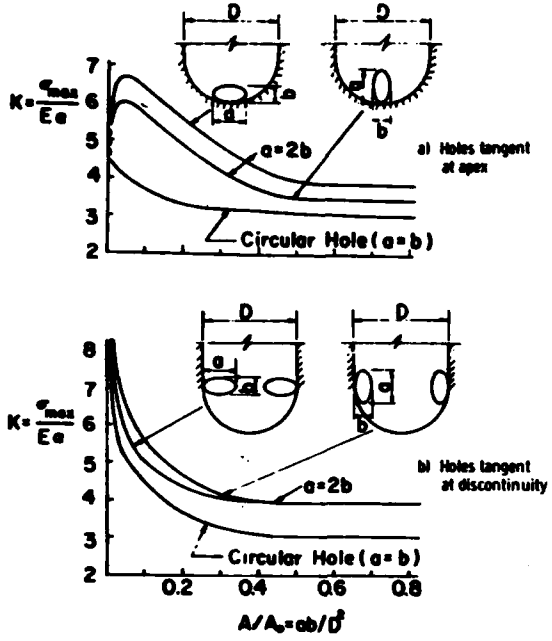

Figure 1.62. Parametric stress concentration factors (K vs A/A_0) for various elliptical holes in plates with bonded boundary, subjected to restrained shrinkage.

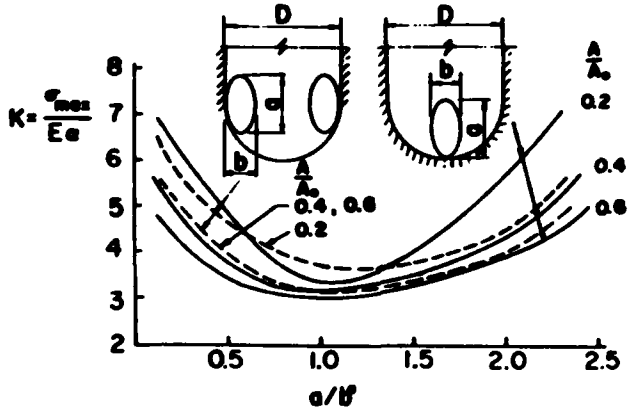

Figure 1.63. Parametric stress concentration factors (K vs a/b) for various ratios of elliptical holes in plates with bonded boundaries, subjected to restraint shrinkage.

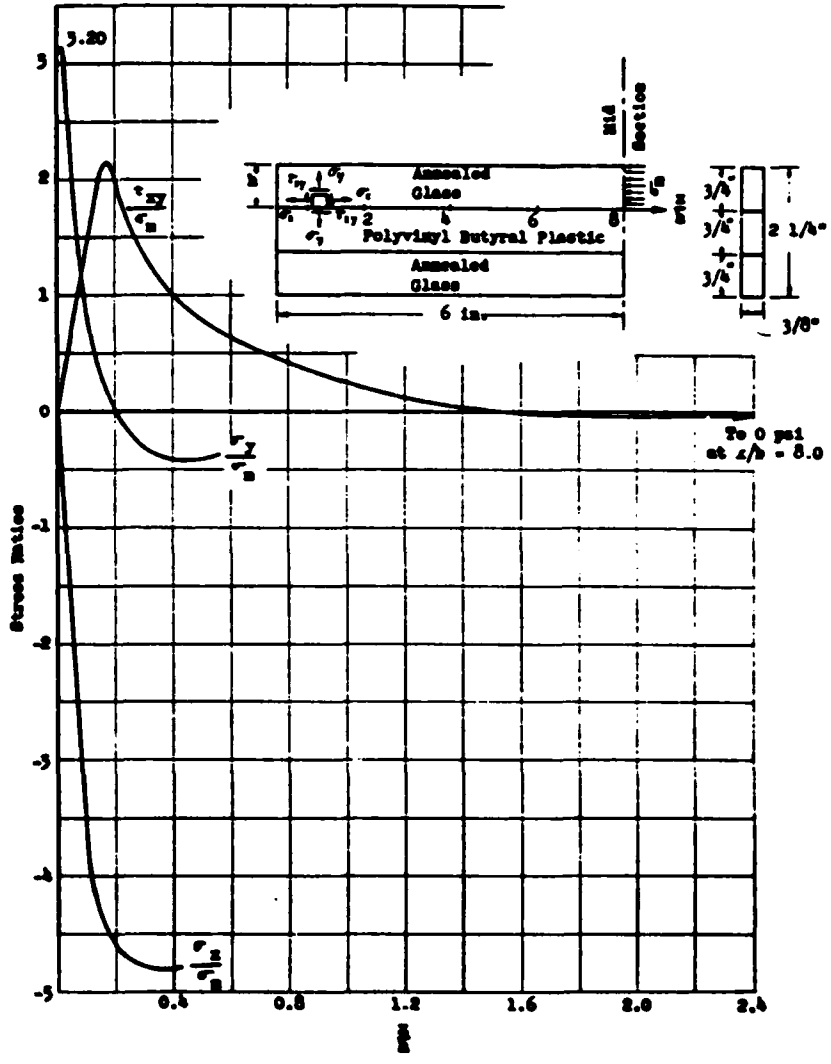

Figure 1.64. Normal and shear-stress distribution along glass-plastic interface at—20 F. (Positive stress ratios denote either tension or type of shear shown in sketch.)

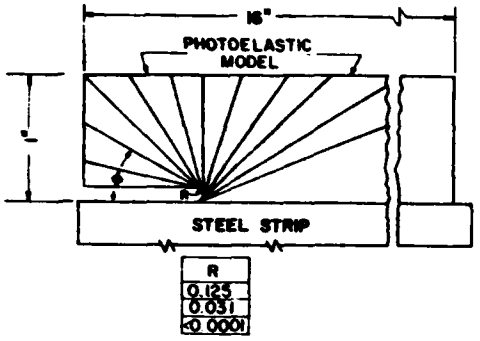

Figure 1.65. Dimensions of the photoelastic model subjected to restrained shrinkage showing progression of cuts to obtain various angles.

probably not circular. It has been estimated, however, that the crack tip has a curvature of less than 0.0001 in.

Stress concentration factors for end angles ϕ varying from 0 to 180 deg and corners radii $R = \frac{1}{8}$, $\frac{1}{32}$ and $< \frac{1}{10,000}$ in. are plotted in Figure 1.66. It is interesting to see that peaks of stress concentration occur at approximately $\phi = 90$ deg as well as $\phi = 0$. The optimum acute angle seems to be in the neighborhood of 60 deg.

In the results shown in Figure 1.66, the triangles and the solid circles and squares are data points obtained using two different machining techniques. The scattering of the data can be seen in the figure.

The position of the point of maximum stress is not located at the interface but somewhere above. This position changes as the angle ϕ changes. Figure 1.67 shows the variation for $R = 0.125$. It is interesting to know that for this case, the position and value of the s.c.f. practically do not change when ϕ changes from 0° to 110°.

More information can be found in [70]. Enlarged isochromatics are shown in Figure 1.68.

Stress concentration associated with cracks near a rigid boundary and subjected to restrained shrinkage. If the circular end of the slots shown in Figure 1.58 is made smaller and smaller, the matrix stress increases. Figure 1.69 shows the geometry of a slot made with the smallest width of all the slots that ended with a simple radius (and were tested in the program). Figure 1.70 shows the isochromatic pattern obtained from this model. The K factor is 9.2.

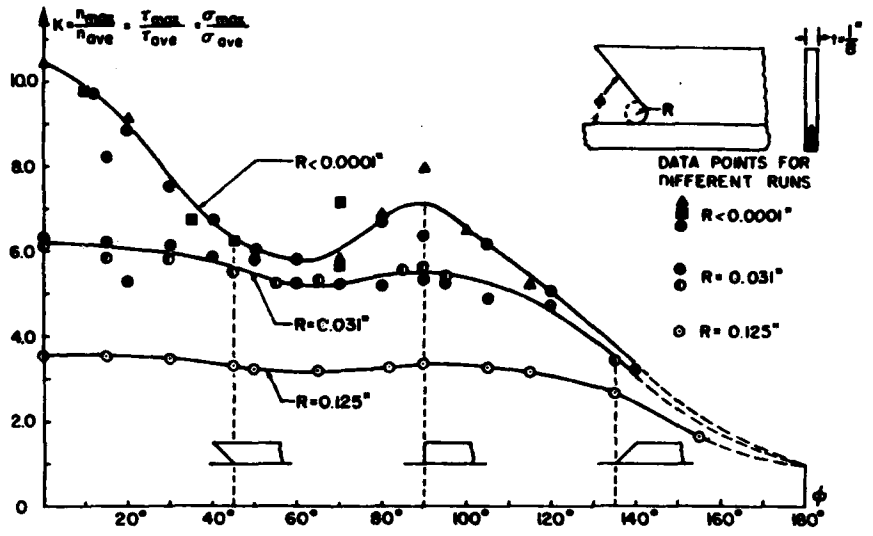

Figure 1.66. Parametric stress concentration factors for various angular corners.

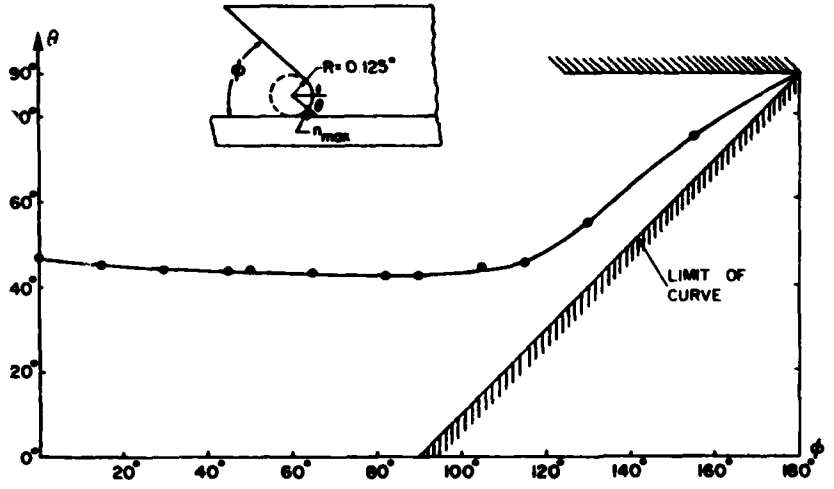

Figure 1.67. Positions of maximum stress at various angular corners.

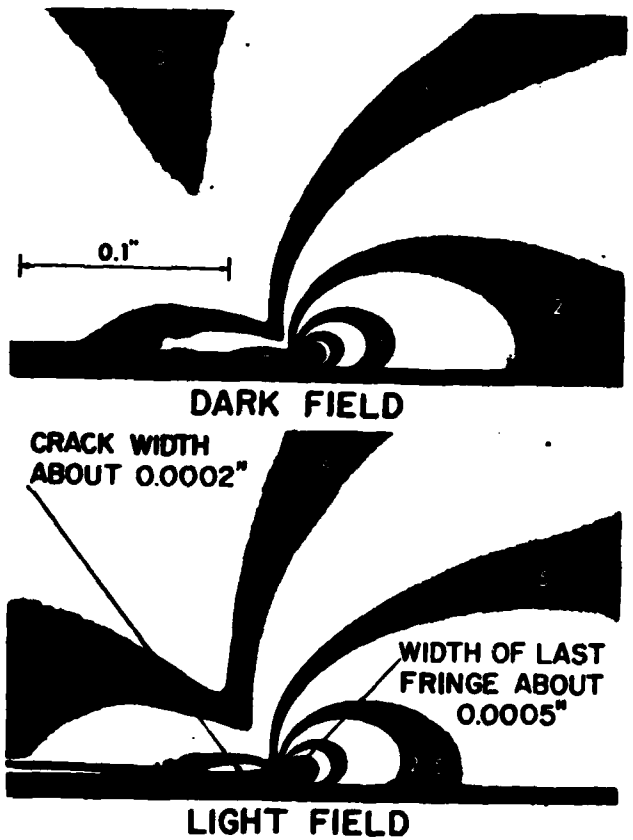

Figure 1.68. Enlargements of isochromatic field in the neighborhood of the corner of a crack.

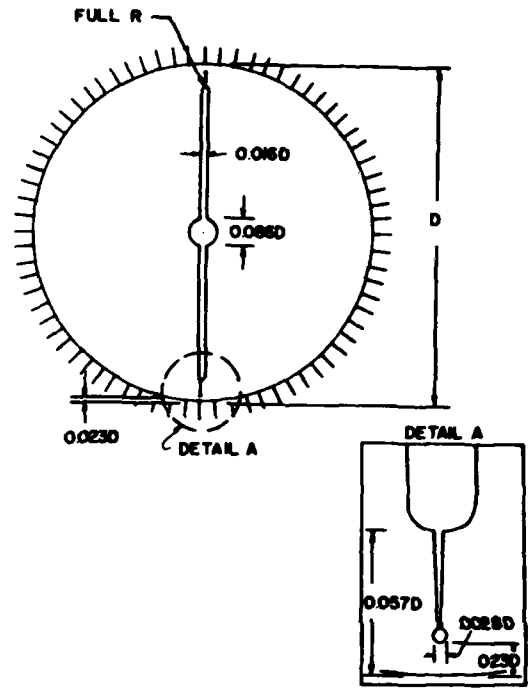

Figure 1.69. Circular disk with a slot ended with a small circular hole and subjected to restrained shrinkage.

The analysis of this type of model may be questioned. First the thickness of the model is about 12 times the radius at the tip of the slot. The surfaces of the model are in a condition of plane stress. The central portion of the model through the thickness can be thought to approach plane strain. The photoelastic analysis gives the result of an integral effect along the path of light. This is probably not a serious limitation. There is evidence to show that the difference between the two extreme situations of plane stress and plane strain ($\varepsilon_z = 0$) is not too large.

A more serious difficulty is the high level of the stress. As the radius becomes smaller, the same load produces higher stress and at some point the assumption of a linear relation between stress, strain and birefringence breaks down. This non-linear response can be avoided to some extent by reducing the load. It is believed that in the pattern shown in Figure 1.70 the fringe orders are not sufficiently great to exhibit

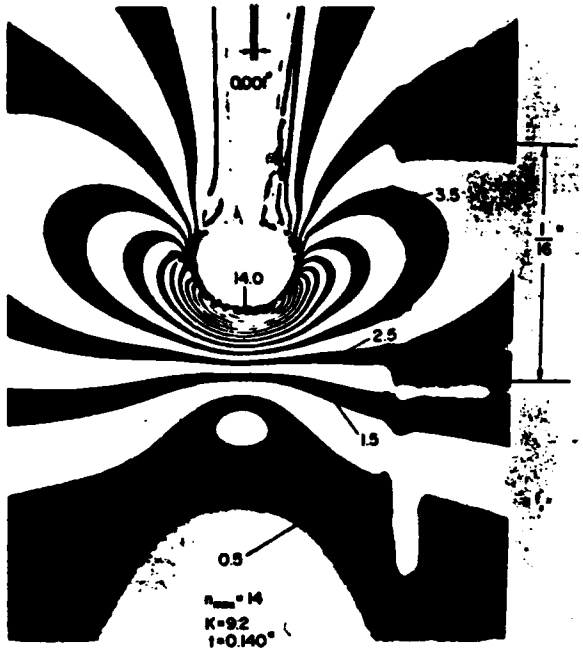

Figure 1.70. Isochromatics at the tip of a slot ended with a small hole in a circular disk subjected to restrained shrinkage.

marked non-linearity and it can be seen that the radius is not appreciably increased.

When these ideas are extended to the case of a crack, similar difficulties are encountered. In the isochromatic patterns around the slot it can be seen that most of the response takes place within a distance from the slot boundary, of the order of one slot width. It follows that a model of a crack must be viewed within approximately one crack width to obtain an estimate of the stresses at the tip.

Figure 1.71 shows the pattern around one crack with a shape similar to the one shown in Figure 1.69. The crack was started with a knife, and propagated spontaneously to the position shown in the figure. At the tip there may exist a much higher fringe order than the 10 or so fringes that can be seen in the photograph, and the three-dimensional and non-linear effects may be important.

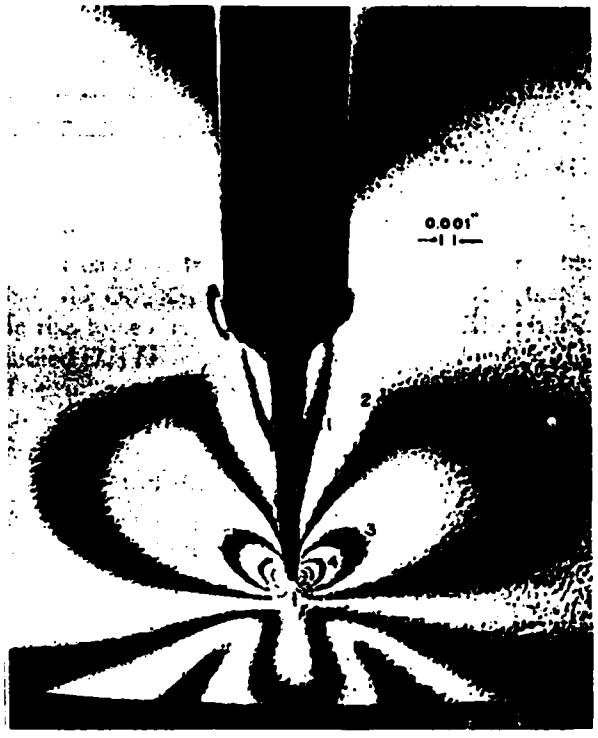

Figure 1.71. Isochromatics at the tip of a crack cut with a knife and propagated spontaneously in a circular disk subjected to restrained shrinkage.

It is to be noted that the maximum stress that is at the axis of the crack in Figure 1.70, shifts to the side of the crack in Figure 1.71. The distance between the bottom of the crack and the rigid boundary is 0.05 in. in the first case, and 0.015 in the second. The situation is also shown, in dimensionless manner, in Figure 1.58.

Stress concentrations in a rectangular plate with circular perforations along its two bonded edges and subjected to restrained shrinkage. In some cases stress concentrations associated with a hole or a fillet may be decreased by repeating the discontinuity. The geometry of the problem to be dealt with here is shown in Figure 1.72. The stresses are

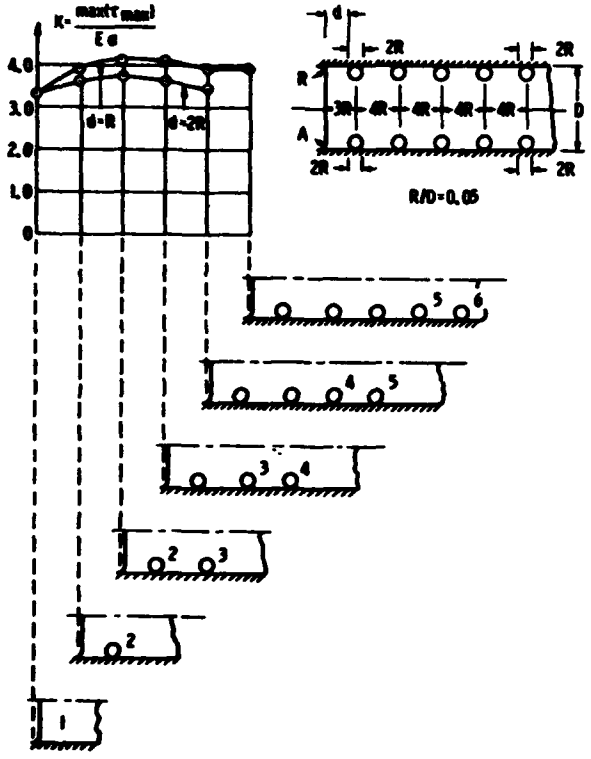

Figure 1.72. Stress concentration in rectangular plates with rows of holes along two bonded boundaries, subjected to restrained shrinkage.

determined for the case of no hole, one hole, and successively for 2, 3, 4 and 5 holes. The maximum stress occurs always at point *A* as shown in the figure. The presence of holes tangentially to the boundaries did not decrease the s.c.f. Lengthening the distance between the first hole and the fillet reduced the s.c.f. but not to a level lower than the one present when there were no holes [71].

1.6 Stress concentrations in some specific problems

Most of the problems studied and the solutions of which are reviewed in Section 1.3 as well as most of the stress concentrations reported in Sections 1.4 and 1.5 correspond to more or less idealized geometries. So

will be the situation of the three-dimensional and the dynamic cases to be dealt in Sections 1.7 and 1.8. In this section some solutions will be presented for cases which still are of general interest, but corresponding to more specific applications.

Stress concentrations at the fillet of internal flanges. When a machine element contains an internal flange the resultant loading in the cylinder often is parallel to the axis, but eccentric (Figure 1.73). It is also frequently the case that these flanges have to be very narrow which requires that the fillet connecting the flange to the shell to be small, giving rise to severe stress concentrations. The stress distribution has been studied [72] for various positions of the load *P* along the radial line *CO*. The influence of the cylinder thickness *t* and the flange thickness *T* are considered. Figures 1.74 to 1.78 show the results obtained, parametrically as function of eccentricity and for several ratios of the diameter of the cylinder to the thickness of the cylinder and of the flange.

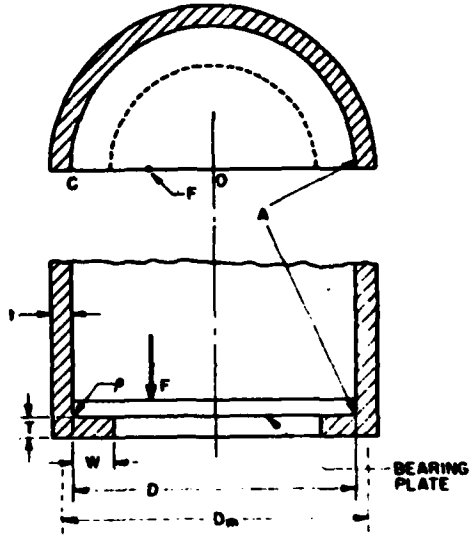

Figure 1.73. Internal flange at the end of a hollow cylinder. The axial and eccentric load is transmitted to the flange by means of a plate.

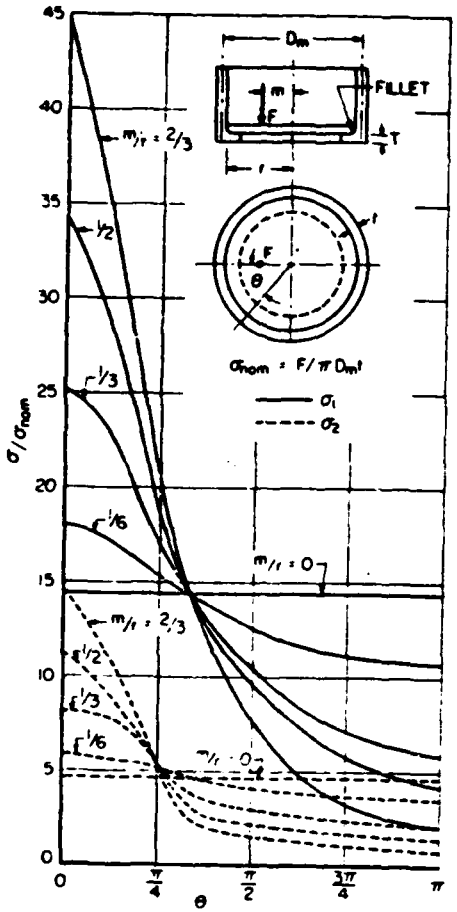

Figure 1.74. Principal stresses at the bottom of the fillet for different eccentricities of load. $D_m/t = 13$, and $D_m/T = 25$.

Stress concentrations in pressurized circular shells with discontinuities, with or without stiffeners. This is the summary [73] of a series of research programs dealing with the experimental determination of stresses, strains and displacements in pressurized circular vessels with a circular hole. The hole can be either plain or reinforced by a ring. The vessels were either of constant thickness or stiffened by transverse internal ribs. The solutions obtained correspond to internal pressure

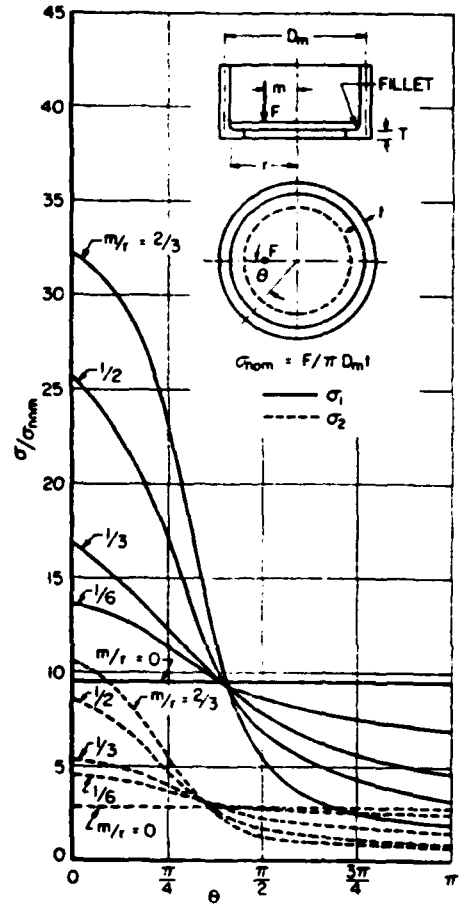

Figure 1.75. Principal stresses at the bottom of the fillet for different eccentricities of load. $D_m/t = 21$, and $D_m/T = 25$.

loading but can easily be adapted to external pressure loading, with the exception of local variations due to the manner of plugging the hole.

Six geometric variations were studied:

Case 1 plain hole-unstiffened shell
Case 2 plane hole-stiffened shell

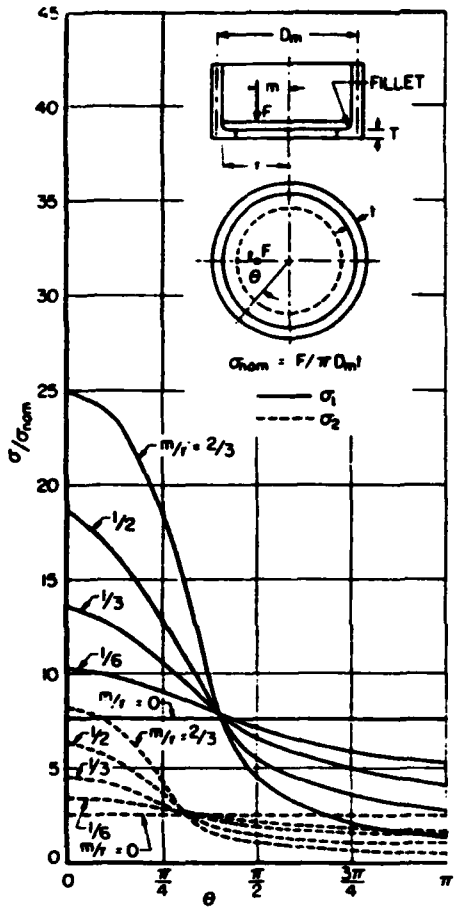

Figure 1.76. Principal stresses at the bottom of the fillet for different eccentricities of load. $D_m/t = 30$, and $D_m/T = 25$.

Case 3 small reinforced hole-unstiffened shell
Case 4 large reinforced hole—unstiffened shell
Case 5 reinforced hole—stiffened shell—hole between ribs
Case 6 reinforced hole—stiffened shell—hole through ribs.

The geometries of the vessels analyzed are represented in Figure 1.79. The hole size varied from $1-\frac{1}{4}$ in. to $2-\frac{3}{8}$ in. The edge of the hole

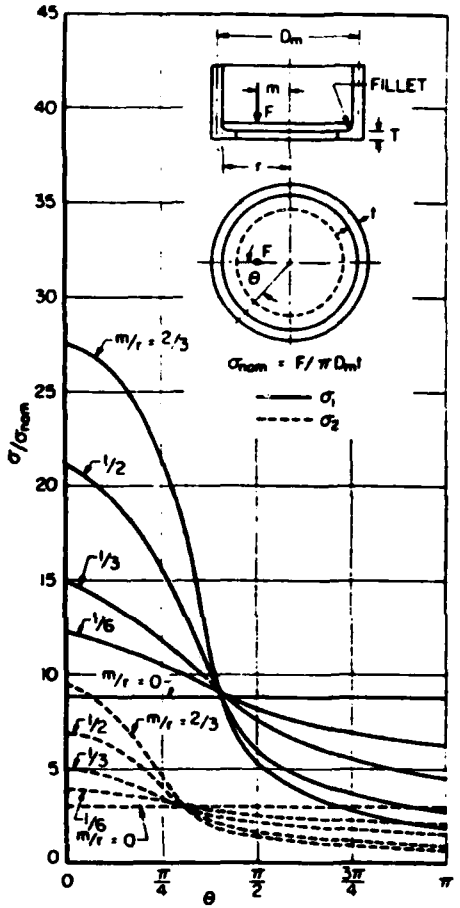

Figure 1.77. Principal stresses at the bottom of the fillet for different eccentricities of load. $D_m/t = 30$, and $D_m/T = 35$.

was reinforced by means of a ring, the outer diameter of which was $\frac{1}{2}$ in. larger than hole diameter for cases 3, 4 and 5 and $\frac{5}{8}$ in. larger for case 6. The height of the reinforcing ring was $\frac{1}{2}$ in. for cases 3 and 5, $\frac{9}{16}$ in. for case 4, and $1-\frac{1}{4}$ in. for case 6. The height of the reinforcing ring for case 6 was such that it reached the inner radius of the rib through which the hole was passed and thus served to replace the rib in the region at the hole.

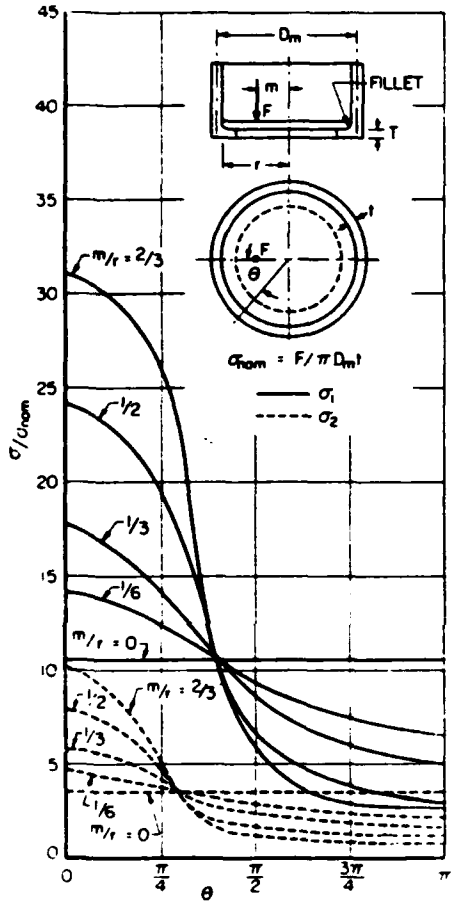

Figure 1.78. Principal stresses at the bottom of the fillet for different eccentricities of load. $D_m/t = 30$, and $D_m/T = 50$.

The radii of the fillets between rib and shell, between reinforcing ring and shell, and between rib and reinforcing ring were all $\frac{1}{16}$ in. with the single exception of the fillets in case 4, which were $\frac{1}{8}$ in.

Internal pressure was applied to the vessels. In order to contain the pressure, plugs made of silicone rubber were placed in the holes. The plugs had a shoulder that rested on the inner surface and were kept in place by the pressure.

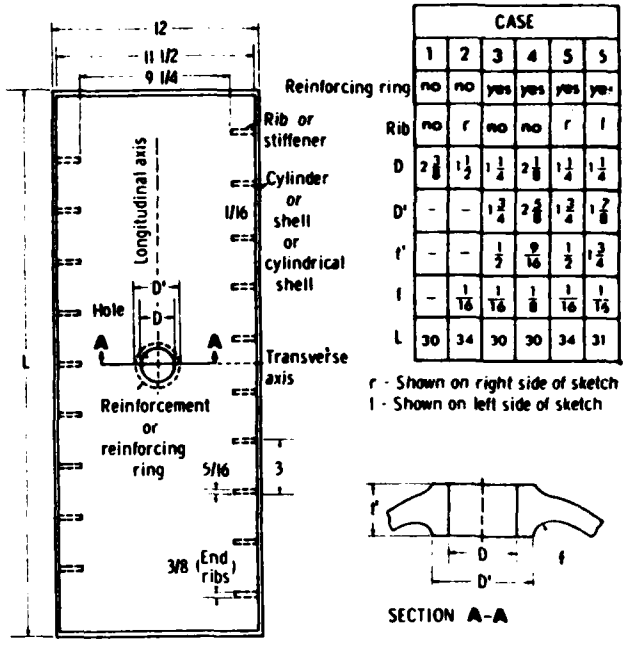

Figure 1.79. Geometry of six cylindrical vessels with a hole and various reinforcements.

The stress analysis was conducted using brittle coatings, electrical resistance strain gages and three-dimensional photoelasticity. Figure 1.80 shows a typical detail of the isochromatic patterns obtained. Figure 1.81 includes a table showing the position and the value of the stress concentration factors for all the cases studied. The complete details of these analyses are given in [74–78].

The stresses in Figure 1.81 are normalized by dividing the actual stresses obtained from the tests by the factor pR/t, where p is test pressure, R the radius of the middle surface of the shell, and t the shell thickness. For the case of a thin-walled cylinder with no reinforcement under pressure, pR/t is well known to be the theoretical stress in the circumferential (hoop) direction, $\sigma_{\theta\theta}$. The longitudinal (axial) stress for the same case is also well known to be $\sigma_{zz} = pR/2t$. Thus the lowest possible maximum stress in a thin unstiffened cylinder would have the normalized stress value of 1.0 for $\sigma_{\theta\theta}/pR/t$. In the case of a cylinder stiffened with ribs, equilibrium would require that the axial stress be at least $\sigma_{zz}/(pR/t) = 0.5$. These minima should be kept in mind in considering the values reported in Figure 1.81.

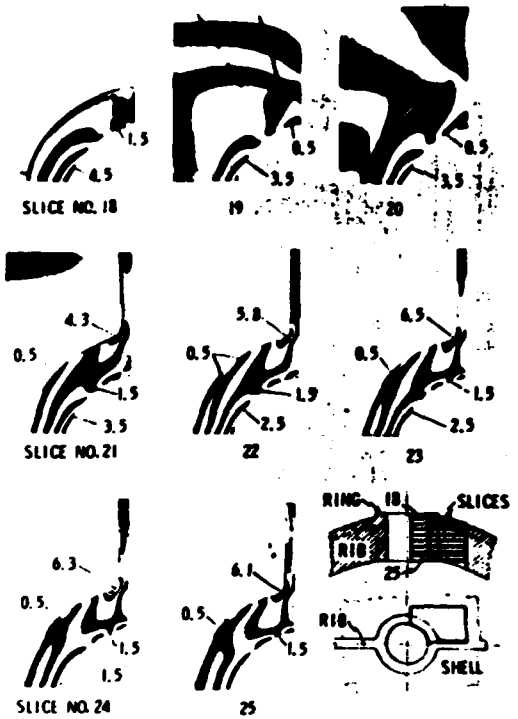

Figure 1.80. Isochromatics in slices through the hole reinforcing ring of case 6.

Stress concentrations at or near a square corner in the neighborhood of a hydrostatically loaded circular hole. Several papers have been published recording stress distributions in square plates and strips of finite width, with a pressurized hole [79–82]. An illustrative result will be shown here. Figure 1.82 shows the geometry of the plate and the variable position of the hole, and the stress distribution along the boundary of the hole. Figure 1.83 shows the value of the maximum stress anywhere in the plate. It is significant that the stress concentration changes location, from the boundary of the hole to the boundary of the plate, as the edge of the hole approaches the edge of the plate. The results are given in dimensionless form taken the pressure as reference (see Section 1 on definition of stress concentration factors).

		Locations of Stress Concentrations	Case 1	Case 2	Cases 3 and 4		Case 5	Case 6
			Plain shell with a nonreinforced hole	Ribbed shell with a nonreinforced hole	Plain shell with two reinforced holes		Ribbed shell with a reinforced hole on bay	Ribbed shell with a reinforced hole on rib
		D/2R	0.202	0.128	0.106	0.181	0.106	0.106
		ring-shell fillet radius / t			0.25	0.50	0.25	0.25
Outer Surface of Shell	$\frac{\sigma_{\theta\theta}}{pR/t}$	At edge of hole	3.90	2.30	1.70	2.10	1.45	1.70
	$\frac{\sigma_{\theta\theta}}{pR/t}$	At fillet of ring and shell			1.10	1.60	1.10	0.98
	$\frac{\sigma_{zz}}{pR/t}$	At edge of hole	2.20	2.10	0.52	0.90	0.85	0.40
	$\frac{\sigma_{zz}}{pR/t}$	At fillet of ring and shell			0.85	1.10	0.95	0.70
Inner Surface of Shell	$\frac{\sigma_{\theta\theta}}{pR/t}$	At edge of hole	3.65	2.70	1.45	1.55	1.15	0.35
	$\frac{\sigma_{\theta\theta}}{pR/t}$	At fillet of ring and shell			1.10	1.15	1.00	1.25
	$\frac{\sigma_f}{pR/t}$	At fillet of ring and rib						1.95
	$\frac{\sigma_{zz}}{pR/t}$	At edge of hole	-1.25	-0.55	0.50	0.50	0.49	-1.10
	$\frac{\sigma_{zz}}{pR/t}$	At fillet of ring and shell			0.50	0.65	0.45	
	$\frac{\sigma_f}{pR/t}$	At fillet of ring and shell					0.13*	1.80
	$\frac{\sigma_f}{pR/t}$	At fillet of rib nearest hole		1.65			1.25	1.05
	$\frac{\sigma_f}{pR/t}$	At fillet of rib through hole						1.60

* At this fillet no well-defined maximum was recorded. The stress increased continuously over the fillet.

Figure 1.81. Stress concentration factors associated with circular holes in cylindrical shells.

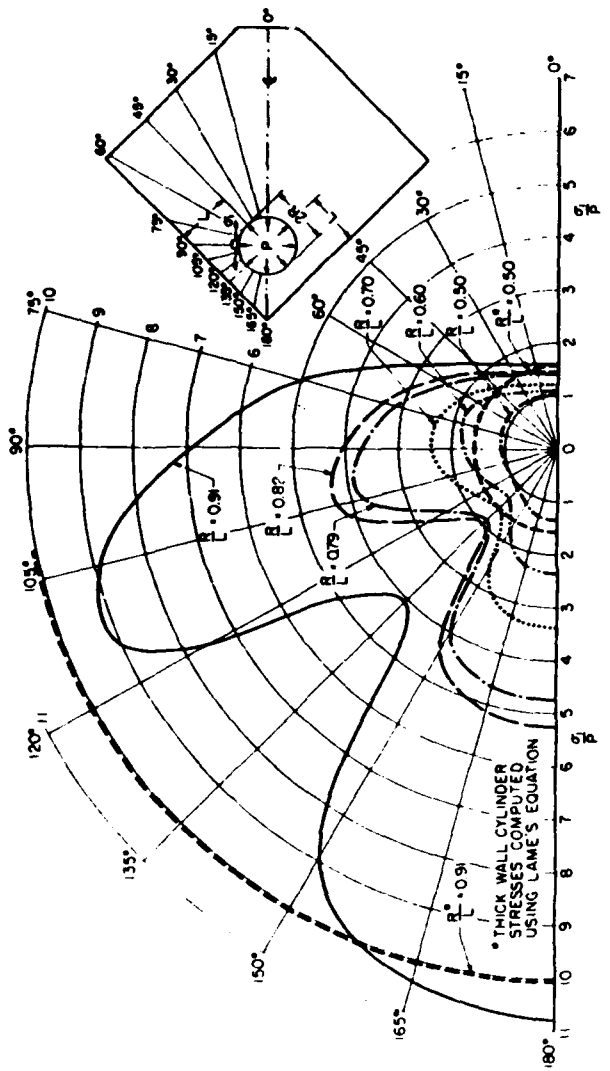

Figure 1.82. Hydrostatically loaded circular hole in the neighborhood of a corner. Stress distribution along the boundary of the hole.

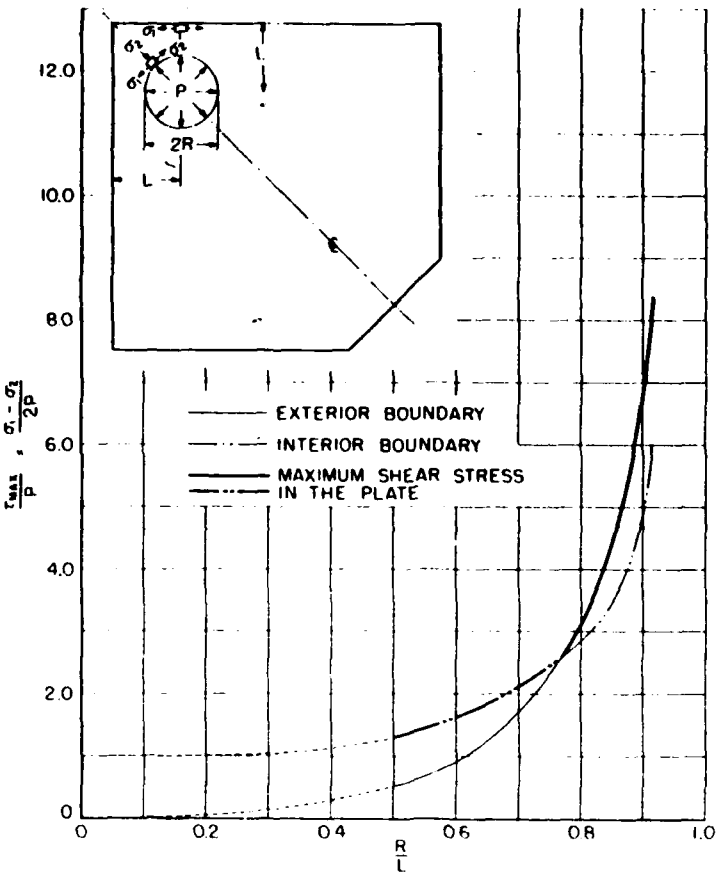

Figure 1.83. Hydrostatically loaded circular hole in the neighborhood of a corner. Maximum shear stress in the plate.

1.7 Stress concentrations in three-dimensional problems

The determination of stress concentrations in three-dimensional problems is considerably more difficult than the determination in the case of two-dimensional problems, both theoretically and experimentally. As could be expected, most of the contributions refer to stress concentrations on free surfaces of three-dimensional bodies because although the method used may be three-dimensional, the stress distribution problem is essentially two-dimensional. Some three-dimensional solutions that may be of interest, either in industrial applications or for the methodology, will be presented in this section. Solutions to other similar problems have been summarized in [86].

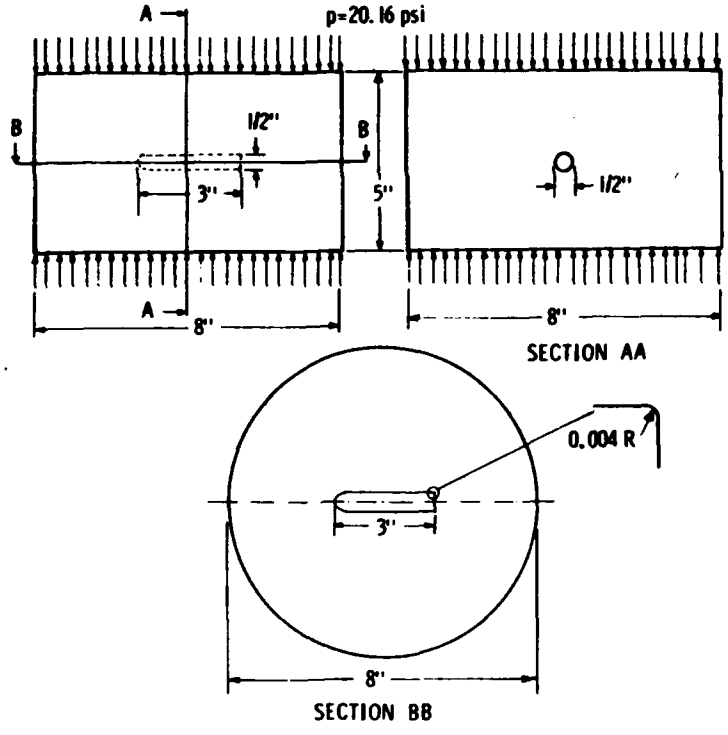

Figure 1.84. Circular bar embedded in a matrix and loaded perpendicular to axis of bar.

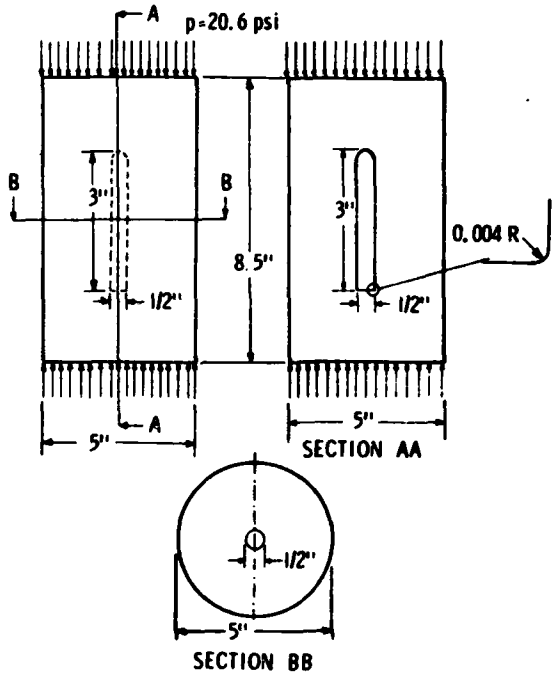

Figure 1.85. Circular bar embedded in a matrix and loaded parallel to axis of bar.

Stress concentration at flat and spherical ends of a circular bar embedded in a matrix in a triaxial stress field. The problem is defined in Figures 1.84 and 1.85. An illustration of the physical evidence is shown in Figure 1.86.

The most significant results related to stress concentrations are shown in Figures 1.87 and 1.88. The stresses are given in a dimensionless manner making the results applicable to all cases of rigid bars embedded in softer matrices. The peak tangential shear stresses on the interface at the hemispherical end take place at approximately an angle of 55° with the axis (measured from the tip of the hemispherical end). They are shown in Figure 1.89. Further information can be found in [83].

Stress concentration at the ends of pressurized cylindrical holes. The experiments were conducted using cylinders the diameter of which was

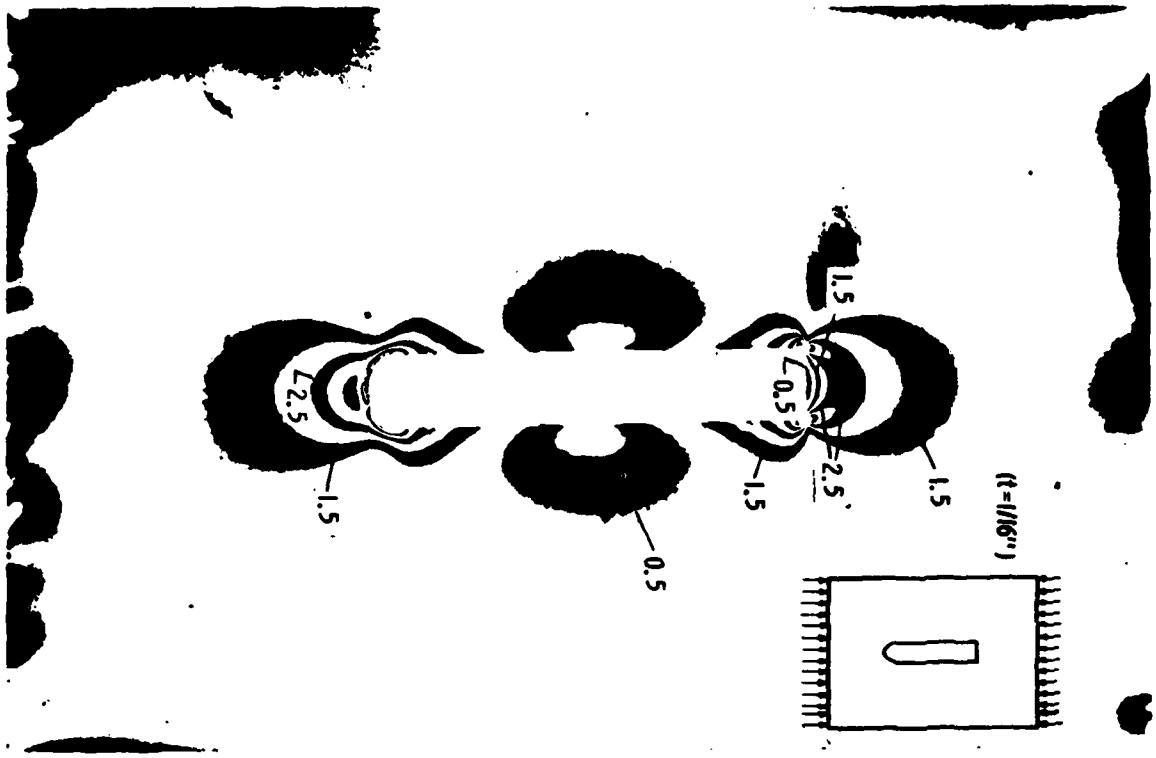

Figure 1.86. Light field isochromatic pattern for meridian slice.

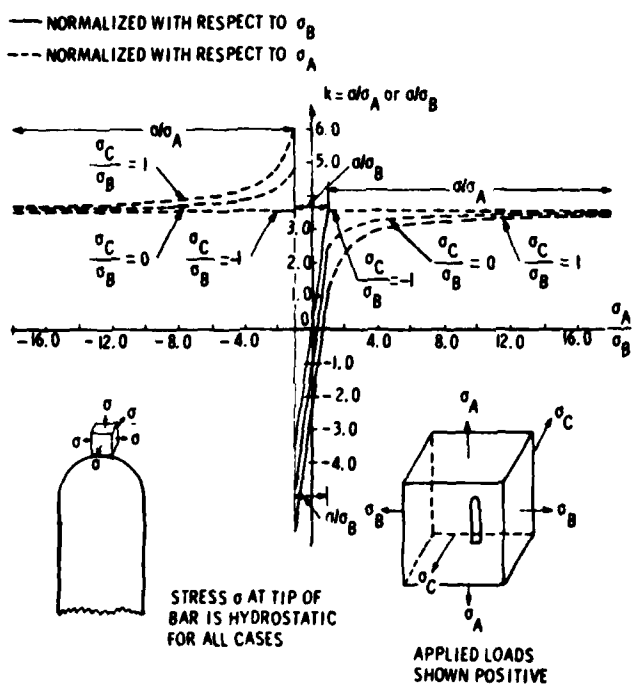

Figure 1.87. Stress-concentration factor at the hemispherical end of a circular bar embedded in a matrix and subjected to triaxial loading.

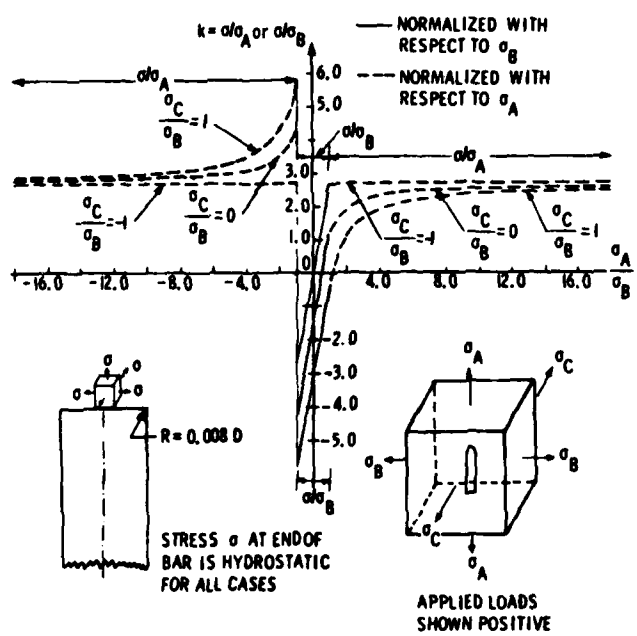

Figure 1.88. Stress-concentration factor at center of flat end of circular bar embedded in a matrix and subjected to triaxial loading.

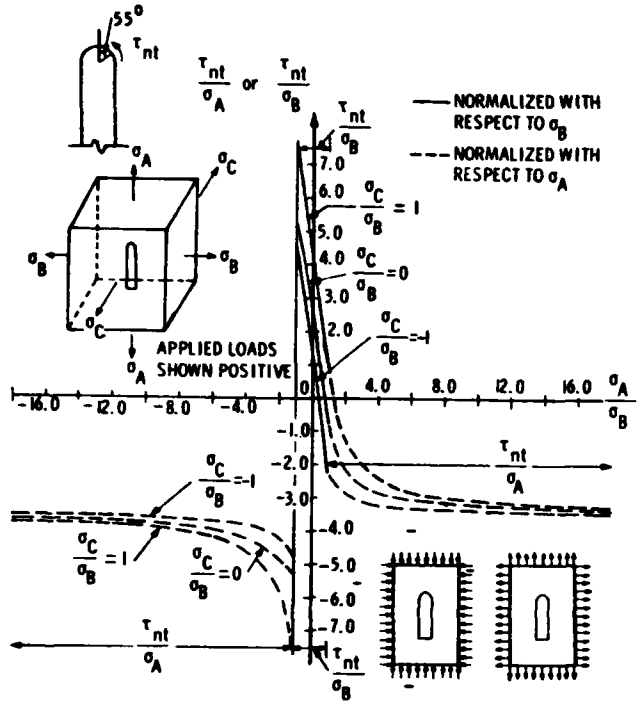

Figure 1.89. Normalized tangential shear stress τ_{nt} on the hemispherical end of an embedded circular bar at a point 55° from the axis of the bar and the σ_B stress plane.

about four times the diameter of the hole [84]. The results obtained can be used as first approximation for any large cylinders with small axial holes or for the infinite medium. Three hole end geometries were investigated. One had a hemispherical end, the other two had flat ends with fillets (radius 0.58 and 0.17 of the radius of the hole) connecting the ends and the sides. The stress distributions are shown in Figures 1.90 to 1.92 in dimensionless form, referred to the pressure. The circumferential component of the stress is little sensitive to the fillet radius changes, while the meridional component is much more dependent on the fillet radius. However, the increase in the fillet radius sharpness from 0.58 to 0.17 of the cylinder radius does not increase appreciably the stress concentration factor.

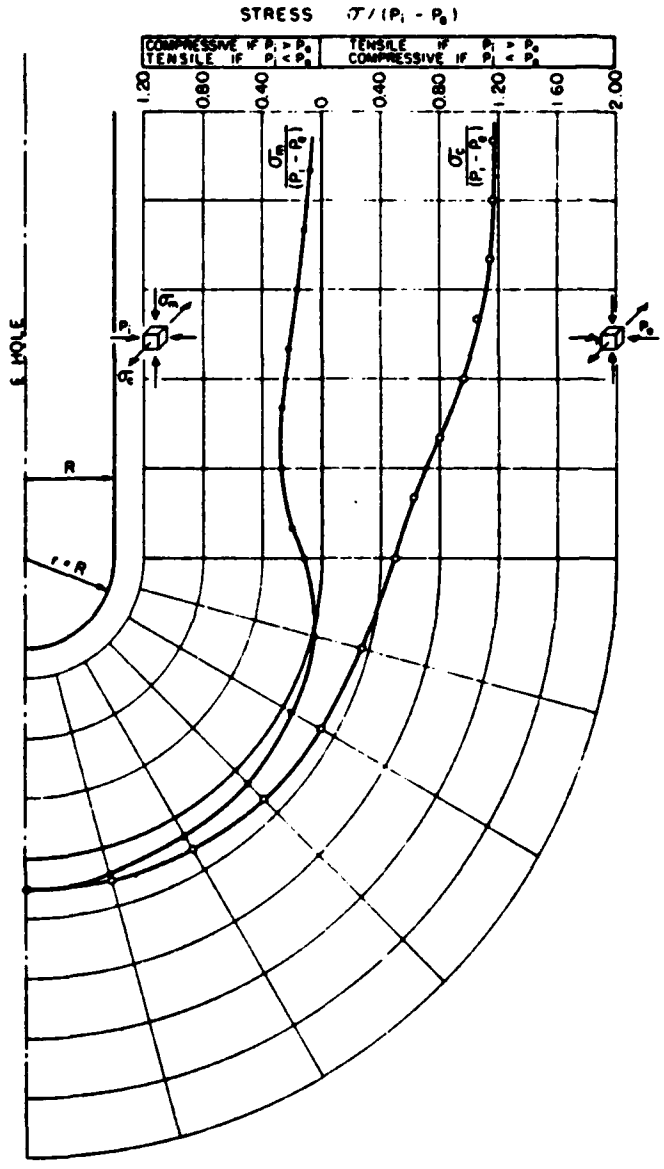

Figure 1.90. Distribution of the two principal stresses tangential to the surface of the hole with hemispherical end.

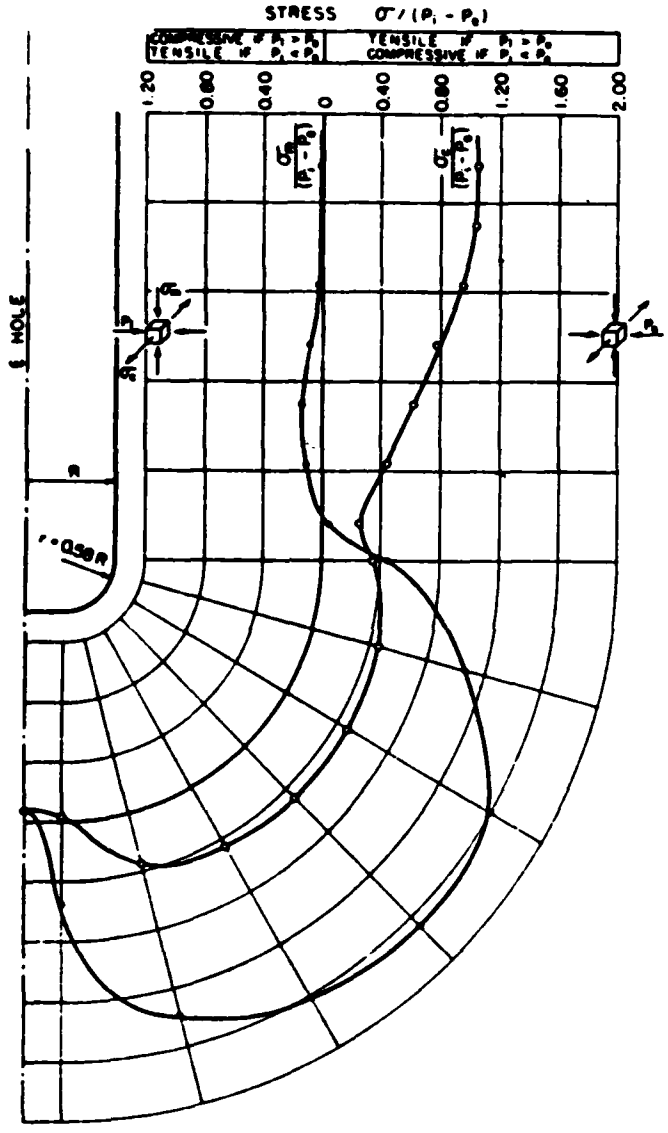

Figure 1.91. Distribution of the two principal stresses tangential to the surface of the hole with flat end and fillet radius equal to 0.58 the radius of the hole.

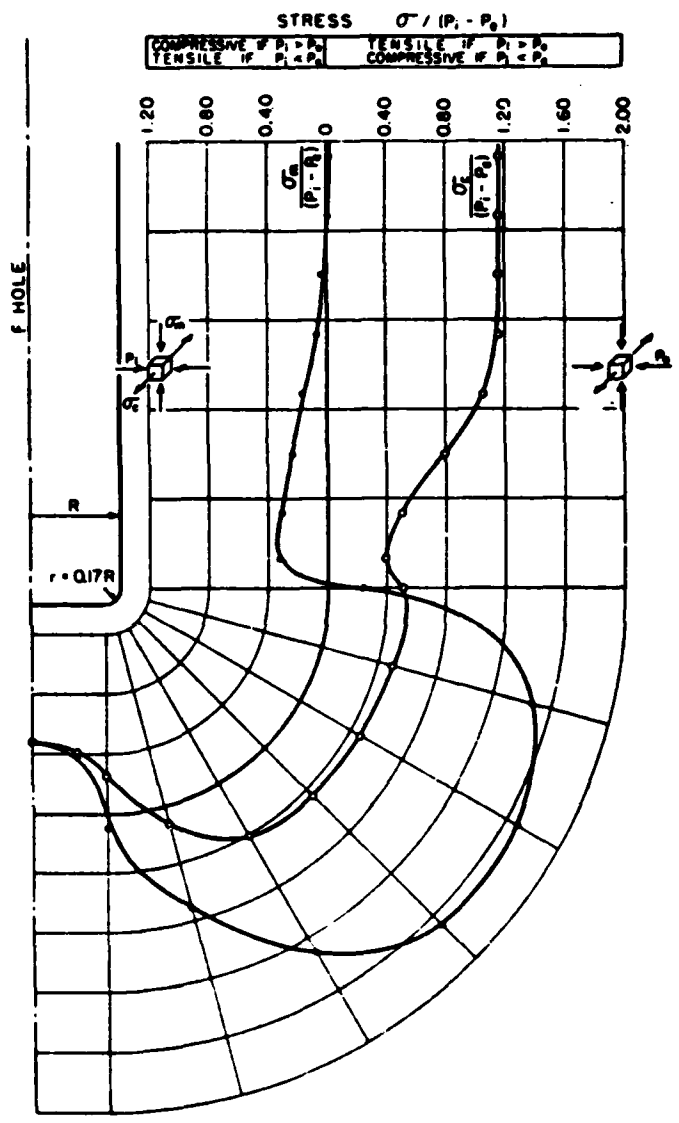

Figure 1.92. Distribution of the two principal stresses tangential to the surface of the hole with flat end and fillet radius equal to 0.17 the radius of the hole.

Stress concentrations associated with the restrained shrinkage of cylinders with toroidal cavities. Three hollow cylinders (one of them with a dome-shaped end) were bonded on the outside surface to shells. The geometry of each cylinder and its corresponding shell is defined in the sketches in Figures 1.93 to 1.94. The meaning of the dimensionless quantities $2L/2b$, b/a, $d/(b-a)$ and t/b are also indicated there. That part of the external surface which is bonded is also shown in the figures. Three-dimensional photoelasticity was used to "freeze" the photoelastic and moiré response. The shells are several times more rigid than the material of the cylinders at the time of 'freezing' the isochromatics. Displacement components were obtained using moiré effects, by photographing a cross-grating on slices of the cylinders, annealing them, and analyzing with a one-way grating. Illustrative examples of the records obtained are shown in Figures 1.93 to 1.98. More information can be found in [85]. The stress concentrations are tabulated in Table 1.1.

TABLE 1.1

Peak values of normalized maximum stresses in the three cylinders

Cylinder	Geometry			$\frac{F_z}{E\alpha_z^*}$	Interface restraint at $z=0$		Maximum stresses At $\begin{cases} r=a \\ z=0 \end{cases}$		See figures for location
	$\frac{2L}{2b}$	$\frac{b}{a}$	$\frac{d}{b-a}$	For 1/8" slice Units: fringe^{-1}	$\bar{\varepsilon}_z = \alpha_z^*$	$\frac{\bar{\varepsilon}_\theta}{\bar{\varepsilon}_z}$	$\frac{\sigma_\theta}{E\alpha_z^*}$	$\frac{\max \tau_{max}}{E\alpha_z^*}$	$\frac{\max \sigma_1}{E\alpha_z^*}$
I	2.60	2.70	0.25	0.91	0.0032	1.84	16.1	6.6	13.2
II	1.25	2.40	0.33	0.81	0.0033	1.97	9.7	5.7	12.9
III	1.29	2.33	0.29	0.63	0.0055	0.88	6.1	4.0	13.8

Stress concentration at the interface of an elbow embedded in a shrinking matrix. The geometry of the square bar is shown in Figure 1.99. The bar is much more rigid than the matrix. The maximum shear strains, and the shear strains γ_{nl} in the plane of symmetry, are shown in Figures 1.100 and 1.101. Three-dimensional photoelasticity was used for the analysis. More information can be found in [86].

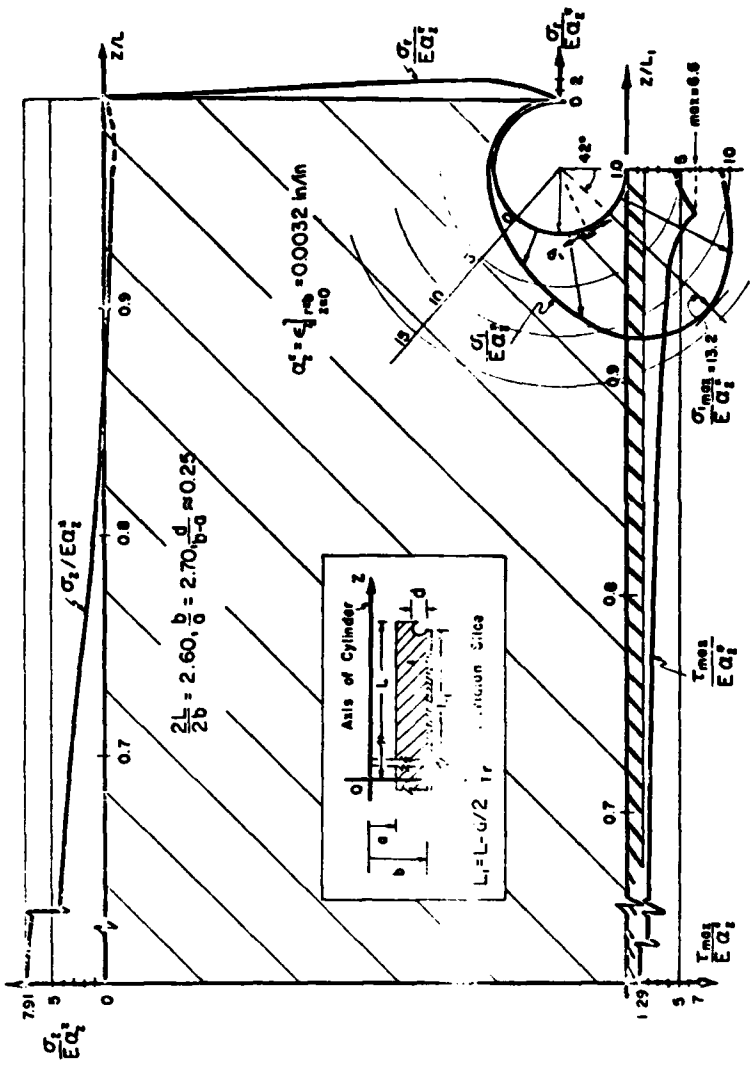

Figure 1.93. Normalized stresses at the boundaries of a meridian plane in hollow cylinder I, bonded on part of the outside surface to a shell and subjected to restrained shrinkage.

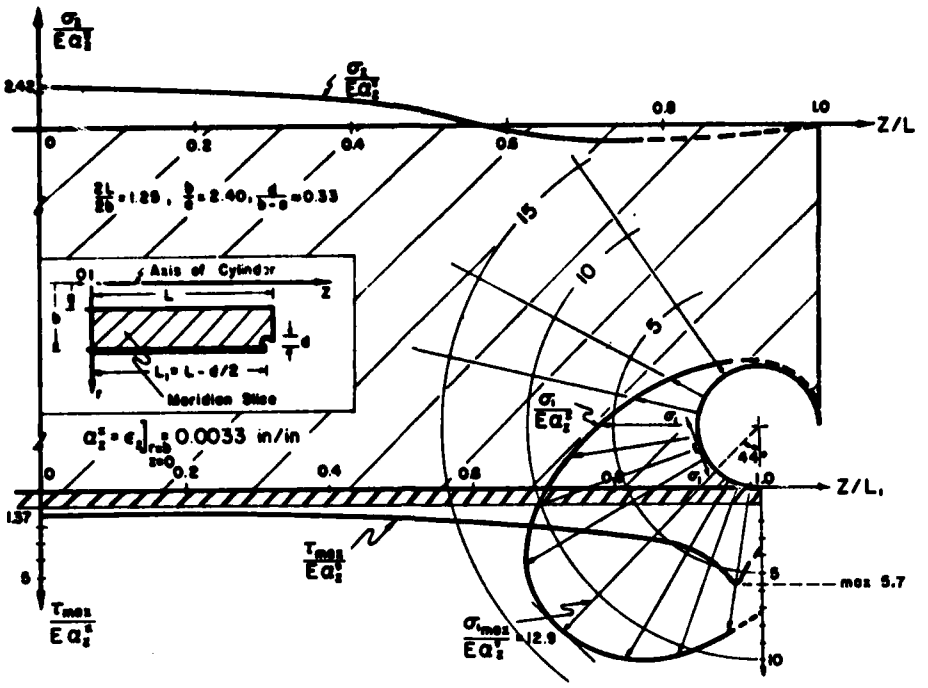

Figure 1.94. Normalized stresses at the boundaries of a meridian plane in hollow cylinder II, part of the outside surface to a shell and subjected to restrained shrinkage.

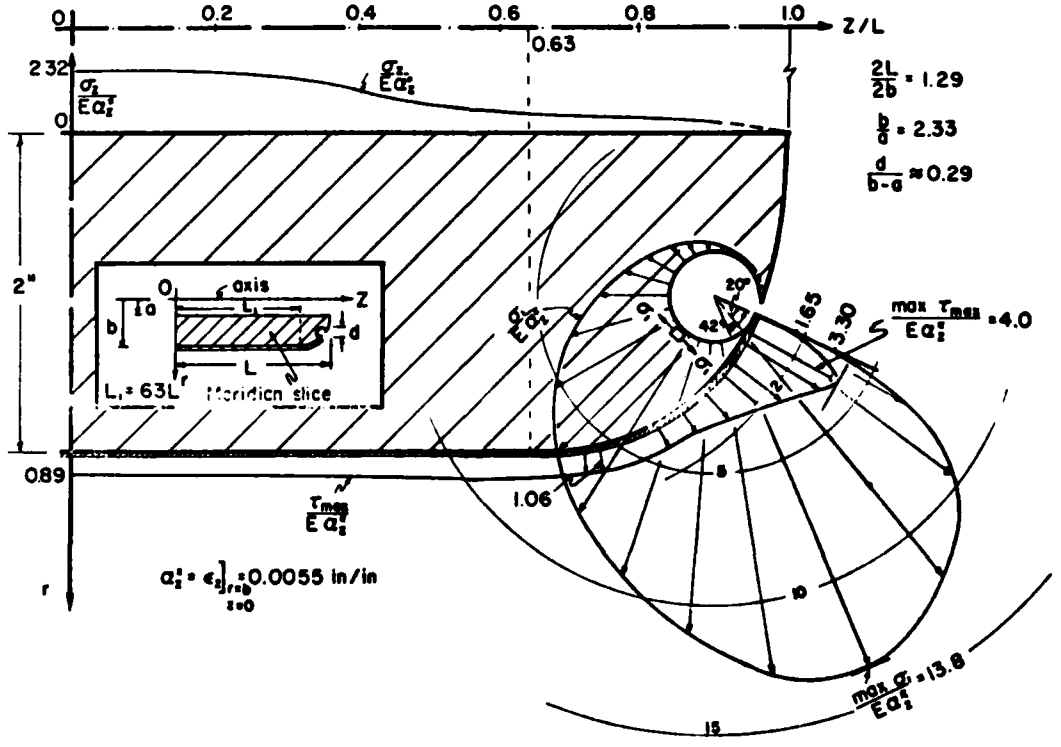

Figure 1.95. Normalized stresses at the boundaries of a meridian plane in a hollow cylinder with dome shape end (cylinder III), bonded on part of the outside surface to a shell and subjected to restrained shrinkage.

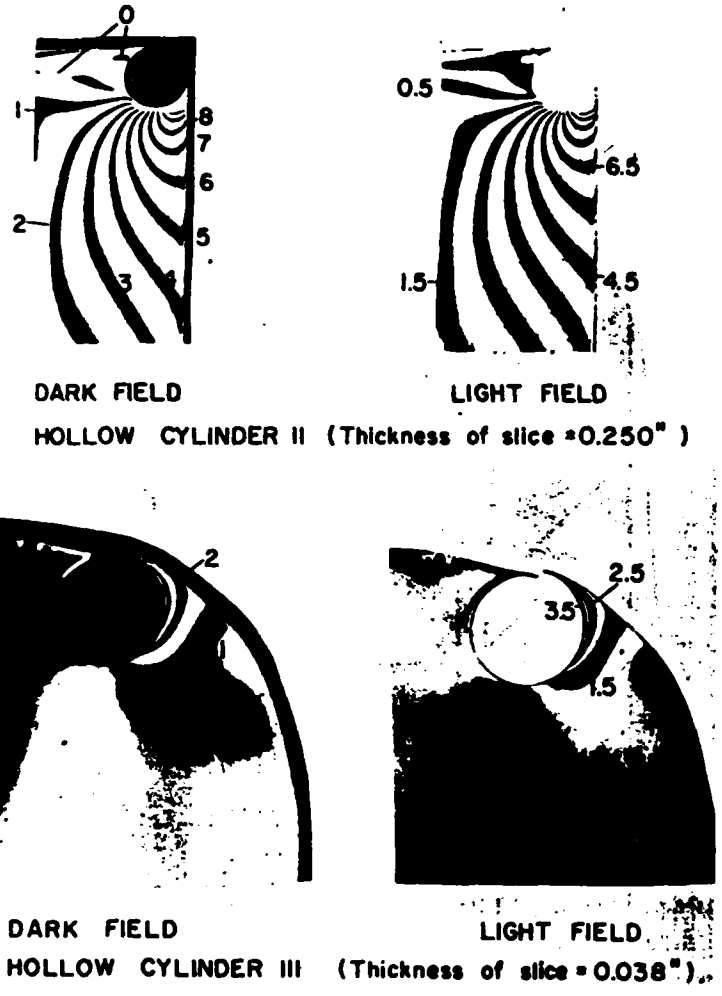

Figure 1.96. Isochromatics near the toroidal cavities on the meridian planes of hollow cylinders II and III.

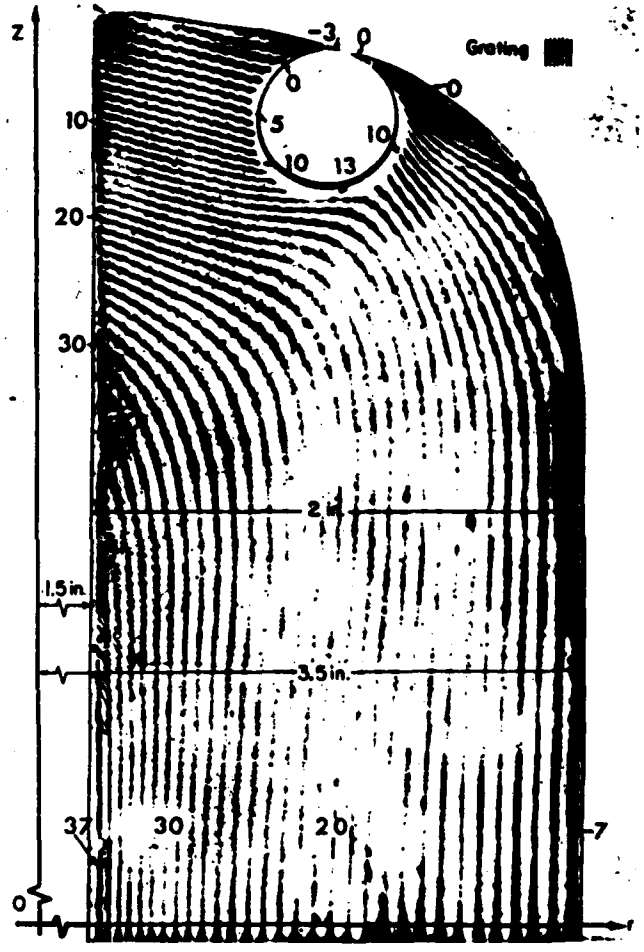

Figure 1.97. Isothetics u_r in a meridian plane of the hollow cylinder with a dome shape end (cylinder III). Note: The radial displacements are given by the expression $u_r = 0.001\,(n + 2r)$ where n is the fringe order and u and r are expressed in inches.

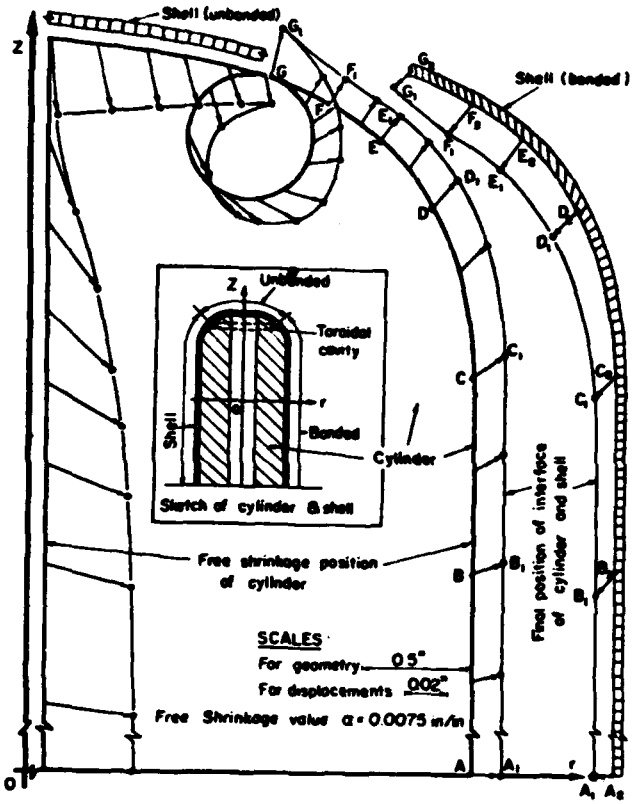

Figure 1.98. Boundary displacements for shell and hollow cylinder with a dome shape end (cylinder III).

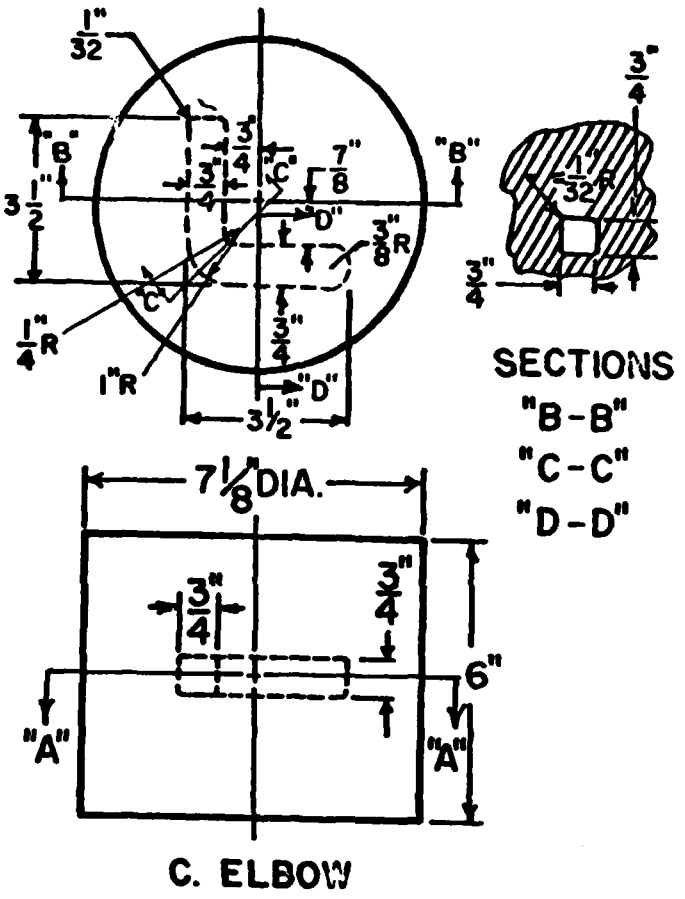

MATERIAL : INSERTS – HYSOL 4290 EPOXY
MATRIX – SAMPSONS EPOXY

Figure 1.99. Geometry of the rigid elbow embedded in the shrinking matrix.

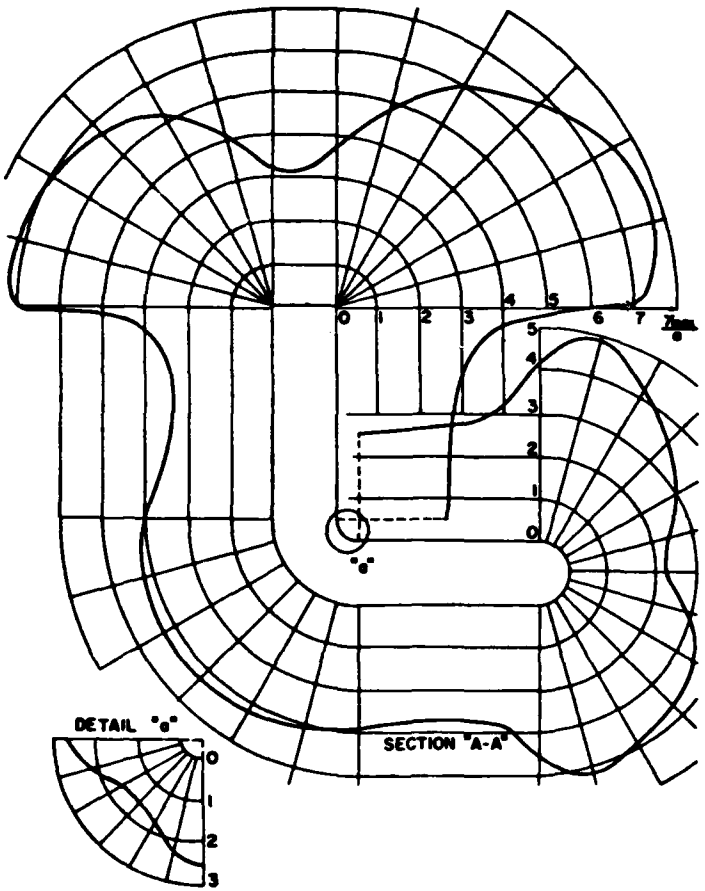

Figure 1.100. Maximum shear strain in the plane of symmetry at the interface between a matrix and an embedded elbow with a flat and a circular end. (restrained shrinkage).

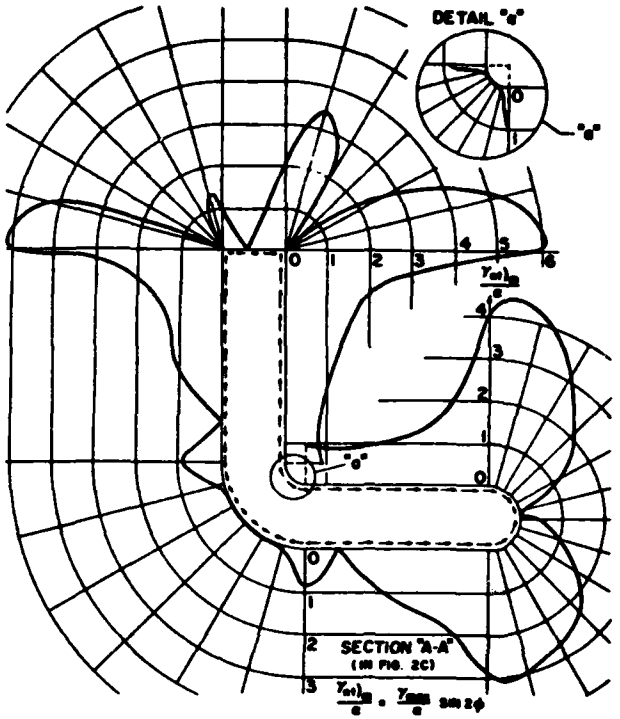

Figure 1.101. Shear strains in the plane of symmetry and tangential to the interface between a matrix and an embedded elbow with a flat and a circular end (restrained shrinkage).

Stress concentration at the interface of two circular bars embedded in a shrinking matrix. In one of the cases studied the two bars were aligned [86], in the other the axis of the bars made an angle of 14°. The geometry is shown in Figure 1.102. Three-dimensional photoelasticity was used for the analysis. The maximum shear strains at the interface are shown in Figures 1.103 and 1.104.

Stress concentrations in cylinders with small perforations and outside surface partially bonded to a rigid case, when subjected to restrained shrinkage. The boundary conditions are defined in Figures 1.105 and 1.106. The stress concentration factors and the position of the points at which they take place are shown in Figures 1.107 and 1.108.

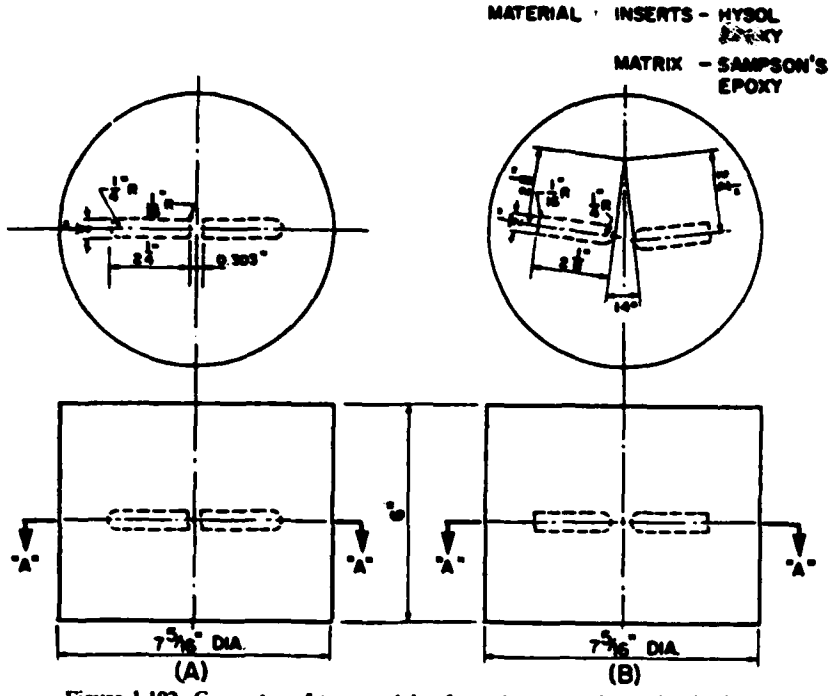

Figure 1.102. Geometry of two models of matrices cast about circular bars.

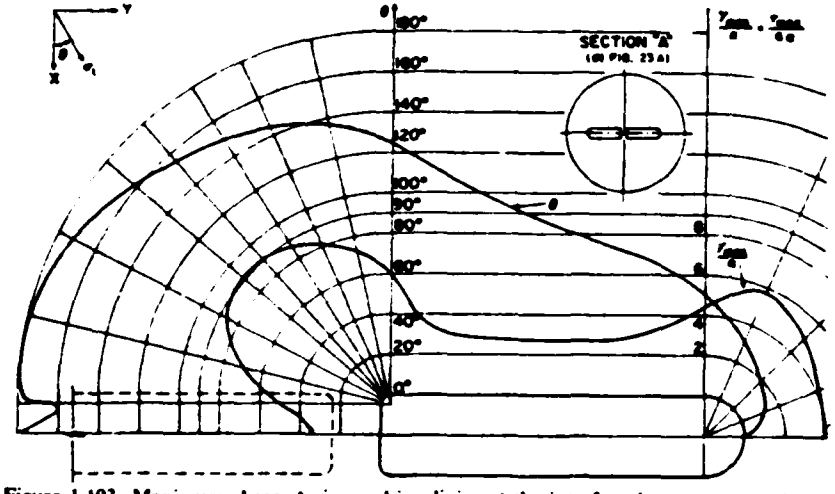

Figure 1.103. Maximum shear strains and isoclinics at the interface between a matrix and two aligned circular bars separated a short distance by the matrix. (restrained shrinkage).

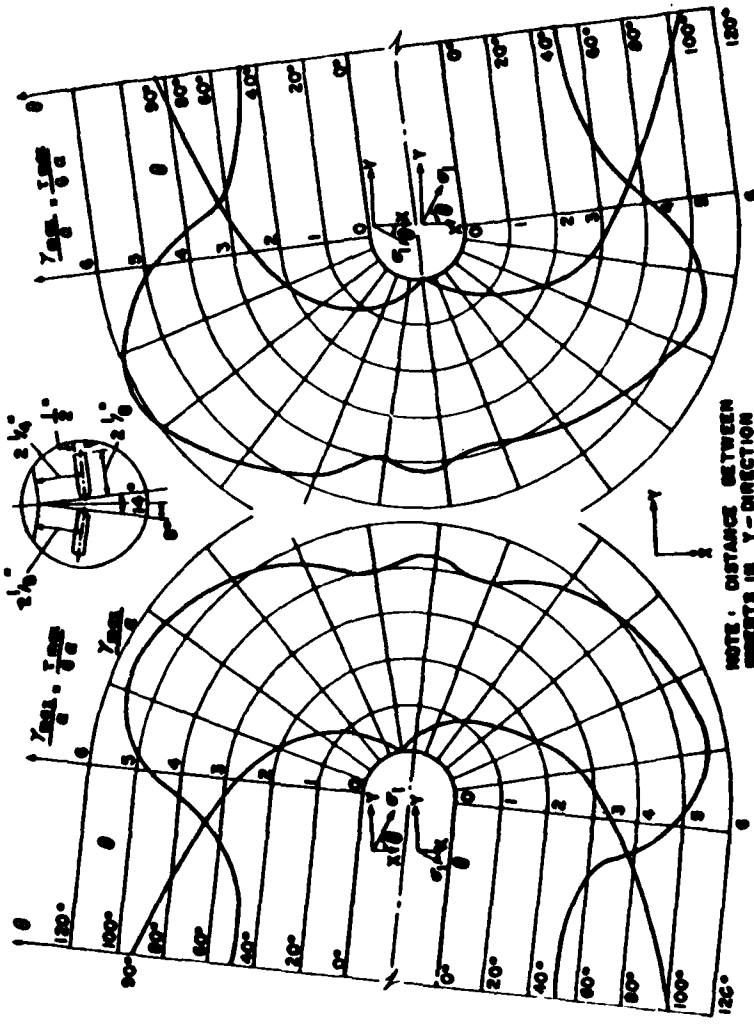

Figure 1.104. Maximum shear strains and isoclinics at interfaces between a matrix and two non-aligned circular bars separated a short distance by the matrix.

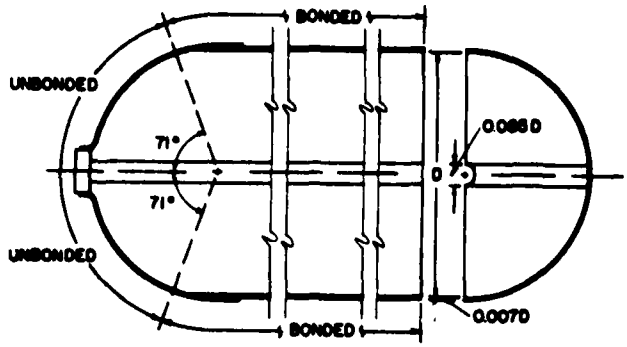

NOTE: STIFFENING ELEMENTS NOT SHOWN

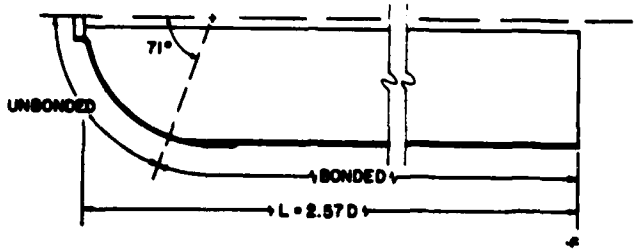

Figure 1.105. Three-dimensional model representing the present geometry of the rocket grain and shell.

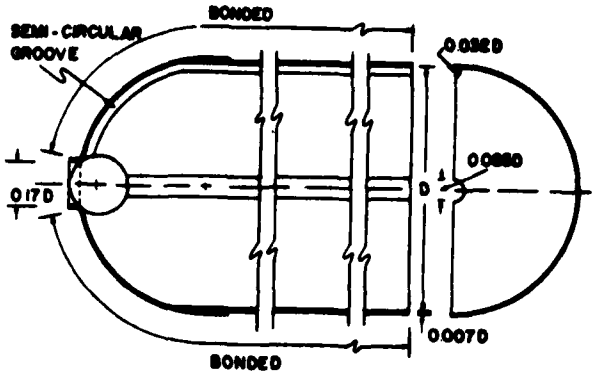

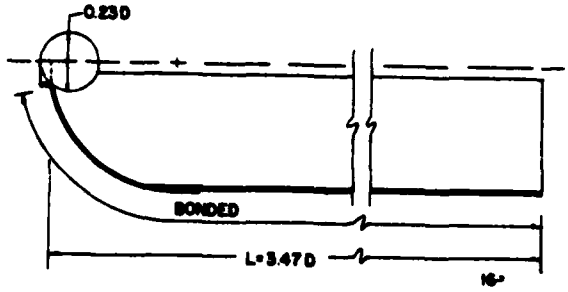

Figure 1.106. Geometry of the three-dimensional model with modifications to reduce stress concentrations.

SLICE NO.	LOCATION	$K = \frac{\sigma_{max}(r_{max})}{E\alpha^2}$
1		5 8
2, 2A	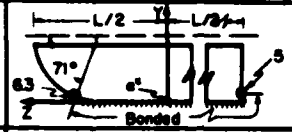	6.3 5
3	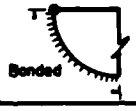	3
4, 4A	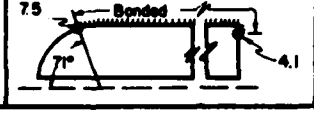	7.5 4.1

$\sigma_z|_{x=y=z=0} = \bar{\sigma}_z = \alpha^2$

The stress concentration takes place at the points marked by a dot

Figure 1.107. Stress concentration factors for the present geometry of the rocket grain.

SLICE NO.	LOCATION	$K = \frac{\sigma_{max}(r_{max})}{E\alpha^2}$
1		5 4.5
2		3
3		2.7
3A	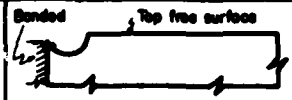	2.5
3B	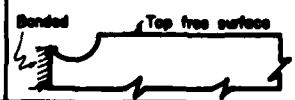	2.4
3C	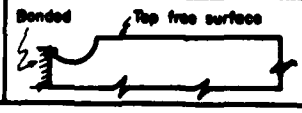	2.5

$\sigma_z|_{x=y=z=0} = \bar{\sigma}_z = \alpha^2$

The stress concentration takes place at the points marked by a dot.

Figure 1.108. Stress concentration factors for the modified geometry of the rocket grain.

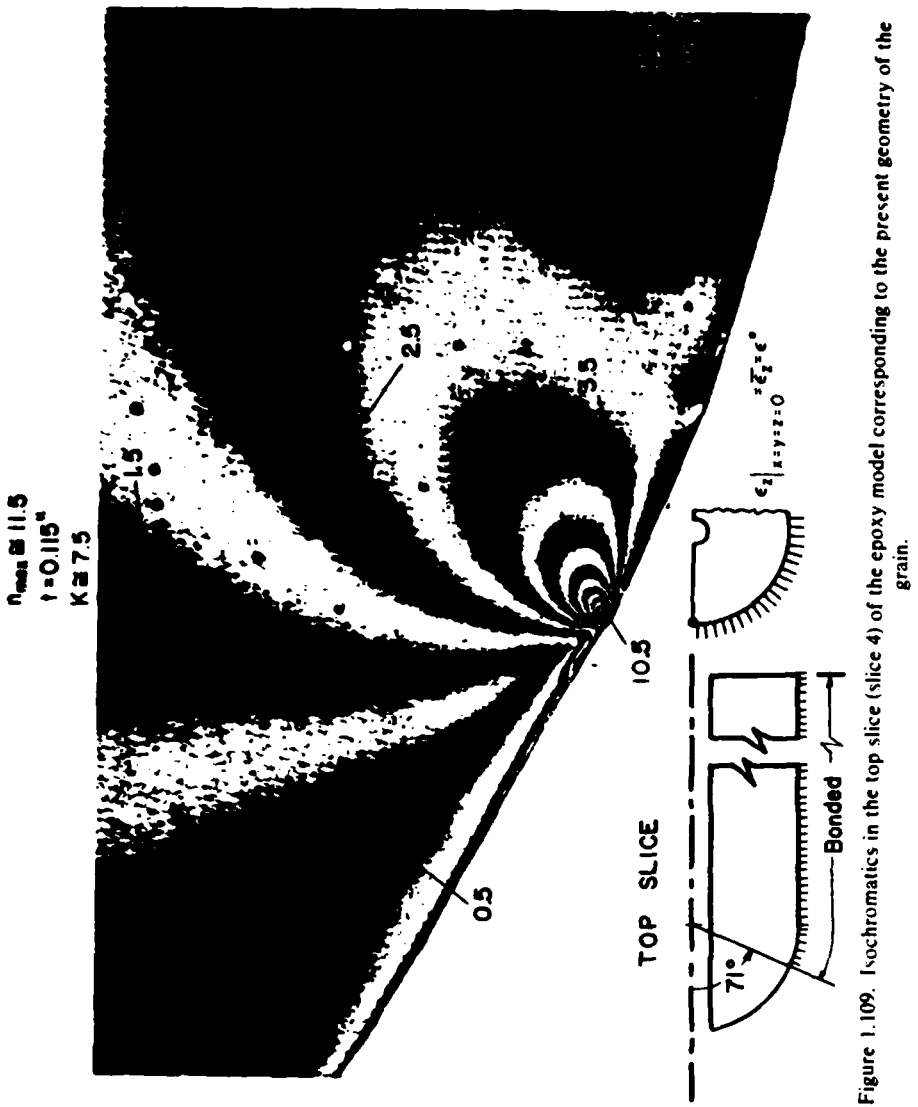

Figure 1.109. Isochromatics in the top slice (slice 4) of the epoxy model corresponding to the present geometry of the grain.

The isochromatic pattern in Figure 1.109. is particularly significant in fracture mechanics. The separation between the shrinking body and the bonded case developed spontaneously. The width of the gap in the neighborhood of the point of concentration is of the order of 0.001 in. The thickness of the observed slice was 0.115 in. The pattern indicates a finite s.c.f.

Stress concentrations in a cubic box subjected to concentrated loads. The geometry and boundary conditions are defined in Figure 1.110. The distribution of the two principal stresses along the diagonal on the inside and outside surfaces is shown in Figures 1.111 and 1.112. Distributions of other stresses in the box can be found in [87]. The results

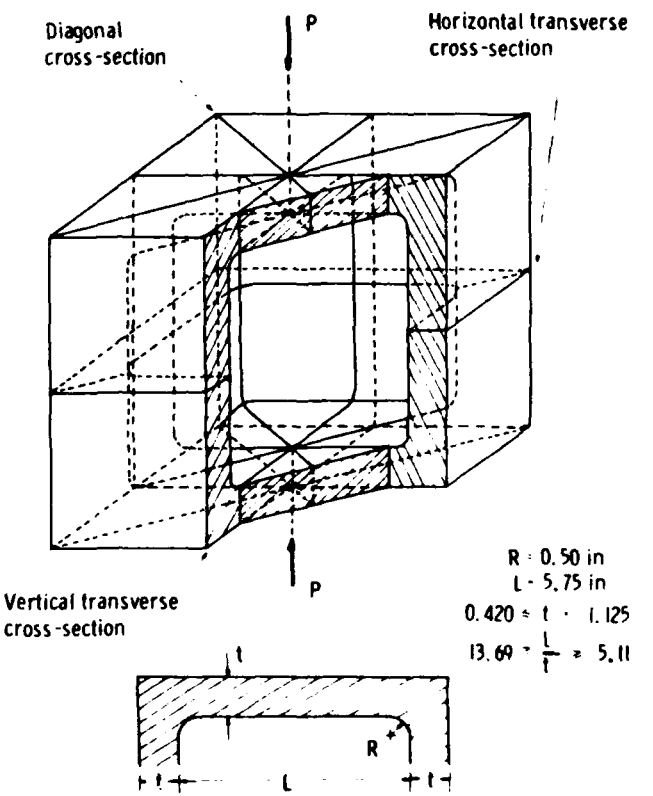

Figure 1.110. Geometry and loading of a cubic box subjected to a concentrated load at the center of two opposite faces.

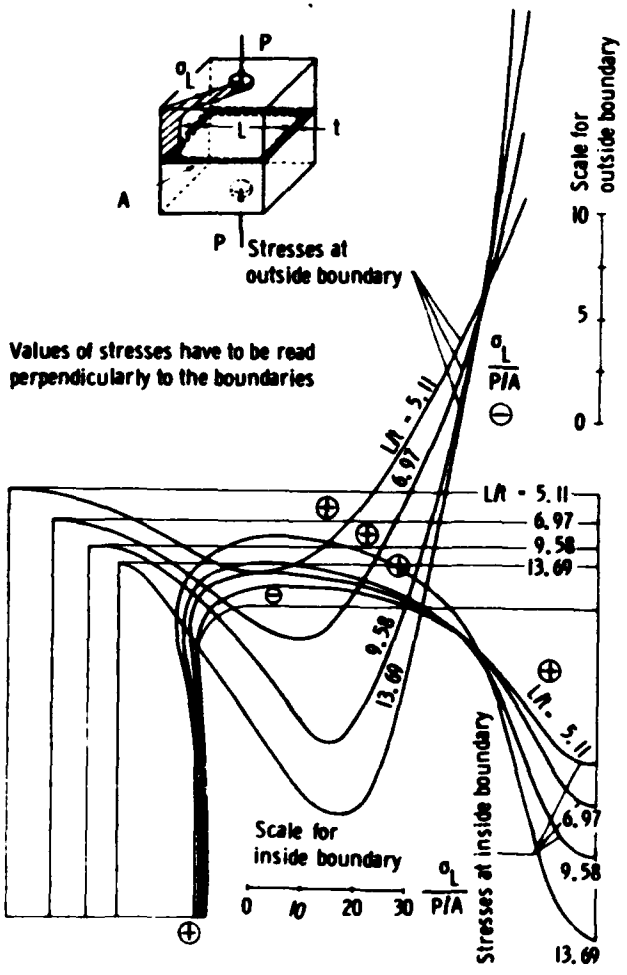

Figure 1.111. Stresses in the longitudinal direction at the intersection of the diagonal cross-section with the inside and outside surfaces, on a cubic box subjected to a concentrated load at the center of two opposite faces.

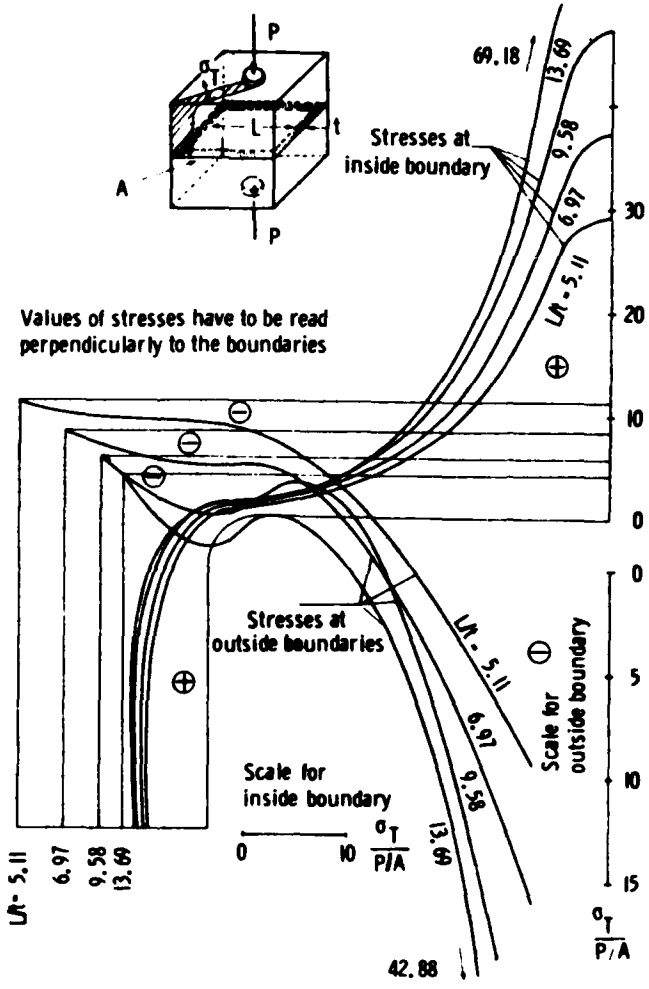

Figure 1.112. Stresses in the transverse direction at the intersection of the diagonal cross-section with the inside and outside surfaces, on a cubic box subjected to a concentrated load at the center of two opposite faces.

are equally applicable to the case of loads applied to the inside boundary by changing the sign of the stresses shown in the figures.

Stress concentrations in a cubic box subjected to pressure. The same box showed in Figure 1.110 has been subjected to internal pressure. The distribution of stresses at some typical cross sections is shown in Figures 1.113 to 1.114. The distribution of other stresses in the box can be found in [88]. Results are equally applicable to the case of external pressure by changing the sign of the stresses shown in the figures.

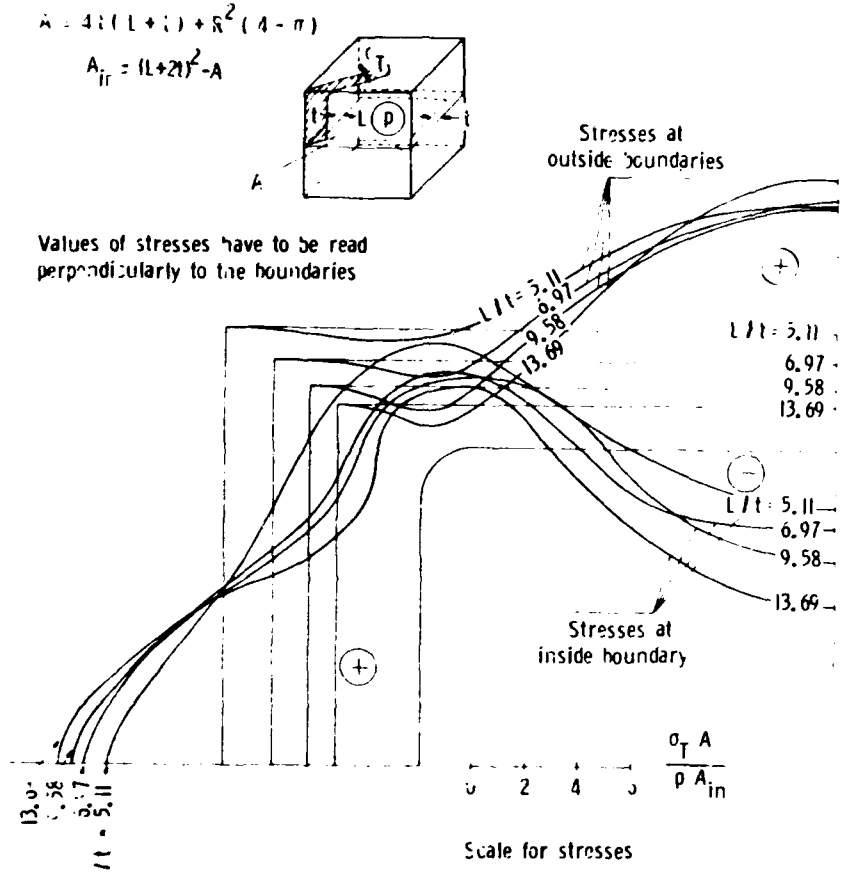

Figure 1.113. Stresses in the transverse direction at the intersection of the diagonal cross-section with the inside and outside surfaces, on a cubic box subjected to internal pressure

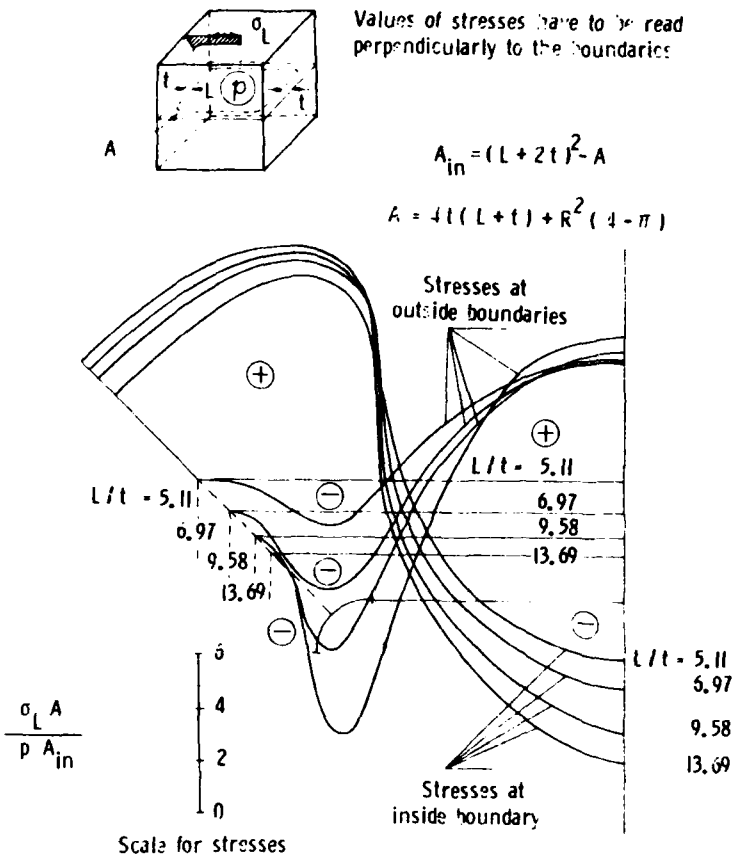

Figure 1.114. Stresses in the longitudinal direction at the intersection of the transverse cross-section with the inside and outside surfaces on a cubic box subjected to internal pressure.

1.8 Dynamic stress concentration factors*

The deformations and stresses generated, when dynamic loads are applied to a body, propagate through the body in the form of waves. At discontinuities within the body, the waves are reflected and refracted, that is, scattered, which may result in a local intensification of the stresses known as a dynamic stress concentration.

The theory associated with the propagation of stress waves in solids was developed during the last half of the 19th century as an extension of the theory of elasticity. Since no experimental means existed at that time for checking the theory, the subject was for the most part neglected during the first half of this century. With the development of electronic equipment and new plastic materials during and after World War II, experimental studies of wave propagation became possible and interest in the subject revived.

Most of the first experimental work in wave propagation was conducted using electrical resistance strain gages. This method gives a continuous time record of a dynamic event but limits observations to discrete points on the surface of the body. This lack of full-field information provided the motivation for studies in dynamic photoelasticity.

Theoretical dynamic stress concentration studies. One of the earliest theoretical investigations of dynamic stress concentrations (d.s.c.f.) was made by Nishimura and Jimbo [89]. They determined the stresses in the vicinity of a spherical inclusion in an elastic solid which is subjected to a dynamic tensile-compressive force with harmonic time variation. Stress concentrations around a spherical cavity, a rigid sphere, and an elastic spherical inclusion were discussed in detail. They showed that at certain wave frequencies, the d.s.c.f. are larger than the static ones.

In an important theoretical paper, which is widely used for experimental comparisons, Baron and Matthews [90] presented the solution for an infinitely long cylindrical cavity in an infinite elastic medium which is acted or by a plane shock wave whose front is parallel to the axis of the cavity. An integral transform technique was used to determine the stress field produced in the medium as the incoming shock wave is diffracted by the cavity. Although the problem is considered for pressure waves with

* The author is indebted to Prof. W. Riley, of Iowa State University, for preparing this section.

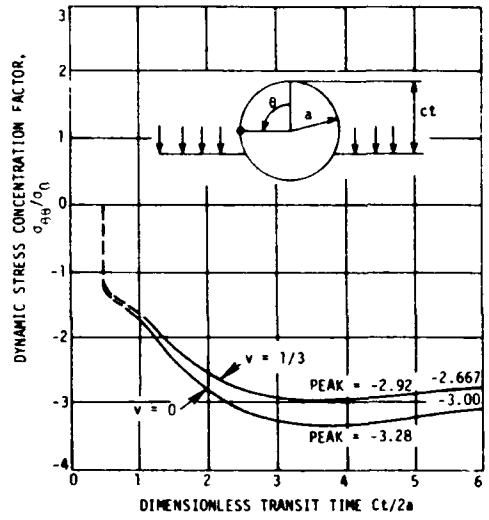

Figure 1.115. Dynamic s.c.f. as a function of dimensionless transit time for different values of Poisson's ratio, for an infinitely long cylindrical cavity in an infinite medium (Baron and Matthews).

a step distribution in time, the results obtained for this case may be used as influence coefficients to determine, by Duhamel integrals, the stress field produced by waves with time-varying pressures. Numerical results are presented in Figure 1.115 for the normalized hoop stress $\sigma_{\theta\theta}/\sigma_0$ at a point on the cavity boundary 90 degrees from the point of initial contact of the wave front with the boundary as a function of dimensionless transit time $Ct/2a$ for two different values of Poisson's ratio ν. These results indicated that the hoop stress on the cavity boundary is amplified by the dynamic loading in the ratio of 3.28 to 3 or approximately 9 percent for the case of Poisson's ratio $\nu = 0$. For the more realistic case of Poisson's ratio $\nu = \frac{1}{3}$, the results are 2.92 to 2.667 which corresponds to an increase in s.c.f. for the dynamic loading of approximately $9 - \frac{1}{2}$ percent.

In a more recent study, Pao [91] determined stress concentrations around a circular cavity in an infinitely extended, thin, elastic plate during passage of plane compressional waves. The problem is the dynamic counterpart of Kirsch's static problem discussed earlier. Briefly, the d.s.c.f. $\sigma_{\theta\theta}/\sigma_0$ were found to be dependent on the incident wave length λ and on Poisson's ratio ν for the plate material. At certain

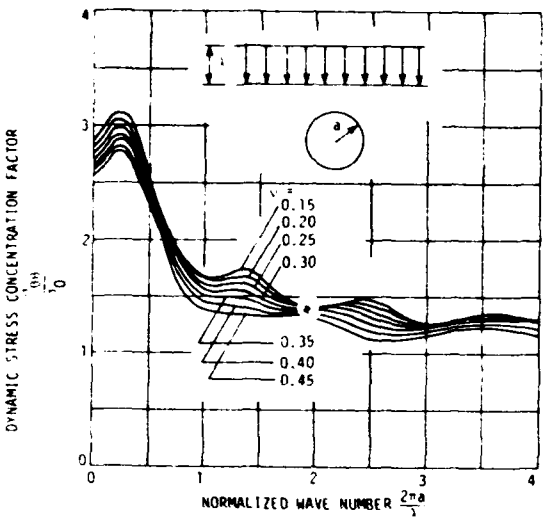

Figure 1.116. Dynamic s.c.f. as a function of normalized wave number for different values of Poisson's ratio, for a circular cavity in an infinite thin plate (Pao).

wave lengths, the d.s.c.f. were larger than those encountered under static loading as shown in Figure 1.116. For the seven values of Poisson's ratio (between 0.15 and 0.45) shown in the figure, the ratios of the d.s.c.f. to the static s.c.f. ranged between 1.09 and 1.10. Thus, the maximum amplification in stress due to dynamic loading appears to be about 10 percent. The results of this study clearly indicate that at very short wave lengths, a significant reduction in s.c.f. occurs under dynamic loading conditions.

Finally, the transient response for a rigid spherical inclusion in an elastic medium can be found in a paper by Mow [92]. An extensive theoretical treatment of diffraction of elastic waves and dynamic stress concentrations can be found in a monograph by Mow and Pao [93].

Experimental dynamic stress concentration studies. One of the first experimental investigations of a dynamic stress problem was made by Wells and Post [94] who determined the dynamic stress distribution surrounding a running crack started from an edge of a plate in tension. A multiple spark technique of the type originated by Schardin was employed to obtain full field photographs of the photoelastic (relative retardation) fringe patterns at various times during the dynamic event. In

addition, absolute retardation measurements were made in similar models with running cracks by means of an optical interferometer so than individual principal stresses could be determined. Even though the s.c.f. at the tip of the crack could not be determined, the results of this study indicated that the dynamic stress distributions in the vicinity of the crack were essentially the same as static distributions.

The first experimental determination of a dynamic stress concentration factor was reported by Durelli and Dally [95] who studied the stress distribution around a central circular hole in a strut subjected to an axial impact type of loading. The model was machined from a low modulus photoelastic material having a modulus of elasticity of approximately 600 psi. The photoelastic fringe patterns during the dynamic event were recorded with a Fastax camera operating at approximately 12,000 frames per second. A selection of frames from the Fastax record are shown in Figure 1.117. The results of the study indicated that the d.s.c.f. was not significantly different from the static s.c.f. if the nominal stress for the dynamic determination is taken as the stress which would have been present in the strut at the center of the hole at the same instant if the hole had not been present. For the

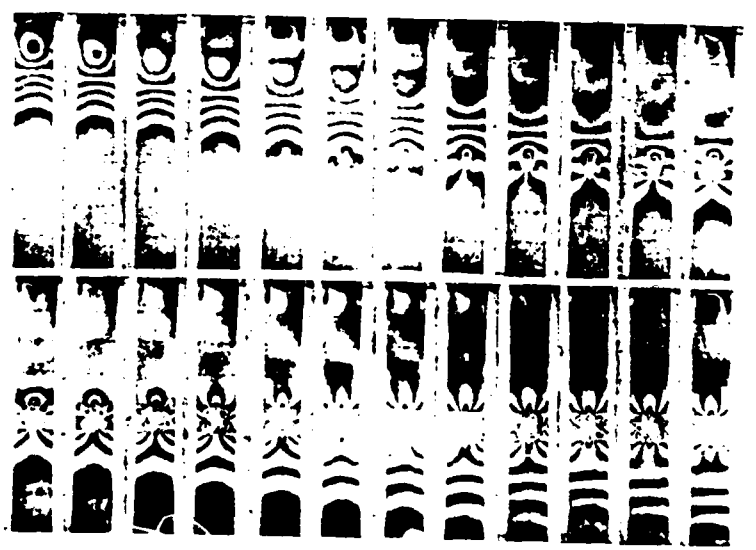

Figure 1.117. Progress of stress wave past a central circular hole in an axially loaded bar (Durelli and Dally).

dynamic loading used, the ratio of pulse length to hole diameter was approximately 16.

In a related study, Dally and Halbleib [96] determined d.s.c.f. in axially loaded struts with central circular holes having hole diameter to strut width ratios d/w of 0.15, 0.33, 0.50 and 0.67. The results indicated that the d.s.c.f. were essentially the same as the static factors for d/w ratios less than 0.35. For d/w ratios larger than 0.35, the ratio of the d.s.c.f. to the static s.c.f. became progressively smaller than 1 as the d/w ratio was increased.

During the same interval of time that the strut studies were conducted (1959–1963), Durelli and Riley [97–101] conducted a series of dynamic photo-elasticity investigations to determine d.s.c.f. associated with circular, elliptical, and square holes in large plates subjected to impact and explosive loadings. In the plate models, the discontinuities were located along a radial line 30° from the centerline of the plate as shown in Figure 1.118. The loading of the model was accomplished by dropping a weight to impact on the top edge of the plate or by detonating a small charge of lead azide explosive. The ratio of pulse length to hole diameter for the falling weight loading [97–100] was approximately 40 if the pulse length is taken as twice the rise time from zero to peak multiplied by the wave

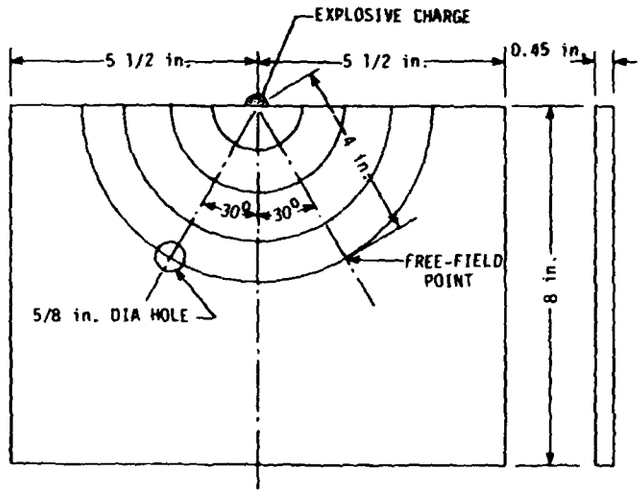

Figure 1.118. Sketch of a plate showing the location of the hole and the symmetric free-field point, for study of wave propagation around a hole. (Durelli and Riley).

front velocity. The results of the studies using falling weight loadings indicated that the dynamic compressive stresses on the hole boundary (circular, elliptical, or square) were larger than they would be in an equivalent static field. The ratio of maximum dynamic compressive stress to maximum static compressive stress was between 1.05 and 1.20 for the different models. The dynamic tensile stresses on the hole boundary were always smaller than they would be in an equivalent static field. The portion of the stress pulse studied in these models was approximately 75 percent of the front of the pulse. Thus, the peak stresses on the hole boundary were not observed. A study of a greater portion of the pulse would be possible only with larger plates or pulses of shorter duration. This was accomplished by using the explosive loadings.

When an explosive is detonated on the edge of a plate [101], both dilatational and distortional stress waves are produced. These waves propagate radially from the point of detonation of the explosive with different velocities. Thus, as the stress wave propagates, the two waves which were simultaneously generated tend to separate. Sufficient separation was achieved in the plate studies with explosive loadings to permit determination of dynamic stress concentrations due to stress fields associated with both types of waves. The rise from zero to peak of the dilatational wave indicates that the ratio of pulse length to hole diameter was approximately 10 for the explosive loading studies. A representative set of photoelastic fringe patterns for a plate with a circular hole resulting from detonation of an explosive on the edge of the plate are shown in Figure 1.119. Stress distributions on the hole boundary and at the symmetric free-field point during passage of the dilatational wave are shown in Figure 1.120. A comparison of the static and dynamic distributions shown in the figure indicates that the dynamic stresses are approximately 15 percent greater than the static stresses computed using the free-field stresses and the Kirsch [30] solution. At a later time, the hole is located in a stress field associated primarily with the distortional wave. As shown in Figure 1.121, the static and dynamic stress distributions are in good agreement at these times.

In a related series of studies, Durelli and Daniel [102] placed circular holes at different locations with respect to the point of impact of the falling weight. The results are in agreement with the preceeding discussion.

A further study of dynamic stress distributions around a circular hole in a large plate was conducted by Daniel and Riley [103]. In this study a

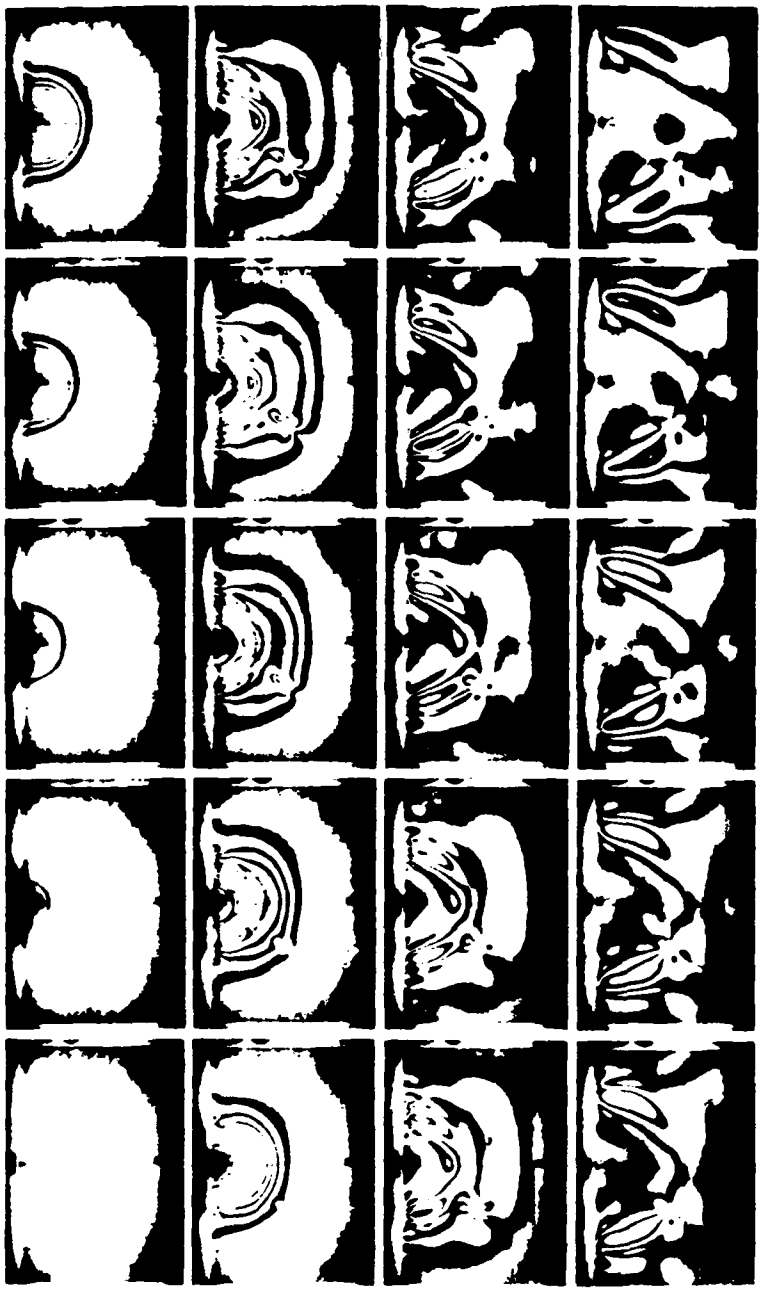

Figure 1.119. Stress wave propagation past a circular hole in a plate. The stress wave was generated by detonating a 70 mg charge of lead azide on the top edge of the plate. Photographs were taken with a Fastax camera at 6780 frames per second. (Durelli and Riley).

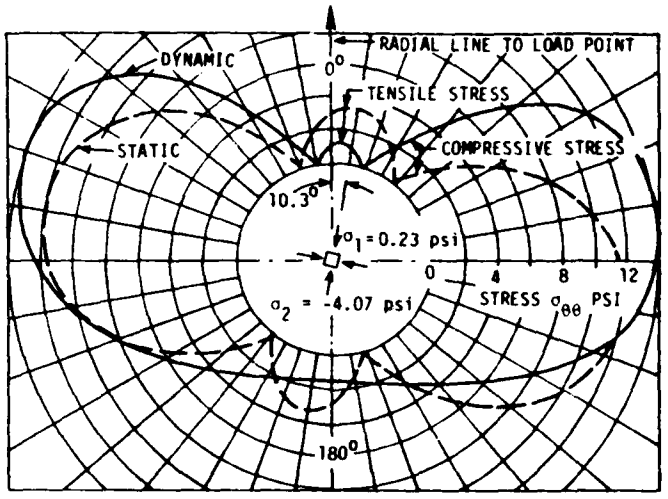

Figure 1.120. Static (free field, dotted line) and dynamic stress distributions on the hole boundary resulting from the dilational wave. (Durelli and Riley).

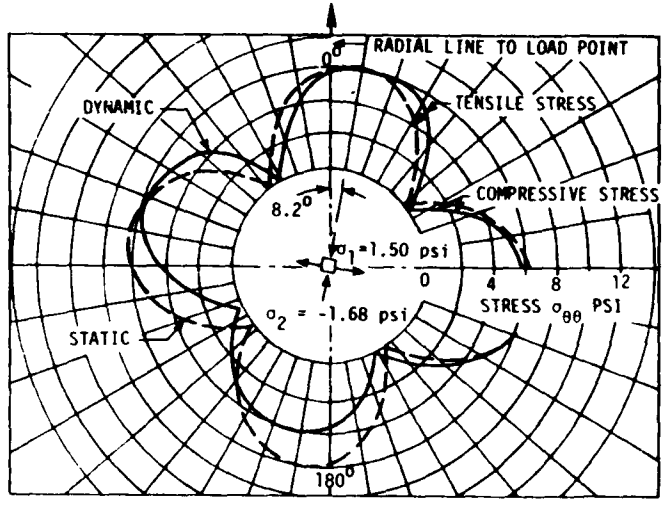

Figure 1.121. Static (free field, dotted line) and dynamic stress distributions on the hole boundary resulting from the distortional wave. (Durelli and Riley).

plane pressure (dilatational wave) was generated in the plate passing an air shock wave of fast rise and slow decay along an edge of the plate. A series of photographs of the photoelastic fringe patterns produced by the plane pressure wave propagating past the hole are shown in Figure 1.122. Detailed photographs of the photoelastic fringe patterns in the vicinity of the hole during passage of the front of the pressure pulse are shown in Figure 1.123. The results indicate that the d.s.c.f. is much lower than the static one initially as the front of the pressure pulse moves past the hole Figure 1.124. At later times, the dynamic factor exceeds the static factor by approximately 13 percent as shown in Figure 1.124. The velocity of propagation of the zero order fringe (wave front) was measured at 4400 inches per second. The results of the study are in agreement with the theoretical predictions of Baron and Matthews [90]. A study of dynamic stress distributions around a rigid circular inclusion in a large plate due to a plane pressure wave was conducted by Riley [104]. The dynamic distributions were not significantly different from static distributions computed using free-field stresses.

Photoelastic studies of dynamic stress distributions around a circular hole in a large plate due to a plane pressure wave generated by the detonation of an explosive charge of lead azide on the edge of the plate were performed by Fang, Hemann, and Achenbach [105]. Measurements were carried out for three ratios of hole diameter to pulse length. Dimensionless hoop stress as a function of time for one of the models is shown in Figure 1.125. Theoretical and experimental values of dimensionless maximum hoop stress $\sigma_{\theta\theta}/\sigma_0$ as a function of hole diameter to pulse length ratio $2a/\lambda$ are shown in Figure 1.125. The experimental determinations are in excellent agreement with the theoretical results of Mow and Pao [93].

Electrical resistance strain gage methods have been used by Shea [106] to evaluate dynamic stress concentration factors as a function of hole diameter to pulse length ratio. Thin plexiglas plates with central circular holes were used for the study. A plane pressure pulse was generated in the plates by detonating a length of 'Primacord' explosive along an edge of the plate. Results of the study are shown in Figure 1.126. These results indicate that there is a pronounced variation of the dynamic stress-concentration factor with pulse frequency. In regions of pulse length shorter than the diameter of the hole, the stress concentration factor drops off significantly. The theoretical predictions of Pao [91] are shown in the figure for comparison.

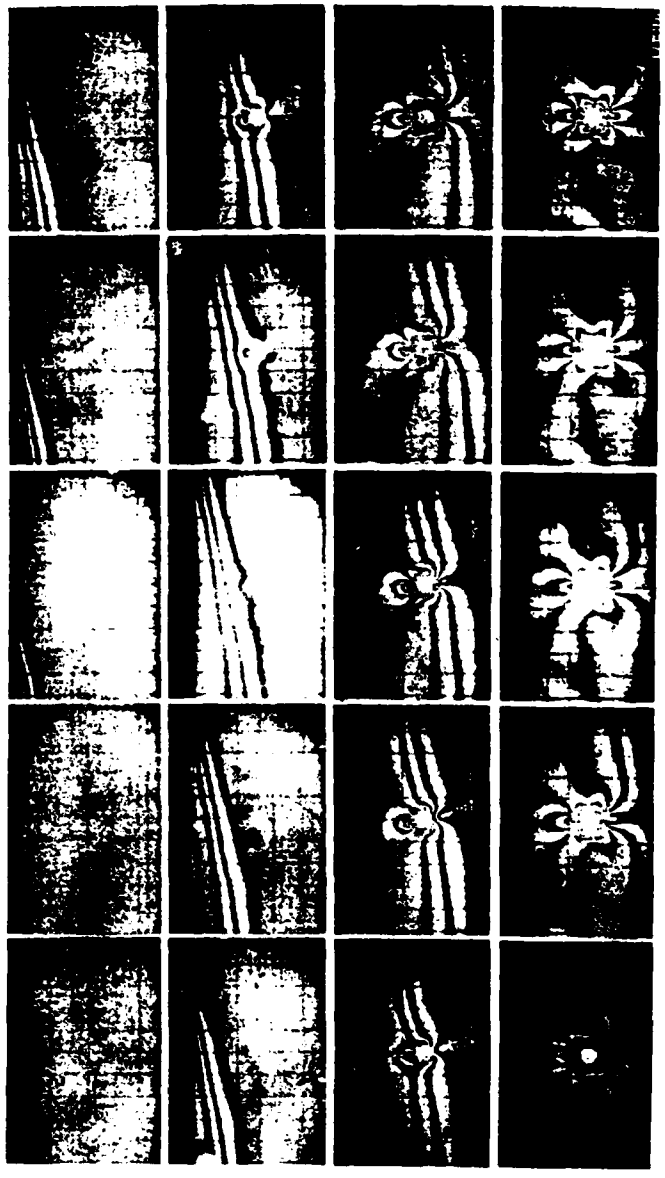

Figure 1.122. Stress wave propagation past a circular hole in a plate. The plane stress wave was generated by an air shock wave moving across the top edge of the plate. (Daniel and Riley).

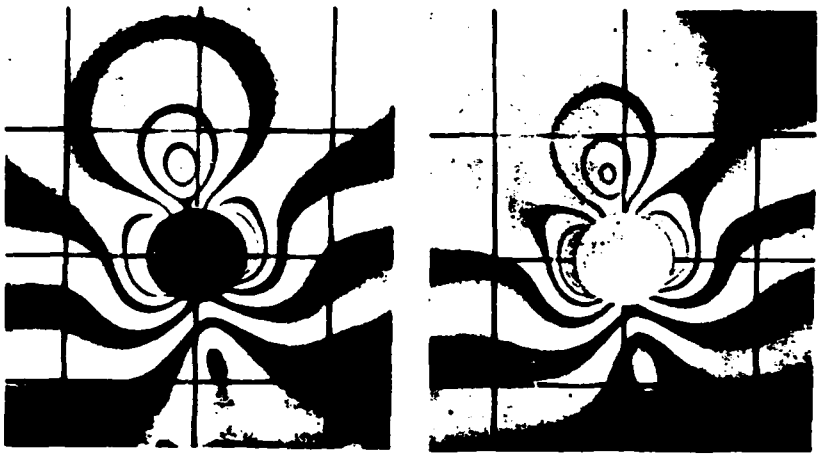

Figure 1.123. Photoelastic fringe patterns in the vicinity of the hole as the plane stress wave moves past the hole. (Daniel and Riley).

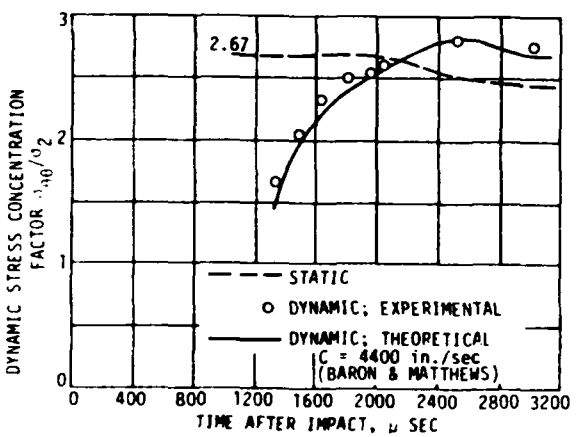

Figure 1.124. Comparison of experimental and theoretical values of maximum dynamic tangential stress on the hole boundary. (Daniel and Riley).

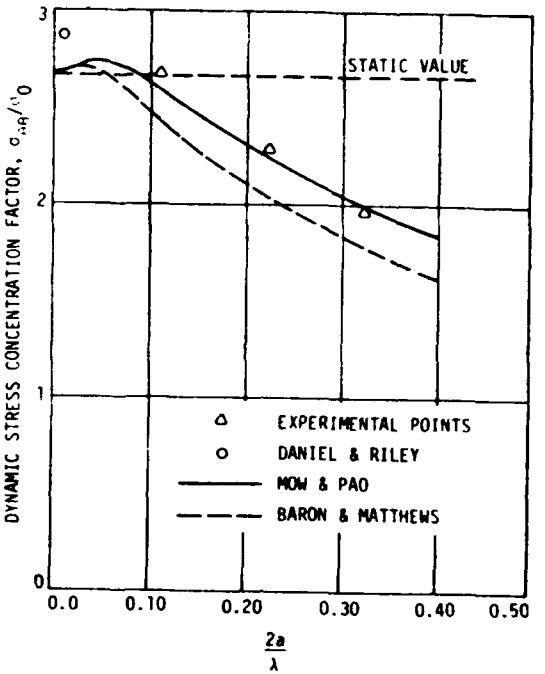

Figure 1.125. Comparison of theoretical and experimental values of the maximum dimensionless tangential stress for different hole diameter to pulse length ratios. (Fang, Hemann, and Achenbach).

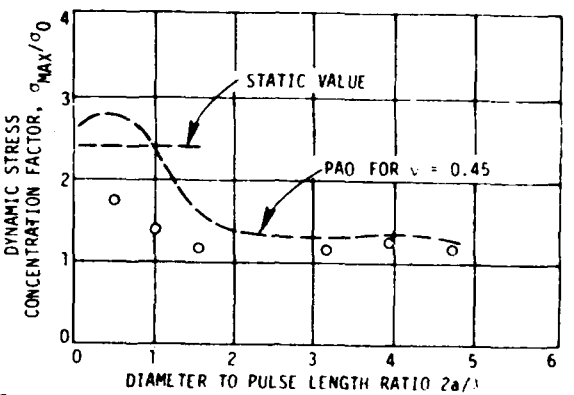

Figure 1.126. Experimental and theoretical s.c.f. as a function of the hole diameter to pulse length ratio in a plexiglass plate with central circular hole. (Shea).

1.9 Unconventional approaches to the study of stress concentrations

It is well known that the strength of brittle materials and the fatigue strength of ductile materials, in general, decreases as the size of the body increases. It is also well known that when strain gradients are present the strength of brittle materials, and the fatigue strength of ductile materials also decrease as the gradient decreases. It is also true that the onset of static yielding in the presence of stress concentrations occurs at higher loads than might be expected on the basis of the stress concentration factors calculated using theory of elasticity. On the other hand, it is also true that the presence of flaws frequently weakens the strength of a body. All these facts raise the question of the significance of the stress concentration factors as usually determined. Different schools of thought have tried to look at the situation and have taken different points of view.

Even more important than the significance of the theoretical concept of stress in mechanics, is the previous problem that develops from the fact that it is impossible to measure a stress, since by definition stress is a limiting process. Stress has to be determined indirectly, from measurements of force, or from measurements of force and displacements.

Attempts have been made at averaging the stress obtained theoretically, over the structural elements of physical bodies. Two of the contributions on the subject are one due to Neuber and the other to Gurney. Considerations on the effect of possible flaws have given origin to recent development in fracture mechanics. Theoretical developments in elasticity have included the possible influence of other elasticity constants besides E and ν. Finally the idea has come of determining the stress, not from displacement measurements and strain determinations but from values of the fracture of brittle materials. Several of these 'unconventional' approaches to the determination of stress concentration factors will be reviewed in this section.

Neuber's particle theory. After showing the failure of the traditional theory in the zone of stress concentrations, Neuber [38, 51] states that it is necessary to accept a particle of finite dimensions as a basic concept, rather than the infinitesimal parallelpiped, but that is only necessary to do so in the zone of disturbance. He suggests that the size of the particle (width ε) became a new constant of the material. The stresses acting on

this particle are the stresses computed using the classic theory of elasticity, but averaged over the surface of the particle. Neuber had developed simplified equations using the classic theory, and applying his 'theory of pointed notches' to the 'particle' at the bottom of the notch he arrives to the conclusion that the expressions giving the stress concentration factors have the same form in both cases, but that in the pointed notch theory the value of the radius of curvature ρ at the bottom of the notch has to be replaced by ρ' which is equal to one half the dimension of the particle.

This new stress concentration factor α_s is a 'technical' stress concentration factor, and has to be conceived as a limit value as the radius becomes smaller and smaller. The limit value of the stress concentration factor for a sharp shallow circumferential notch under shear or torsion is then

$$\alpha_s = \sqrt{\frac{2t}{\varepsilon}} = \sqrt{\frac{t}{\rho'}} \tag{1.60}$$

rather than the value of the infinitesimal theory $\alpha_t = \sqrt{t/\rho}$ which tends to infinity.

Similarly for deep sharp circumferential notches under shear or torsion the limiting technical factor is:

$$\alpha_s = \frac{2}{\pi}\sqrt{\frac{2a}{\varepsilon}} = \frac{2}{\pi}\sqrt{\frac{a}{\rho'}} \tag{1.61}$$

rather than the value of the infinitesimal theory

$$\alpha_t = \frac{2}{\pi}\sqrt{\frac{a}{\rho}} \tag{1.62}$$

and for the case of the deep sharp notch on both sides of a plate subjected to axial load:

$$\alpha_s = \frac{4}{\pi}\sqrt{\frac{2a}{\varepsilon}} = \frac{4}{\pi}\sqrt{\frac{a}{\rho'}} \tag{1.63}$$

rather than

$$\alpha_k = \frac{4}{\pi}\sqrt{\frac{a}{\rho}} \tag{1.64}$$

Neuber adds finally two considerations: (1) that the flank angle of the notch, which he neglected in all his developments, becomes very important when the radius of curvature at the bottom of the notch is very small. The stress concentration factors drops as the flank angle increases; (2) the deformation at the bottom of the notch is appreciable for sharp notches and its effect is to decrease the stress concentration. All these influences are taken into account using ρ the half of the length of the particle, and ω the flank angle, in the final equation:

$$\alpha_k = 1 + \frac{\alpha'_{k-1}}{1 + \frac{\pi}{\pi - \omega}\sqrt{\frac{\rho'}{\rho}}} \tag{1.65}$$

where α_k is the 'technical' stress concentration factor, and α'_k the infinitesimal one.

It is regrettable that an attempt was made at substantiating the particle theory with experimental strain analysis measurements. The author's conclusion that the particle size in steel is about 0.96 mm, (in the second edition a somewhat different reasoning gives 0.30 mm) and that the value also applies to photoelastic materials does not seem to take into consideration the accuracy and precision of mechanical and optical measurements. The selected Fischer's 'Strain Measurements' published in 1932, were conducted using mechanical strain gages on steel specimens with radii as small as 2.5 mm. A relatively high level of error could have been expected. On the other hand, the way Armbruster's tests, which contradict the theory, are disposed of, shows a regrettable tendency to fit facts to theories. Reference to the classic book of Coker and Filon would have avoided unfortunate comparisons.

The particle theory is still a good assumption to interpret rupture. It does not seem that it can be verified with usual birefringence measurements, nor with measurements obtained from mechanical strain gages. An attempt at verifying the couple-stress theory with photoelastic measurements has been recently made by Shiryaer [115] but it does not seem to prove the point either. The author claims that the stress concentration factor decreases from 2.7 to 2 when a hole in a plate is reduced in size from a radius of 4 mm to a radius of 0.5 mm. Techniques to determine fringe values, however, at the edge of holes 0.5 mm. in diameter are very delicate and subjected to numerous errors when the thickness of the specimen is 10 times the radius of the discontinuity. The gradient of the stresses becomes very high requiring high resolution of the

fringe, the 'space' effect at the edge is relatively more pronounced, and so is the three dimensional effect. It is quite possible that the apparent decrease in s.c.f. is due to the fact that fringes cannot be detected, rather than to the effect of 'particles' or 'couple stresses'.

Gurney's stress averaging over an atom. The particle considered by Neuber is not physically defined, and its size is computed indirectly. From the context, and the comparisons with experimental determinations, it seems to correspond approximately to the grains in some metals, for instance the chromium–chromium carbide shown in Figure 1.6, or the inclusions in the rocket solid propellant shown in Figure 1.5. No attempt was made to analyze what may happen at the level of the atomic structure.

Gurney [107] tries to average the stresses predicted by elasticity theory over the volume occupied by an atom. The computation is conducted for a small length ϵ at the end of an elliptical crack of length 2a, having radius ρ. (Neuber's notation is used for easier continuity in the development of this way of thinking.) Because of simplicity in handling the equations, the stress concentration factors are computed for the case of equal biaxiality. Gurney concludes that whereas the real value is $2t/s$, t and s being the semiaxes of the ellipse, when the radius equals the length over which the stress is averaged, the effective stress concentration (or average effect) or 'technical' value is only 1.1 t/s. If the radius of curvature is made zero, the effective stress concentration factor is

$$1.8\sqrt{\frac{t}{\epsilon}} \tag{1.66}$$

Therefore decreasing ρ at the end of the crack from ϵ to zero, only increases the average stress over ϵ by about 70%.

Cox's studies on microscopic flaws. If a plate containing a hole with its axis perpendicular to the plane of the plate is stressed in the plane of the plate, the maximum stress is tangential to the free edge of the hole, and is the only one with non-zero value of three principal stresses at the point. A material with a system of such holes would fail under a uniaxial state of stress, irrespective of the law of failure of the material and irrespective of the loading conditions in the plane of the plate. It is also true that the ratio of the ultimate stress under shear and the ultimate

stress under uniaxial tension applied to the plates as a whole would depend only on the geometry of the hole and the ratio between the strength of the material under uniaxial tension and compression. Cox [108] adds that if by experiments materials do not conform to this reasoning, it would mean that the rate of variation of stress in the neighborhood of the point of maximum stress must have also an influence on failure. (This conclusion could of course have been obtained otherwise.)

The author considers also the case of cylindrical holes oriented at random and representative of flaws that could be microscopic or even submicroscopic in size, provided that their size is still large by comparison with the atomic structure of the material.

He concludes that internal flaws are unlikely to account for the mechanical properties of engineering materials. He adds that experimental results do not support the hypothesis that the low strength of materials in relation to estimates of their strength based on thermodynamic data, may be explained by assuming that all materials contain numerous sub-microscopic flaws. The conclusion seems to go against the present trends in the analysis of fracture.

Notch sensitivity. Discussions on 'particles' on which the stress is averaged, on the effect of stress on 'atoms,' or on microscopic or submicroscopic 'flaws' present in a material, are sometimes motivated by theoretical thinking. Theoreticians try to better simulate the physical reality. Frequently, however, these studies belong to the attempts of engineers to make the results of the theory of elasticity useful to solve problems in design.

In few words the fact is that materials seldom if ever fail with a reduction in strength of the magnitude of the stress concentration factor. Theoretically inclined people may look at the situation talking about the influence of stress on atoms. Engineers try to explain it using words like 'notch sensitivity,' or 'volume of material' subjected to the maximum stress, or to some percentage of it. Contributions of Peterson (2) and Lipson [40] can be included in this last group of studies.

The notch sensitivity index can be expressed as:

$$q = \frac{K_f - 1}{K_t - 1} \tag{1.67}$$

with values varying from 0 for materials ignoring the presence of the

concentration, to 1 for materials behaving ideally as could be predicted from theory of continuum. In equation (1.67), K_f is the so-called 'fatigue stress concentration factor' given by:

$$K_f = \frac{\text{endurance limit of specimens without a notch}}{\text{endurance limit of specimens with a notch}} \tag{1.68}$$

and K_t is what has been called here s.c.f.

The concept of 'notch sensitivity' does not hide completely the fact that s.c.f. are determined using loads at failure. From equation (1.67), it follows that:

$$K_t = \frac{K_f - 1}{q} + 1 \tag{1.69}$$

This approach determines therefore the s.c.f. by measuring two loads at failure, one acting on the notched body and the other acting on the plain body.

Size and stress concentration. Concepts like 'notch sensitivity' try to explain the difference in behavior of different materials in which the same notch or groove is present. But another fact complicating behavior has also to be considered. It is the fact that the same material, subjected to the same level of stress may behave differently depending on its size. Reference is made here to the classic work of Weibull, recently reviewed by Freudenthal [109]. A contribution has also been made in [110] to explain at the same time the size and gradient of stress influence, and the sensitivity of the material to the presence of the discontinuity. It is sufficient to test the material to failure using two specimens with different stress gradients. The relationship between stress and volume v of material subjected to 95 percent of the maximum stress, or more, is given by:

$$\sigma = \sigma_s \left(\frac{v_s}{v}\right)^{\ln(\sigma_r/\sigma_s)/\ln(v_r/v_s)} \tag{1.70}$$

where σ is the maximum stress at the point of failure, v is the volume of material subjected to 95 per cent or more of the maximum stress, and r and s correspond to tests conducted on the different specimens. When the material has been calibrated by conducting tests on two specimens,

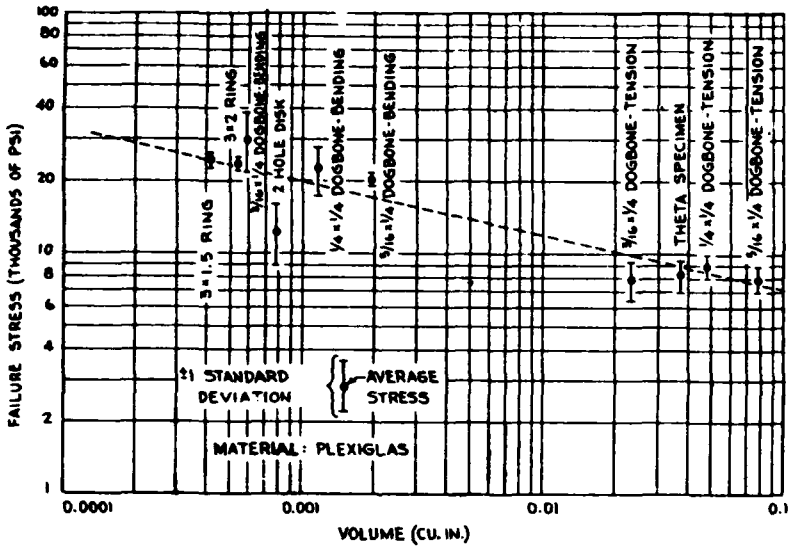

Figure 1.127. Value of σ_1 at failure vs. volume subjected to 95% of σ_1, or more, for plexiglas specimens.

and σ_r, σ_s, v, and v_s are known, the tensile strength can be obtained from

$$\sigma = c(v)^{-k} \tag{1.71}$$

where c and k are constants. The relationship comes directly from the plot of the straight line on log-log paper. An illustration is shown in Figure 1.127. The value 95% has been selected for convenience, but could be related to statistical concepts.

Here again s.c.f. is computed by measuring two loads at failure, P that produces failure in a body of volume v and P_s that produces failure in a body of volume v_s. It is sufficient to replace in equation (1.70) $\sigma/\sigma_s = P/P_s$ thus:

$$\text{s.c.f.} = \frac{\sigma}{\sigma_s} = \frac{P}{P_s} = \left(\frac{v_s}{v}\right)^{(\ln(\sigma_r/\sigma_s)/\ln(v_s/v_r))} \tag{1.72}$$

This approach emphasizes the concept that the s.c.f. is not a constant quantity, ideally determined, but depends on the specimen taken as reference. It also suggests that the reference could be made absolute if a

maximum limit like E/10, or a fundamental particle with a size of order 0.0001 in. could be determined and its concept clarified.

Couple stresses and micropolar elasticity. Recent developments in the classical theory of elasticity also attempt, in a different way, to bring stress concentrations factors down to the values obtained from experiments. Among the most important, the theories of 'couple stresses' and 'micropolar elasticity' should be mentioned. Both require the introduction of new material constants, with dimensions of a length, and give results which depend on the relative size of the discontinuity and the characteristic new constants of the material. These new constants in a more elaborated and refined way do a work similar to the one attempted by Neuber with the use of 'particles' (Section 1.9). An illustration of the variation in the stress concentration factors associated with an elliptical hole in an infinite plate subjected to uniaxial loading is shown in Figure 1.128 as obtained by Kim and Eringen [111] using micropolar elasticity. A similar illustration of the variation in the stress concentration factor associated with a circular hole in an infinite plate subjected to uniaxial loading is shown in Figure 1.129, as obtained by Mindlin [112] using the theory that includes couple stresses in the equations of equilibrium. Sternberg and Muki studied the problem of the crack [113] and Hartranft

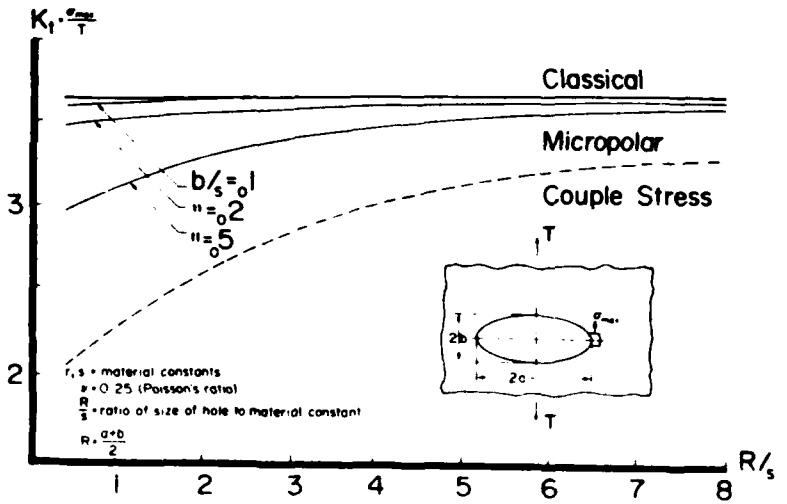

Figure 1.128. Stress concentration factors for an elliptical hole, according to several theories. (Kim and Eringen).

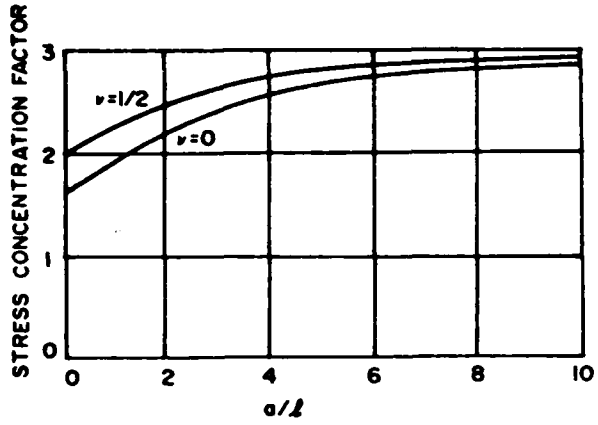

Figure 1.129. Stress concentration factor at a circular hole in a field of simple tension: variation with ratio of radius of hole to material constant 1. (couple-stress theory, by Mindlin).

and Sih [114] the problem of the circular inclusion, also using couple-stress theory. Shiryaer [115] claims to have proved experimentally the decrease in the value of the s.c.f. as the size of a hole decreases, using photoelasticity. As pointed out earlier the evidence is not convincing.

Stress intensity factors. The so-called stress intensity factors have been rationalized and determined, independently, by several authors. They all have the same basic form: a constant times the square root of a length (usually half the length of a crack)

$$K = p\sqrt{\pi t} \tag{1.73}$$

The stress at the end of the major axis of an elliptical hole, subjected to a single load perpendicular to that major axis, in terms of the radius of curvature at that point is given by equation (1.48). When ρ is very small in relation to t, equation (1.48) can be approximated by:

$$\sigma \simeq 2p\sqrt{\frac{t}{\rho}} \tag{1.74}$$

(Recall that t is half the axis of the ellipse and ρ the radius of curvature at the base of the notch.)

This equation is of the same form as the one giving the typical stress

intensity factor, equation (1.73). The relationship is obvious:

$$\sigma = p\frac{2}{\sqrt{\rho}}\sqrt{t}; \quad K = p\sqrt{\pi}\sqrt{t} \tag{1.75}$$

Catalogs of values of stress intensity factors for numerous problems have been published by Cartwright and Rooke [116]. Sih [117, 118], Tada, Paris and Irwin [119], and Rooke and Cartwright [120]. Most of the solutions reported have been obtained analytically, or using numerical methods.

Conclusions. It follows from the previous considerations that the mathematical concept of stress concentration factor cannot be used in a direct simple manner to explain or to predict fracture. In a micro scale, matter is not continuous and cannot be divided indefinitely without changing its properties. It is true that in general a body with a stress concentration of k does not fail when the point at which the concentration is located is subjected to a stress equal to $k\sigma_{av} = \sigma_u$, σ_u being the ultimate stress in calibrating specimens tested at the same temperature, at the same strain rate and to the same number of loading cycles. It usually takes higher stress than $k\sigma_{av}$, which leads to the studies summarized above trying to explain why the load at fracture may be higher than the theoretically predicted.

References

[1] Roark, R. J. and Young, W. C., *Formulas for Stress and Strain*, Fifth edition, McGraw-Hill (1975). The first edition was published in 1938.

[2] Peterson, R. E., *Stress Concentration Factors*, John Wiley and Sons, New York, pp. 316 (1974). A first version: Peterson, R. E.: 'Stress Concentration Design Factors' was published by Wiley in 1953.

[3] Griffel, W., *Handbook of Formulas for Stress and Strain*, Frederick Ungar Publishing Co., pp. 418 (1966).

[4] Tetelman, A. S. and McEvily, A. J., *Fracture of Structural Materials*, Wiley (1967).

[5] Savin, G. N., *Stress Distribution Around Holes*, Kiev (1968), Transl. NASA, TTF-607, p. 997 (Nov. 1970). The first edition: Savin, G. N., Concentration of Stress Around Holes was published in 1951 by the State Publishing House of Technical Theoretical Literature. Trans. Pergamon Press (1961).

[6] Durelli, A. J., Phillips, E. and Tsao, C., *Introduction to the Theoretical and Experimental Analysis of Stress and Strain*, McGraw-Hill (1958).

[7] Durelli, A. J., *Applied Stress Analysis*, Prentice-Hall (1967).

[8] Durelli, A. J., The Difficult Choice, Feature Article in *Applied Mechanics Reviews*, pp. 1167–1178 (Sept. 1977).
[9] Collatz, L., *The Numerical Treatment of Differential Equations*, 3rd. Ed. Trans. by P. G. Williams, Springer-Verlag, N. Y. (1966).
[10] Hulbert, L. E., The Numerical Solution of Two-Dimensional Problems of the Theory of Elasticity, *Ph.D. Dissertation*, Ohio State University (1963).
[11] Muskhelishvili, N. T., *Some Basic Problems of the Mathematical Theory of Elasticity*, Translated by J. R. M. Radok, P. Noordhoff Ltd., Groningen, The Netherlands (1963).
[12] Wilson, H. B. Jr., Mathematical Determination of Stresses and Displacements in Star-perforated Grains, *AIAA Journal* 2, pp. 1247–1253 (July 1964).
[13] Wilson, H. B., Jr. and Becker, E. B., *An Effective Numerical Method for Conformal Mapping of Simply Connected Regions*, Developments in Mechanics, Vol. 3, Part I: Solid Mech. and Mat., John Wiley and Sons, Inc., pp. 403–414 (1967).
[14] Richardson, M. K. and Wilson, H. B., Jr., *A Numerical Method for the Conformal Mapping of Finite Doubly Connected Regions*, Developments on Theoretical and Applied Mechanics, Vol. 3, pp. 305–321, edited by W. A. Shaw, Pergamon Press (1967).
[15] Laura, P. A., Conformal Mapping of a Class of Doubly Connected Regions, *Ph.D. Dissertation*, The Catholic University of America (1965).
[16] Rao, A. K., Review of Continuum, Finite Element and Hybrid Techniques in the Analysis of Stress Concentration in Structures, *Nuclear Engineering and Design*, Vol. 31, pp. 427–433 (1974).
[17] Dunham, R. S. and Becker, E. B., TEXGAP the Texas Grain Analysis Program, *TICOM Report 73–1*, The University of Texas at Austin (Aug. 1973).
[18] Bushnell, D., *Difference Models Versus Finite-elements Models*, Numerical and Computer Methods in Structural Mechanics, Academic Press, New York, pp. 291–336 (1973).
[19] Key, S. and Krieg, R., *Comparison of Finite-element and Finite-difference Methods*, Numerical and Computer Methods in Structural Mechanics, Academic Press, New York, pp. 337–352 (1973).
[20] Perrone, N. and Kao, R., A General Finite Difference Method for Arbitrary Meshes, *International Journal of Computers and Structures*, 5, pp. 45–57 (April 1975).
[21] Zienkiewicz, O. C., in volume The Mathematics of Finite-elements and Applications, edited by J. R. Whiteman. *Proceedings of Brunel University Conference, April 1972*, Academic Press (1973).
[22] Oden, J. T., Finite-element Applications in Nonlinear Structural Analysis, in *Proceedings of ASCE Symposium on Application of Finite Element Methods in Civil Engineering*, Nashville (1969) ed. by W. H. Rowan, Jr. and R. M. Hackett, Vanderbilt Univ. (1969).
[23] Durelli, A. J., Parks, V. J. and Feng, H., Evaluation of Grid Data to Determine Displacements and Strains, *Journal of Strain Analysis*, Vol. 2, No. 3, pp. 181–187 (July 1967).
[24] Fischer, G., Versuche ueber die Wirkung von Kerben an elastische beanspruchten Biegestaeben, *Dissertation Aachen* (1932), V. D. I. Verlag, Duesseldorf (1932).
[25] Durelli, A. J., Phillips, E. and Tsao, C., *Introduction to the Theoretical and Experimental Analysis of Stress and Strain*, McGraw-Hill (1958).
[26] Parks, V. J. and Durelli, A. J., Moiré Patterns of Partial Derivatives of Displacement Components, *Journal of Applied Mechanics*, Vol. 33, pp. 901–906 (1966).
[27] Erf, R. K. (ed.) *Holographic Non-destructive Testing*, Academic Press, (1974).

[28] Erf, R. K. (ed.) *Speckle Metrology*, Academic Press (1978).
[29] Bickle, L. W., The response of Strain Gages to Longitudinally Sweeping Strain Pulses, *Experimental Mechanics*, Vol. 10, No. 8, pp. 333–337 (August 1970).
[30] Kirsch, G., Ueber einige Eigenschaften des ebenen Problems der Elastizitaetstheorie, *Zeit. des Ver. Deutscher Ing.* Vol. 42, pp. 787–807 (1890).
[31] Inglis, C. E., Stresses in a Plate Due to the Presence of Cracks and Sharp Corners, Trans. Inst. Naval Arch. London, England, 1913; *Engineering*, Vol. 95, p. 415 (1913).
[32] Durelli, A. J., Phillips, E. A. and Tsao, C. H., *Introduction to the Theoretical and Experimental Analysis of Stress and Strain*, McGraw-Hill (1958).
[33] Kosolov, G. V., *On One Application of the Theory of Complex Variable Functions to Plane Problems of the Mathematical Theory of Elasticity*, Yurger (1909).
[34] Isida, M., On the Tension of a Semi-infinite Plate with an Elliptic Hole, *Science Papers of Faculty of Engineering*, Tokushima University, Vol. 5, No. 1 (Feb. 1955).
[35] Durelli, A. J., Parks, V. J. and Feng, H. C., Stresses Around an Elliptical Hole in a Finite-Plate Subjected to Axial Loading, *Journal of Applied Mechanics*, pp. 192–195 (March 1966).
[36] Coker, E. G. and Filon, L. N. G., *A Treatise on Photo-elasticity*, Cambridge University Press (1931).
[37] Lehr, E., *Spannungsverteilung in Konstruktionselementen*. Auswertung der bisheringen Forschungsergebnisse für die praktische Anwendung. VDI-Verlag, Berlin (1934).
[38] Neuber, H., *Theory of Notch Stresses: Principles for Exact Stress Calculation*. Transl. of Kerbspannungslehre: Grundlagen fuer genaue Spannungsrechnung, Springer, Berlin (1937), by David Taylor Model Basin, Washington, D. C. Nov. 1945.
[39] Roark, R. J. and Young, W. C., *Formulas for Stress and Strain*: Fifth ed., McGraw-Hill (1975). The first edition was published in 1938.
[40] Lipson, C., Noll, G. and Clock, L., *Stress and Strength of Manufactured Parts*, McGraw-Hill, (1950).
[41] Savin, G. N., *Stress Distribution Around Holes*, Kiev (1968), Transl. NASA, TTF-607, pp. 997 (Nov. 1970). A first version: Savin, G. N., Concentration of Stress Around Holes, was published in 1951 by the State Publishing House of Technical Theoretical Literature. Trans. Pergamon Press (1961).
[42] Foeppl, L. and Sonntag, G.: *Tafeln und Tabellen zur Festigkeitslehre*. R. Oldenburg, Muenchen (1951).
[43] Peterson, R. E., *Stress Concentration Factors*: John Wiley and Sons, New York, pp. 316 (1974). A first version: Peterson, R. E.: Stress Concentration Design Factors was also published by Wiley in 1953.
[44] Griffel, W., *Handbook of Formulas for Stress and Strain*, Frederick Ungar Publishing Co., p. 418 (1966).
[45] Nisitani, H.: *Solutions of Notch Problems by Body Force Method*. Mechanics of Fracture, ed. by G. C. Sih, Noordhoff Intern. Publish. Alphen aan den Rijn., Vol. 5, pp. 1–68.
[46] Heywood, R. B., *Photoelasticity for Designers*, Pergamon Press (1969).
[47] Hogan, M. B., A Survey of the Literature Pertaining to Stress Distribution in the Vicinity of a Hole and the Design of Pressure Vessels, Bull. No. 48, *Utah Engineering Experimental Station*, Vol. 41, No. 2 (Aug. 1950).
[48] Neuber, H. and Hahn, H. G., Stress Concentration in Scientific Research and Engineering, *Applied Mechanics Reviews*, Vol. 19, No. 3 (March 1966).

[49] Sternberg, E., Three-dimensional Stress Concentrations in the Theory of Elasticity, *Applied Mechanics Reviews*, Vol. 11, pp. 1–4 (Jan. 1958).

[50] Durelli, A. J., The Difficult Choice, *Applied Mechanics Reviews*, Vol. 30, No. 9, pp. 1167–1178 (Sept. 1977).

[51] Neuber, H., *Theory of Notch Stresses*: Principles of Exact Calculation of Strength with Reference to Structural Form and Material. Transl. of Kerbspannungslehre: Grundlage für genaue Festigkeit Berechnung mit Beruecksichtigung von Konstruktion's form und Werkstoff. Springer, Berlin (1958) by U.S. Atomic Energy Comm. AEC-tr-4547, Chap. X, (June 1961).

[52] Durelli, A. J., Parks, V. J. and Lopardo, V. J., Stresses and Finite Strains Around an Elliptic Hole in Finite Plates Subjected to Uniform Load, *International Journal of Non-Linear Mechanics*, Vol. 5, pp. 397–411 (1970).

[53] Durelli, A. J., Parks, V. J., Lopardo, V. J. and Chen, T. L., Normalized Stresses Around an Elliptic Hole in a Finite Plate of Linear Material Subjected to Large Uniform In-plane Loading, *Experimental Mechanics*, Vol. 13, No. 10 pp. 441–444 (Oct. 1973).

[54] Chen, T. L. and Durelli, A. J., Stress Field in a Sphere Subjected to Large Deformations, *International Journal of Solids and Structures*, Vol. 9, pp. 1035–1052 (1973).

[55] Chen, T. L. and Durelli, A. J., Displacements and Finite-Strain Fields in a Hollow Sphere Subjected to Large Elastic Deformations, *International Journal of Mechanical Science*, Vol. 16, pp. 777–788 (1974).

[56] Durelli, A. J. and Mulzet, A. P., Large Strain Analysis and Stresses in Linear Materials, *Journal of Engineering Mechanical Division*, Proc. ASCE., June 1965, pp. 65–91.

[57] Durelli, A. J., Parks, V. J. and Feng, H., Experimental Methods of Large Strain Analysis, *International Journal of Non-Linear Mechanics*, Vol. 2, pp. 387–404 (1967).

[58] Durelli, A. J., Parks, V. J. and Chen, T. L., Stress and Finite-Strain Analysis of a Circular Ring Under Diametral Compression, *Experimental Mechanics*, pp. 210–214 (May 1969).

[59] Durelli, A. J., Parks, V. J. and Bühler Vidal, J. O., Linear and Non-Linear Elastic and Plastic Strains in a Plate with a Large Hole Loaded Axially in its Plane. *International Journal of Non-Linear Mechanics*, Vol. 11, pp. 207–211 (1976).

[60] Durelli, A. J. and Parks, V. J., Photoelastic Stress Analysis in the Bonded Interface of a Strip with Different End Configurations, *American Ceramic Society Bulletin*, Vol. 46, No. 6, pp. 586 (June 1967).

[61] Durelli, A. J., Parks, V. J. and Bhadra, P., Experimental Determination of Stresses and Strains in a Rectangular Plate Subjected to Biaxial Restrained Shrinkage, *British Journal of Applied Physics*, Vol. 17, pp. 917–926 (1966).

[62] Parks, V. J. and Durelli, A. J., Stress Distribution at Variously Shaped Corners in Plates, Bonded on Two Long Edges, and Subjected to Restrained Shrinkage, Mech. Behavior Working Group, Interagency Chemical Rocket Propulsion Group, *CPIA Bulletin*, No. 119, Vol. 1, pp. 365–392 (Nov. 1966).

[63] Durelli, A. J., Parks, V. J., and del Rio, C. J., Stresses in Square Slabs with Different Edge Geometries, when Bonded on One Face to a Rigid Plate and Shrunk, *Experimental Mechanics*, Vol. 7, No. 11, pp. 481–484 (Nov. 1967).

[64] Duffy, J., The Elastic Wedge under Mixed Boundary Conditions, *Technical Report*, No. 1, Div. Engng., Brown Univ., DA-G4-1-April (1961).

[65] Theocaris, P. S. and Dafermos, K., The Elastic Strip Under Mixed Boundary Conditions, *Applied Mechanics*, 31, (Trans. Amer. Soc. Mech. Engrs., 86, pp. 714–716) (Dec. 1964).

[66] Aleck, B. J., Thermal Stresses in a Rectangular Plate Clamped Along an Edge, *Journal of Applied Mechanics*, 16, pp. 118–22 (1949).

[67] Parks, V. J., Durelli, A. J. and Chen, T. L., Stresses in a Restrained Shrinking Disk with a Central Slot, *AIAA Journal*, Vol. 6, No. 6, pp. 1181–1182 (June 1968).

[68] Durelli, A. J., Parks, V. J. and Lee, Han-Chow, Stress Concentrations Around Elliptical Perforations in Shrunk Plates with Bonded Boundaries, *Journal of Spacecraft and Rockets*, Vol. 5, No. 2, pp. 1499–1501 (Dec. 1968).

[69] Durelli, A. J. and Tsao, C. J., Determination of Thermal Stresses in Three-Ply Laminates., *Journal of Applied Mechanics*, Vol. 22, No. 2, pp. 190–193 (June 1955).

[70] Parks, V. J., Chiang Fu-pen and Durelli, A. J., Maximum Stress at the Angular Corners of Long Strips Bonded on One Side and Shrunk. *Experimental Mechanics*, pp. 278–281 (June 1968).

[71] Durelli, A. J., Parks, V. J. and Chen, T. L., Stress Concentrations in a Rectangular Plate with Circular Perforations Along its Two Bonded Edges and Subjected to Restrained Shrinkage, *Strain*, Vol. 5, No. 1, pp. 1–4 (Jan. 1969).

[72] Hofer, K. E. and Durelli, A. J., Stress Distribution at the Fillet of an Internal Flange, *Journal of Applied Mechanics*, Vol. 28, E, No. 4. pp. 618–623 (Dec. 1961).

[73] Durelli, A. J. and Parks, V. J., Stresses in Pressurized Circular Shells with Discontinuities, with or without Stiffeners, *Journal of Ship Research*, Vol. 16, No. 2, pp. 140–147 (1972).

[74] Durelli, A. J., del Rio, C. J., Parks, V. J. and Feng, H., Stresses in a Pressurized Cylinder with a Hole, *Journal of Structure Division Proceedings ASCE*, Vol. 93, paper No. 5524, pp. 383–399 (Oct. 1967).

[75] Durelli, A. J., Parks, V. J. and Lee, H. C., Stresses in a Perforated Ribbed Cylindrical Shell Subjected to Internal Pressure, *International Journal of Solids and Structures*, Vol. 5, No. 6, pp. 573–586 (June 1969).

[76] Durelli, A. J., Parks, V. J. and Lee, H. C., Stresses in a Pressurized Cylindrical Shell with Two Unequal Diametrically Opposite Reinforced Circular Holes, *Acta Mechanica*, Vol. X, No. 3–4, pp. 161–179 (1970).

[77] Durelli, A. J., Parks, V. J. and Lee, H. C., Stresses in a Pressurized Ribbed Cylindrical Shell with a Reinforced Hole, *Report to Naval Ship Research and Development Center*, (Feb. 1969).

[78] Durelli, A. J. et al. Stresses in a Pressurized Ribbed Cylindrical Shell with a Reinforced Circular Hole Interrupting a Rib, Trans. ASME, *Journal of Engineering for Industry*, Series B, Vol. 93, No. 4, pp. 897–904 (Nov. 1971).

[79] Durelli, A. J. and Barriage, J. B., Stress Distribution in Square Plates with Hydrostatically Loaded Central Circular Holes, *Journal of Applied Mechanics*, Trans. ASME, Vol. 77, pp. 539–544 (1955).

[80] Durelli, A. J. and Riley, W. R., Stress Distribution in Strips with Hydrostatically Loaded Central Circular Holes, Proc. Mid-Western Conf. on Solid Mechanics, pp. 81–93 (Oct. 1955).

[81] Durelli, A. J. and Kobayashi, A. S., Stress Distributions Around Hydrostatically Loaded Circular Holes in the Neighborhood of Corners, *Journal of Applied Mechanics*, Vol. 26, No. 1, pp. 150–152 (March 1959).

[82] Riley, W. F., Durelli, A. J. and Theocaris, P. S., Further Stress Studies on a Square Plate with a Pressurized Central Circular Hole., Proc. 4th Annual Conf. on Solid Mech., Univ. of Texas, Austin, Texas, Sept. 1959, pp. 91–107.

[83] Parks, V. J., Durelli, A. J., Chandrashekhara, K. and Chen, T. L., Stress Distribution Around a Circular Bar, with Flat and Spherical Ends, Embedded in a Matrix in a Uniaxial Stress Field, *Journal of Applied Mechanics*, pp. 578–586 (Sept. 1970).

[84] Riley, W. F. and Durelli, A. J., Boundary Stresses at the Ends of Pressurized Cylindrical Holes Axially Located in a Large Cylinder, *Proceedings SESA*, Vol. XVII, No. 1, pp. 115–126 (Dec. 1959).

[85] Durelli, A. J., Parks, V. J. and Del Río, C. J., *Stresses, Strains and Displacements Associated with the Restrained Shrinkage of Cylinders with Toroidal Cavities*, Recent Advances in Engineering Science, Ed. A. C. Eringen, Vol. 3, pp. 521–540, Gordon and Breach, Sc. Publishers, NY (1968).

[86] Durelli, A. J., Parks, V. J., Feng, H. C. and Chiang, F., Strains and Stresses in Multiply Connected Inserts, Mechanics of Composite Materials, Proc. 5th Symposium on Naval Structural Mechanics, Ed. by Wendt, Liebowitz and Perrone, Pergamon, 1970, pp. 299–335.

[87] Durelli, A. J., Pavlin, V., Buhler Vidal, J. O. and Orne, G., Elastostatics of a Cubic Box Subjected To Concentrated Loads, *Strain*, Vol. 13, No. 1, pp. 7–12 (Jan. 1977).

[88] Durelli, A. J., Pavlin, V. and Buhler Vidal, J. O., Elastostatics of Cubic Boxes Subjected to Pressure, *Journal of Pressure Vessel Technique*, Vol. 99, pp. 568–574 (Nov. 1977).

[89] Sezawa, K. and Imbo, Y., A Dynamical Problem of Stress Concentration, *Journal of the Faculty of Engineering*, University of Tokyo, Japan, Vol. 24, p. 101 (1955).

[90] Knight, M. J. and Matthews, A. T., Diffraction of a Pressure Wave by a Cylindrical Cavity in an Elastic Medium, *Journal of Applied Mechanics*, Series E, Vol. 28, No. 3, pp. 343–348 (1961).

[91] Baron, M. L., Dynamic Stress Concentration in an Elastic Plate, *Journal of Applied Mechanics*, Series E, Vol. 29, No. 2, pp. 299–305 (1962).

[92] Baron, M. L., Transient Response of a Rigid Spherical Inclusion in an Elastic Medium, *Applied Mechanics*, Vol. 32, No. 3, pp. 637–000 (September 1965).

[93] Baron, M. L. and Bleich, Y. H., The Diffraction of Elastic Waves and Dynamic Stress Concentrations, RAND Corporation, Report No. R-482-PR, (April 1971).

[94] Baron, M. L. and Parnes, D., *The Dynamic Stress Distribution Surrounding a Running Crack—A Photoelastic Analysis*, *Proceedings of SESA*, Vol. 16, No. 1, pp. 69–92 (1958).

[95] Bleich, H. H. and Davy, J. W., Stress Concentration Factors Under Dynamic Loading Conditions, *Applied Mechanical Engineering Science*, Vol. 1, No. 1, pp. 1–5 (June 1959).

[96] Bleich, H. H. and Riley, W. F., Dynamic Stress Concentrations at Circular Holes in Plates, *Applied Engineering Science*, Vol. 7, No. 1, pp. 23–27 (March 1973).

[97] Durelli, A. J. and Riley, W. F., Stress Distribution on the Boundary of a Circular Hole in a Large Plate During Passage of a Stress Pulse of Long Duration, *Journal of Applied Mechanics*, Vol. 28, No. 2, pp. 245–251 (1961).

[98] Durelli, A. J. and Riley, W. F., Stress Distribution on the Boundary of an Elliptical Hole in a Large Plate During Passage of a Stress Pulse of Long Duration (Major Axis Parallel to the Wave Front), *International Journal of Mechanical Sciences*, Vol.

[99] Durelli, A. J. and Riley, W. F., Stress Distribution on the Boundary of an Elliptical Hole in a Large Plate During Passage of a Stress Pulse of Long Duration (Major Axis Normal to the Wave Front), *Journal of Applied Physics*, Vol. 32, No. 7, pp. 1255–1260 (July 1961).

[100] Durelli, A. J., Riley, W. F. and Carey, J. F., Stress Distribution on the Boundary of a Square Hole in a Large Plate During Passage of a Stress Pulse of Long Duration, Proceedings of the International Symposium on Photoelasticity, Pergamon Press, N.Y., 1963, pp. 251–263.

[101] Riley, W. F. and Durelli, A. J., Stress Distribution on the Boundary of a Circular Hole in a Large Plate During Passage of a Stress Pulse of Short Duration, *Journal of Mechanical Engineering Sciences*, Vol. 3, pp. 62–68 (1961).

[102] Durelli, A. J. and Daniel, I. M., Stress Distribution Around a Circular Hole in a Semi-Infinite Plate under Impact at Different Points on the Edge, *Developments in Mechanics*, Vol. 1, Plenum Press, N.Y., pp. 268–285 (1961).

[103] Daniel, I. M. and Riley, W. F., Stress Distribution on the Boundary of a Circular Hole in a Large Plate Due to an Air Shock Wave Traveling Along an Edge of the Plate, *Journal of Applied Mechanics*, Series E, Vol. 31, No. 3, pp. 402–408 (1964).

[104] Riley, W. F., Photoelastic Study of the Interaction Between a Plane Stress Wave and a Rigid Circular Inclusion, *Journal of Mechanical Engineering Science*, Vol. 6, No. 4, pp. 311–317 (1964).

[105] Fang, S. J., Hemann, J. H. and Achenbach, J. D., Experimental and Analytical Investigation of Dynamic Stress Concentrations at a Circular Hole, *Journal of Applied Mechanics*, Series E, Vol. 41, No. 2, pp. 417–422 (1974).

[106] Shea, R., Dynamic Stress-concentration Factors, *Experimental Mechanics*, Vol. 4, No. 1, pp. 20–24 (1964).

[107] Gurney, C., The Effective Stress Concentration at the End of a Crack Having Regard to the Atomic Constitution of Materials, Aero. Research Council, Report No. 2285, Dec. 1945, His Majesty Stationery, London (1948).

[108] Cox, H. L., Four Studies in the Theory of Stress Concentration, Aero. Research Council, His Majesty Stationery, R and M. No. 2704, London (1953).

[109] Freudenthal, A. M., *Fracture*, ed. by Liebowitz, H., Vol. II, Chap. 6, Academic Press (1968).

[110] Durelli, A. J. and Parks, V. J., Influence of Size and Shape on the Tensile Strength of Brittle Materials, *British Journal of Applied Physics*, Vol. 18, pp. 387–388 (1967).

[111] Kim, B. S. and Eringen, A. C., Stress Distribution Around an Elliptic Hole in an Infinite Micropolar Elastic Plate, *Letters in Applied and Engineering Science*, Vol. 1, pp. 381–390, Pergamon (1973).

[112] Mindlin, R. D., Influence of Couple Stresses on Stress Concentrations, *Experimental Mechanics*, Vol. 3, No. 1, pp. 1–7 (January 1963).

[113] Sternberg, E. and Muki, R., The Effect of Couple-Stresses on the Stress Concentration Around a Crack, ONR report, April 1966 Contract Nonr-220(58)NR-064-431.

[114] Hartranft, R. J. and Sih, G. C., The Effect of Couple Stresses on the Stress Concentration of a Circular Inclusion, *Journal of Applied Mechanics*, (June 1965).

[115] Shiryaer, Ya. M., Stress Concentration Near an Inhomogeneity and Experimental Clarification of the Couple-Stress Effect, *Zhurnal Prikladnoi Mekhaniki i Tekhnicheskoi Fiziki*, No. 4, pp. 142–144, (July–Aug. 1976). Trans. in *Journal of Applied Mechanics and Technical Physics*, Vol. 17, No. 4, pp. 569–571 (May 1977).

[116] Cartwright, D. J. and Rooke, E. P., Approximate Stress Intensity Factors Com-

AD-A120 702 STRESS CONCENTRATIONS(U) MARYLAND UNIV COLLEGE PARK 2/2
SCHOOL OF ENGINEERING A J DURELLI SEP 82 60
N00014-81-K-0186

UNCLASSIFIED F/G 12/1 NL

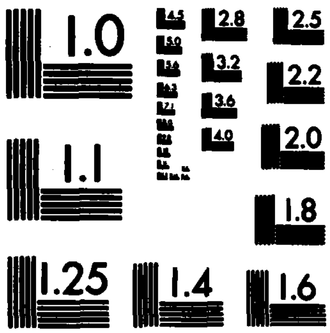

MICROCOPY RESOLUTION TEST CHART
NATIONAL BUREAU OF STANDARDS-1963-A

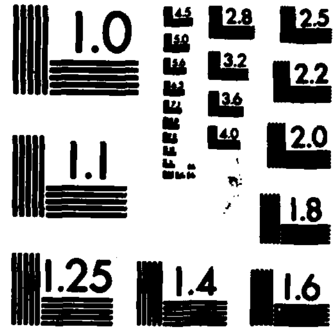

MICROCOPY RESOLUTION TEST CHART
NATIONAL BUREAU OF STANDARDS-1963-A

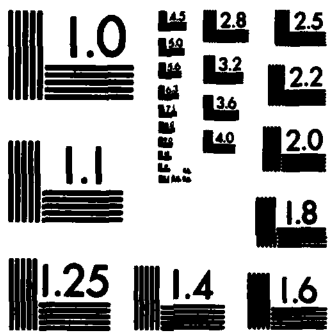

MICROCOPY RESOLUTION TEST CHART
NATIONAL BUREAU OF STANDARDS-1963-A

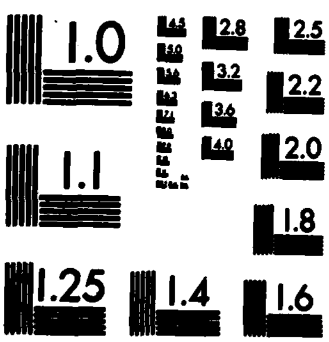

MICROCOPY RESOLUTION TEST CHART
NATIONAL BUREAU OF STANDARDS-1963-A

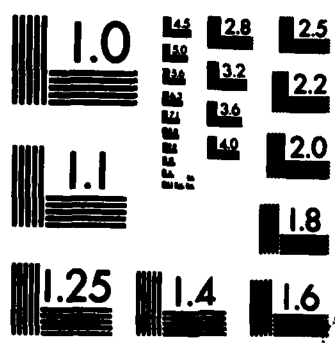

MICROCOPY RESOLUTION TEST CHART
NATIONAL BUREAU OF STANDARDS-1963-A

pounded From Known Solutions, *Engineering Fracture Mechanics*, Vol. 6, p. 563 (1974).

[117] Sih, G. C. (Ed.), *Methods of Analysis and Solutions of Crack Problems*, Noordhoff Int. Publish. (1973).

[118] Sih, G. C., *Handbook of Stress Intensity Factors for Researchers and Engineers*, Inst. of Fract. and Sol. Mech., Lehigh Univ. Bethlehem, PA. 1973.

[119] Tada, H., Paris, P. and Irwin, G., *The Stress Analysis of Cracks Handbook*., Del. Research Corp., Hillertown, PA (1973).

[120] Rooke, D. F. and Cartwright, D. J., *Compendium of Stress Intensity Factors*, Ministry of Defence, Her Majesty's Stationery Office, London (1974).

SECURITY CLASSIFICATION OF THIS PAGE (When Data Entered)

REPORT DOCUMENTATION PAGE

READ INSTRUCTIONS BEFORE COMPLETING FORM

1. REPORT NUMBER: 60	2. GOVT ACCESSION NO.: AD-A120702
3. RECIPIENT'S CATALOG NUMBER:	
4. TITLE (and Subtitle): Stress Concentrations	5. TYPE OF REPORT & PERIOD COVERED:
	6. PERFORMING ORG. REPORT NUMBER:
7. AUTHOR(s): A. J. Durelli	8. CONTRACT OR GRANT NUMBER(s): N00014-81-k-0186
9. PERFORMING ORGANIZATION NAME AND ADDRESS: University of Maryland, College Park, Md.	10. PROGRAM ELEMENT, PROJECT, TASK AREA & WORK UNIT NUMBERS:
11. CONTROLLING OFFICE NAME AND ADDRESS: Office of Naval Research, Dept. of the Navy, Washington, D. C. 20025	12. REPORT DATE: September 1982
	13. NUMBER OF PAGES: 81
14. MONITORING AGENCY NAME & ADDRESS (if different from Controlling Office)	15. SECURITY CLASS. (of this report)
	15a. DECLASSIFICATION/DOWNGRADING SCHEDULE

16. DISTRIBUTION STATEMENT (of this Report)

Distribution of this report is unlimited

DISTRIBUTION STATEMENT A
Approved for public release;
Distribution Unlimited

17. DISTRIBUTION STATEMENT (of the abstract entered in Block 20, if different from Report)

18. SUPPLEMENTARY NOTES

19. KEY WORDS (Continue on reverse side if necessary and identify by block number)

Non-linear Strains
Stress Concentrations
Photoekasticity
Dynamic Stress Concentrations
Notch Sensitivity
Stress Intensity Factors

20. ABSTRACT (Continue on reverse side if necessary and identify by block number)

The scope of this work on "Stress Consentrations" includes critical studies of the presently available handbooks, geometrically non-linear problems, mixed boundary value problems, three-dimensional problems, dynamic stress concentrations and also deals with the advantages and limitations of the methods commonly used to determine stress concentration factors.

DD FORM 1 JAN 73 1473 EDITION OF 1 NOV 65 IS OBSOLETE
S/N 0102-014-6601

SECURITY CLASSIFICATION OF THIS PAGE (When Data Entered)

The work was conducted with the financial support of the Office of Naval Research. The author of the chapter dealing with dynamic stress concentration was Prof. W. F. Riley of Iowa State University. It is unfortunate that these acknowledgements did not find place in the printed text. The author is particularly grateful to Dr. N. Basdekas of ONR for continuing a financial support that permitted the publication of the 60th report of a series that started about 20 years ago. P. Baxter was in charge of several phases of the work reproduction.

ONR DISTRIBUTION LIST

Part 1 - Government
Administrative and Liaison Activities

Office of Naval Research
Department of the Navy
Arlington, Virginia 22217
Attn: Code 474 (2)
Code 471
Code 200

Director
Office of Naval Research
Branch Office
666 Summer Street
Boston, Massachusetts 02210

Director
Office of Naval Research
Branch Office
536 South Clark Street
Chicago, Illinois 60605

Director
Office of Naval Research
New York Area Office
715 Broadway - 5th Floor
New York, New York 10003

Director
Office of Naval Research
Branch Office
1030 East Green Street
Pasadena, California 91106

Naval Research Laboratory (6)
Code 2627
Washington, D.C. 20375

Defense Documentation Center (12)
Cameron Station
Alexandria, Virginia 22314

Navy

Undersea Explosion Research Division
Naval Ship Research and Development
Center
Norfolk Naval Shipyard
Portsmouth, Virginia 23709
Attn: Dr. R. Palmer, Code 177

Naval Research Laboratory
Washington, D.C. 20375
Attn: Code 8400
8410
8430
8440
6300
6390
6380

David W. Taylor Naval Ship Research
and Development Center
Annapolis, Maryland 21402
Attn: Code 2740
28
281

Naval Weapons Center
China Lake, California 93555
Attn: Code 4062
4520

Commanding Officer
Naval Civil Engineering Laboratory
Code L31
Port Hueneme, California 93041

Naval Surface Weapons Center
White Oak
Silver Spring, Maryland 20910
Attn: Code R-10
G-402
K-82

Technical Director
Naval Ocean Systems Center
San Diego, California 92152

Navy (Con't.)

Supervisor of Shipbuilding
U.S. Navy
Newport News, Virginia 23607

Navy Underwater Sound
Reference Division
Naval Research Laboratory
P.O. Box 8337
Orlando, Florida 32806

Chief of Naval Operations
Department of the Navy
Washington, D.C. 20350
Attn: Code OP-098

Strategic Systems Project Office
Department of the Navy
Washington, D.C. 20376
Attn: NSP-200

Naval Air Systems Command
Department of the Navy
Washington, D.C. 20361
Attn: Code 5302 (Aerospace and Structures)
604 (Technical Library)
320B (Structures)

Naval Air Development Center
Warminster, Pennsylvania 18974
Attn: Aerospace Mechanics
Code 606

U.S. Naval Academy
Engineering Department
Annapolis, Maryland 21402

Naval Facilities Engineering Command
200 Stovall Street
Alexandria, Virginia 22332
Attn: Code 03 (Research and Development)
04B
045
14114 (Technical Library)

Naval Sea Systems Command
Department of the Navy
Washington, D.C. 20362
Attn: Code 05H
312
322
323
05R
32R

Commander and Director
David W. Taylor Naval Ship
Research and Development Center
Bethesda, Maryland 20084
Attn: Code 042
17
172
173
174
1800
1844
012.2
1900
1901
1945
1960
1962

Naval Underwater Systems Center
Newport, Rhode Island 02840
Attn: Dr. R. Trainor

Naval Surface Weapons Center
Dahlgren Laboratory
Dahlgren, Virginia 22448
Attn: Code G04
G20

Technical Director
Mare Island Naval Shipyard
Vallejo, California 94592

Navy (Con't.)

U.S. Naval Postgraduate School
Library
Code 0384
Monterey, California 93940

Webb Institute of Naval Architecture
Attn: Librarian
Crescent Beach Road, Glen Cove
Long Island, New York 11542

Army

Commanding Officer (2)
U.S. Army Research Office
P.O. Box 12211
Research Triangle Park, NC 27709
Attn: Mr. J. J. Murray, CRD-AA-IP

Watervliet Arsenal
MAGGS Research Center
Watervliet, New York 12189
Attn: Director of Research

U.S. Army Materials and Mechanics
Research Center
Watertown, Massachusetts 02172
Attn: Dr. R. Shea, DRXMR-T

U.S. Army Missile Research and
Development Center
Redstone Scientific Information
Center
Chief, Document Section
Redstone Arsenal, Alabama 35809

Army Research and Development
Center
Fort Belvoir, Virginia 22060

NASA

National Aeronautics and Space
Administration
Structures Research Division
Langley Research Center
Langley Station
Hampton, Virginia 23365

National Aeronautics and Space
Administration
Associate Administrator for Advanced
Research and Technology
Washington, D.C. 20546

Air Force

Wright-Patterson Air Force Base
Dayton, Ohio 45433
Attn: AFFDL (FB)
(FBR)
(FBE)
(FBS)
AFML (MBM)

Chief Applied Mechanics Group
U.S. Air Force Institute of Technology
Wright-Patterson Air Force Base
Dayton, Ohio 45433

Chief, Civil Engineering Branch
WLRC, Research Division
Air Force Weapons Laboratory
Kirtland Air Force Base
Albuquerque, New Mexico 87117

Air Force Office of Scientific Research
Bolling Air Force Base
Washington, D.C. 20332
Attn: Mechanics Division

Department of the Air Force
Air University Library
Maxwell Air Force Base
Montgomery, Alabama 36112

Other Government Activities

Commandant
Chief, Testing and Development Division
U.S. Coast Guard
1300 E Street, NW.
Washington, D.C. 20226

Technical Director
Marine Corps Development
and Education Command
Quantico, Virginia 22134

Director Defense Research
and Engineering
Technical Library
Room 3C128
The Pentagon
Washington, D.C. 20301

Dr. M. Gaus
National Science Foundation
Environmental Research Division
Washington, D.C. 20550

Library of Congress
Science and Technology Division
Washington, D.C. 20540

Director
Defense Nuclear Agency
Washington, D.C. 20305
Attn: SPSS

Mr. Jerome Persh
Staff Specialist for Materials
and Structures
OUSDR&E, The Pentagon
Room 3D1089
Washington, D.C. 20301

Chief, Airframe and Equipment Branch
FS-120
Office of Flight Standards
Federal Aviation Agency
Washington, D.C. 20553

National Academy of Sciences
National Research Council
Ship Hull Research Committee
2101 Constitution Avenue
Washington, D.C. 20418
Attn: Mr. A. R. Lytle

National Science Foundation
Engineering Mechanics Section
Division of Engineering
Washington, D.C. 20550

Picatinny Arsenal
Plastics Technical Evaluation Center
Attn: Technical Information Section
Dover, New Jersey 07801

Maritime Administration
Office of Maritime Technology
14th and Constitution Avenue, NW.
Washington, D.C. 20230

Universities

Dr. J. Tinsley Oden
University of Texas at Austin
345 Engineering Science Building
Austin, Texas 78712

Professor Julius Miklowitz
California Institute of Technology
Division of Engineering
and Applied Sciences
Pasadena, California 91109

Dr. Harold Liebowitz, Dean
School of Engineering and
Applied Science
George Washington University
Washington, D.C. 20052

Professor Eli Sternberg
California Institute of Technology
Division of Engineering and
Applied Sciences
Pasadena, California 91109

Professor Paul M. Naghdi
University of California
Department of Mechanical Engineering
Berkeley, California 94720

Professor A. J. Durelli
Oakland University
School of Engineering
Rochester, Missouri 48063

Professor F. L. DiMaggio
Columbia University
Department of Civil Engineering
New York, New York 10027

Professor Norman Jones
The University of Liverpool
Department of Mechanical Engineering
P. O. Box 147
Brownlow Hill
Liverpool L69 3BX
England

Professor E. J. Skudrzyk
Pennsylvania State University
Applied Research Laboratory
Department of Physics
State College, Pennsylvania 16801

Professor J. Klosner
Polytechnic Institute of New York
Department of Mechanical and
Aerospace Engineering
333 Jay Street
Brooklyn, New York 11201

Professor R. A. Schapery
Texas A&M University
Department of Civil Engineering
College Station, Texas 77843

Professor Walter D. Pilkey
University of Virginia
Research Laboratories for the
Engineering Sciences and
Applied Sciences
Charlottesville, Virginia 22901

Professor K. D. Willmert
Clarkson College of Technology
Department of Mechanical Engineering
Potsdam, New York 13676

Professor R. S. Rivlin
Lehigh University
Center for the Application
of Mathematics
Bethlehem, Pennsylvania 18015

Universities (Con't)

Dr. Walter E. Haisler
Texas A&M University
Aerospace Engineering Department
College Station, Texas 77843

Dr. Hussein A. Kamel
University of Arizona
Department of Aerospace and
Mechanical Engineering
Tucson, Arizona 85721

Dr. S. J. Fenves
Carnegie-Mellon University
Department of Civil Engineering
Schenley Park
Pittsburgh, Pennsylvania 15213

Dr. Ronald L. Huston
Department of Engineering Analysis
University of Cincinnati
Cincinnati, Ohio 45221

Professor G. C. M. Sih
Lehigh University
Institute of Fracture and
Solid Mechanics
Bethlehem, Pennsylvania 18015

Professor Albert S. Kobayashi
University of Washington
Department of Mechanical Engineering
Seattle, Washington 98105

Professor Daniel Frederick
Virginia Polytechnic Institute and
State University
Department of Engineering Mechanics
Blacksburg, Virginia 24061

Professor A. C. Eringen
Princeton University
Department of Aerospace and
Mechanical Sciences
Princeton, New Jersey 08540

Professor E. H. Lee
Stanford University
Division of Engineering Mechanics
Stanford, California 94305

Professor Albert I. King
Wayne State University
Biomechanics Research Center
Detroit, Michigan 48202

Dr. V. R. Hodgson
Wayne State University
School of Medicine
Detroit, Michigan 48202

Dean B. A. Boley
Northwestern University
Department of Civil Engineering
Evanston, Illinois 60201

Professor H. W. Liu
Syracuse University
Department of Chemical Engineering
and Metallurgy
Syracuse, New York 13210

Professor S. Bodner
Technion R&D Foundation
Haifa, Israel

Professor Werner Goldsmith
University of California
Department of Mechanical Engineering
Berkeley, California 94720

Universities (Con't)

Professor P. G. Hodge, Jr.
University of Minnesota
Department of Aerospace Engineering
and Mechanics
Minneapolis, Minnesota 55455

Dr. D. C. Drucker
University of Illinois
Dean of Engineering
Urbana, Illinois 61801

Professor N. M. Newmark
University of Illinois
Department of Civil Engineering
Urbana, Illinois 61803

Professor E. Reissner
University of California, San Diego
Department of Applied Mechanics
La Jolla, California 92037

Professor William A. Nash
University of Massachusetts
Department of Mechanics and
Aerospace Engineering
Amherst, Massachusetts 01002

Professor G. Herrmann
Stanford University
Department of Applied Mechanics
Stanford, California 94305

Professor J. D. Achenbach
Northwest University
Department of Civil Engineering
Evanston, Illinois 60201

Professor S. B. Dong
University of California
Department of Mechanics
Los Angeles, California 90024

Professor Bart Paul
University of Pennsylvania
Towne School of Civil and
Mechanical Engineering
Philadelphia, Pennsylvania 19104

Professor F. A. Cozzarelli
State University of New York at
Buffalo
Division of Interdisciplinary Studies
Karr Parker Engineering Building
Chemistry Road
Buffalo, New York 14214

Professor Joseph L. Rose
Drexel University
Department of Mechanical Engineering
and Mechanics
Philadelphia, Pennsylvania 19104

Professor B. K. Donaldson
University of Maryland
Aerospace Engineering Department
College Park, Maryland 20742

Professor Joseph A. Clark
Catholic University of America
Department of Mechanical Engineering
Washington, D.C. 20064

Dr. Samuel B. Batdorf
University of California
School of Engineering
and Applied Science
Los Angeles, California 90024

Professor Isaac Fried
Boston University
Department of Mathematics
Boston, Massachusetts 02215

Universities (Con't)

Professor E. Krempl
Rensselaer Polytechnic Institute
Division of Engineering
Engineering Mechanics
Troy, New York 12181

Dr. Jack R. Vinson
University of Delaware
Department of Mechanical and Aerospace
Engineering and the Center for
Composite Materials
Newark, Delaware 19711

Dr. J. Duffy
Brown University
Division of Engineering
Providence, Rhode Island 02912

Dr. J. L. Swedlow
Carnegie-Mellon University
Department of Mechanical Engineering
Pittsburgh, Pennsylvania 15213

Dr. V. K. Varadan
Ohio State University Research Foundation
Department of Engineering Mechanics
Columbus, Ohio 43210

Dr. Z. Hashin
University of Pennsylvania
Department of Metallurgy and
Materials Science
College of Engineering and
Applied Science
Philadelphia, Pennsylvania 19104

Dr. Jackson C. S. Yang
University of Maryland
Department of Mechanical Engineering
College Park, Maryland 20742

Professor T. Y. Chang
University of Akron
Department of Civil Engineering
Akron, Ohio 44325

Professor Charles W. Bert
University of Oklahoma
School of Aerospace, Mechanical,
and Nuclear Engineering
Norman, Oklahoma 73019

Professor Satya N. Atluri
Georgia Institute of Technology
School of Engineering and
Mechanics
Atlanta, Georgia 30332

Professor Graham F. Carey
University of Texas at Austin
Department of Aerospace Engineering
and Engineering Mechanics
Austin, Texas 78712

Dr. S. S. Wang
University of Illinois
Department of Theoretical and
Applied Mechanics
Urbana, Illinois 61801

Industry and Research Institutes

Dr. Norman Hobbs
Kaman AviDyne
Division of Kaman
Sciences Corporation
Burlington, Massachusetts 01803

Argonne National Laboratory
Library Services Department
9700 South Case Avenue
Argonne, Illinois 60440

Industry and Research Institutes (Con't)

Dr. M. C. Junger
Cambridge Acoustical Associates
54 Rindge Avenue Extension
Cambridge, Massachusetts 02140

Dr. V. Godino
General Dynamics Corporation
Electric Boat Division
Groton, Connecticut 06340

Dr. J. E. Greenspon
J. G. Engineering Research Associates
3831 Menlo Drive
Baltimore, Maryland 21215

Newport News Shipbuilding and
Dry Dock Company
Library
Newport News, Virginia 23607

Dr. W. F. Bozich
McDonnell Douglas Corporation
5301 Bolsa Avenue
Huntington Beach, California 92647

Dr. H. N. Abramson
Southwest Research Institute
8500 Culebra Road
San Antonio, Texas 78284

Dr. R. C. DeHart
Southwest Research Institute
8500 Culebra Road
San Antonio, Texas 78284

Dr. M. L. Baron
Weidlinger Associates
110 East 59th Street
New York, New York 10022

Dr. T. L. Geers
Lockheed Missiles and Space Company
3251 Hanover Street
Palo Alto, California 94304

Mr. William Caywood
Applied Physics Laboratory
Johns Hopkins Road
Laurel, Maryland 20810

Dr. Robert E. Dunham
Pacifica Technology
P.O. Box 148
Del Mar, California 92014

Dr. M. F. Kanninen
Battelle Columbus Laboratories
505 King Avenue
Columbus, Ohio 43201

Dr. A. A. Hochrein
Daedalean Associates, Inc.
Springlake Research Road
15110 Frederick Road
Woodbine, Maryland 21797

Dr. James W. Jones
Swanson Service Corporation
P.O. Box 5415
Huntington Beach, California 92646

Dr. Robert E. Nickell
Applied Science and Technology
3344 North Torrey Pines Court
Suite 220
La Jolla, California 92037

Dr. Kevin Thomas
Westinghouse Electric Corp.
Advanced Reactors Division
P. O. Box 158
Madison, Pennsylvania 15663